SEASONAL FORECASTS AND HYDROECONOMIC OPTIMIZATION IN EAST AFRICA

By

Saleh Satti

A dissertation submitted to Johns Hopkins University in conformity with the requirements for the Degree of Doctor of Philosophy

Baltimore, Maryland

June 2016

© 2016 Saleh Satti

All Rights Reserved

Abstract

Improving and adequately assessing seasonal forecasts in East Africa has great implications for food security and water resources planning in the region as they have much to contribute to the "added value" in decision making. Quantifying the value of information added by a forecast can aid in understanding ways to tailor forecasts in management scenarios. This dissertation aims to improve current seasonal forecasts for East Africa by (1) developing a hydroeconomic decision making model (SHOM) to quantify irrigation and hydropower benefits within an optimization framework, (2) identifying a novel method to reveal spatial biases in dynamically-based seasonal forecast systems, and (3) using the model to assess a suite of operational seasonal forecasts for decision makers within the region. Assessment of the analysis done in this dissertation shows several results. First, establishing a control structure upstream of Sudan will increase total benefits. Second objective regionalization can be used to identify spatial discrepancies in dynamical models, and understanding the spatial biases can be used to improve predictions in selected models. Third, seasonal forecasts are most effective in adding value to decision makers during drought years. Finally, models that underestimate values in their predictions relative to actual values produce higher benefits than models that overestimate.

Dedication

This dissertation is dedicated to my family and friends who have supported me. My father Abdel Moneim, my mother Kawther, my sister Sara, and my brothers Mohammed and Ahmed.

Acknowledgements

I would like to thank my Advisor Benjamin Zaitchik, for his patience, support and guidance.

I would like also like to thank Sauleh Siddiqui of JHU Civil Engineering, and Paul Block from the University of Wisconsin-Madison department of Civil and Environmental Engineering.

Additionally I would like to thank my committee members at JHU Earth and Planetary Sciences, Anand Gnanadesikan and Darryn Waugh.

I would like also thank members of the JHU Hydroclimate group, Hamada, Fisseha, Tiffany, Alexi, Jose and Asha for their assistance and support.

Lastly I would like to thank my family, especially my parents for all their support and love.

CONTENTS

List of tables

List of figures

1. Introduction

The challenge for the food insecure portions of the world is to predict the next big hydroclimatic extreme. The impending drought or flood has the capacity to decimate a harvest, cause a regional or global crisis and influence the lives of millions. Advancements in the predictive ability of the latest models rely heavily on an improved understanding of the science behind the processes within our earth system. Improvement in climate forecasting, both short term and long, has been possible with the advent of modern supercomputing which can resolve the complex equations that govern climate dynamics.

Applying this climate information in a meaningful way that aids food and energy production is problematic because most model outputs are riddled with errors and biases. Parsing the output forecasted data in order to ascertain the meaningful portions to decision makers requires identifying and improving on the current limitations of seasonal forecasting. Additionally understanding the decision making process that allows for the optimal use of water in the agricultural and energy sectors is equally important in formulating the decision makers objectives which ultimately impacts food and energy security.

Within the forecasting framework, one approach to discern the value of information (VOI) is by combining the predicted information from forecasting into a an optimization modeling framework that mimics the decision makers utility. VOI studies assess the importance of the forecasting model by assigning an expected

monetary value to the decision makers actions based on the forecasted information. Whereas metrics adopted by the climate community, such as ranked probability skill scores and error calculation assess the general performance of the model they fail to incorporate the needs of the users in the assessment. VOI studies provide a useful manner of assessing forecasts because they can identify the aspects of the forecasts that prove most valuable to the end user and therefore provide useful feedback that can help improve the forecasting capacity of the model.

1.1 Hydroeconomic Optimization

Optimization models are mathematical models that comprise an objective function that is either minimized or maximized and a set of constraints that define the model space and region of feasibility. These models can be applied in multiple management and planning scenarios where an optimal set of decisions is needed.

Within the field of water resources engineering, hydroeconomic optimization models are used in large-scale holistic studies where water management decisions are made in the context of other sectors such as food and energy. Hydroeconomic optimization models use the optimization framework with hydrologic, agronomic and economic inputs to assign costs and benefits to a set of water resources decisions. They are valued in water resources decisions because they can guide basin managers and stakeholders towards an economically optimal management strategy in place of traditional, static systems based on water rights and fixed allocations (Harou et al., 2009). Multiple studies have used hydroeconomic optimization in their management analysis spanning different regions of the world assessing different water resources sectors. Georgakoks et al. 2012 perform a

study on the value of reservoir management adaptation under climate change in Northern California. Yurtal et al. use dynamic programming to maximize hydropower operations in Turkey. Guariso and Whittington (1987) use hydroeconomic optimization of agriculture and energy to assess regional transboundary issues of cooperation in future large scale planning within the Nile.

Hydroeconomic optimization has focused on the Nile, particularly when dealing with the main actors that utilize this resource. Studies have focused in Egyptian use (Guariso et al. 1980) particularly in management of one of the largest hydropower dams in Africa, as well as in Ethiopia where the largest hydropower potential(Block and Strezpek 2010, USBR 1964) is realized. One of the largest contributors and users of Nile, Sudan, is often neglected in standalone hydroeconomic studies. This dissertation introduces the Sudan Hydro-economic Optimization Model (SHOM), which provides a complementary perspective on optimal water resource decision-making in the Eastern Nile. In contrast to earlier modeling efforts, we focus specifically on the Sudanese portion of the Blue Nile and the main stem Nile north of Khartoum. This because Sudan is an understudied and a pivotal player in Nile water resource management and geo-politics.

1.2 Seasonal Precipitation Forecasting

Vast improvements have been made in the field of seasonal forecasting within the last 30 decades. Prediction of precipitation on timescales greater than 10 days has traditionally been problematic due to short term memory in the atmosphere. Forecasts on time scales greater than half a month depend on the other variables within the earth systems with longer memories. Ocean indices, soil moisture, sea surface temperature (SSTs), and sea

level pressure (SLPs) are used predictors in statistical forecasting models that predict precipitation on seasonal time spans. Use of these predictors exhibits accuracy in precipitation forecasting in regions with high variability. Seasonal precipitation forecasting can be divided into two distinct types; dynamical and statistical. Statistical forecast models are not spatially constrained nor do they contain inherent biases (Landman and Goddard 2002). By using dominant large scale modes, and local variables as predictors, statistical models forecast precipitation as the response variable. Variable selection is usually done with some knowledge of the different prevailing weather and climate processes that influence precipitation within the region.

Dynamical forecast are forecasts made on models that rely on resolving physical equations. These models are usually atmospheric models that are forced with SSTs or are sometimes coupled with simple ocean models. Over the three last decade dynamical models have improved in their predictive capacity due to developments in computers as well as the quality of input data particularly with the emergence of satellite based products. The physically based nature of dynamical models allows for processes and mechanisms affecting variability and prediction to be easily discerned. The coarse resolution, complex nature of dynamical forecasts and the inherent biases in the models are issues that pose challenges for the forecasting community which utilize dynamical models. Biases in the models, particularly the spatial nature of biases due to error in precipitation placement receive relatively little attention. Traditionally forecasting predictions for a location are extracted from the corresponding spatial location in the model. This spatial matching does not account for spatial biases in the model output. Past studies have looked into improving prediction by spatially correcting model outputs

(Koster et al. 2008) via a correlation analysis. This challenge of correcting spatial biases lies in the identification of regions where the spatial biases are prominent. Performing an objective regionalization within the area of interest identifies model spatial bias. Regionalization is a statistical technique that clusters data points with similar variability and creates regions with the same response to climate drivers. Today, there has been no comprehensive study into identifying and correcting dynamical model spatial biases. This body of work aims to develop a process that identifies and correct spatial biases within the Max Plank Institute for Meteorology's Atmosphere-ocean General Circulation Model (AGCM) version 4.5 (ECHAM4.5) predictions. Correction of biases in dynamical models are pressing particularly in food and energy insecure regions where forecast outlooks may be improved.

1.3 Value of Information of Forecasts

With the development of the Von Neumann-Morgenstern utility theorem VOI (Value of Information) studies have featured prominently in decision analysis where probilities of risk are derived and the users utility is defined (Katz and Murphy 1997). Prior information in a complex decision making set up can be evaluated and quantified. Like decision analysis, VOI studies can be performed using hydroeconomic optimization, where the optimal set of decisions is monetized. In weather and climate applications decisions are made ex ante when the information is made available. This information provided by forecasts is of great consequence to decision makers and users that utilize them. While traditional measures of forecast error in climatology (e.g. RMSE and RPS) assess the information by assuming a broad, collective end-user i.e. error in forecasts

assume everyone is the end user (Katz and Murphy 1997). VOI studies evaluate forecasts tailored to a particular user. Traditionally VOI studies with short-term climate and weather forecasts have been mainly conducted in the agricultural sectors within the developed world where there is access to reliable forecasts and commercial large scale agricultural data is readily available. Hydroeconomic optimization based VOI studies of seasonal forecasts of other sectors (hydropower) in developing regions of the world exist (Block 2011). This dissertation performs a VOI study using forecasted upstream flows inputted into SHOM in order to investigate the value of Blue Nile seasonal forecasts on hydropower and irrigation production along the Sudanese Blue Nile.

1.4 Dissertation Outline

The first chapter of this dissertation introduces the topics and identifies the areas of research that are addressed in the proceeding chapters. Chapter 2 presents a published peer reviewed paper Satti et al 2015 that introduces a multiobjective hydroeconomic model for the Sudanese Blue Nile (SHOM). This Chapter sets up and explains various parts of the model and performs a sensitivity analysis to both upstream climate conditions, as well as economic value of water for irrigation. Chapter 2 also examines various hypothetical scenarios that affect future water use along the Nile, including the inclusion of the Grand Ethiopian Renaissance Dam (GERD) in Ethiopia and potential changes to the 1959 Nile Agreement. The third chapter is a manuscript currently under submission and peer review. This chapter focuses on identifying spatial biases using objective regionalization in two dynamical models (CFSv2 and ECHAM4.5). This chapter then proceeds to develop a method that improves forecast predictions in one of

the models, ECHAM4.5 by adjusting for the spatial error. Chapter 4 does a VOI study for the Sudanese Blue Nile. A comprehensive model set up combines a precipitation prediction model, a hydrology model and SHOM to produce the value assessment. This VOI set-up compares 3 forecasting models, 1 statistical and 2 dynamical, and deduces the aspects of the forecast that adds value to SHOM. Lastly Chapter 5 presents the conclusions of all the previous chapters.

2. The Question of Sudan: A Hydroeconomic Optimization Model for the Sudanese Blue Nile

Abstract:

The effects of development and the uncertainty of a changing climate in East Africa pose myriad challenges for water managers along the Blue Nile. Sudan's large irrigation potential, hydroelectric dams, and prime location within the basin mean that Sudan's water management decisions will have great social, economic and political implications for the region. At the same time, Sudan's water use options are constrained by tradeoffs between upstream irrigation developments and downstream hydropower facilities as well as by the country's commitments under existing or future transboundary water sharing agreements. Here, we present a model that can be applied to evaluate optimal allocation of surface water resources to irrigation and hydropower in the Sudanese portion of the Blue Nile. Hydrologic inputs are combined with agronomic and economic inputs to formulate an optimization model within the General Algebraic Modeling System (GAMS). A sensitivity analysis is performed by testing model response to a range of economic conditions and to changes in the volume and timing of hydrologic flows. Results indicate that changing hydroclimate inputs have the capacity to greatly influence the productivity of Sudan's water resources infrastructure. Results also show that the economically optimal volume of water consumption, and thus the importance of existing treaty constraints, is sensitive to the perceived value of agriculture relative to electricity as well as to changing hydrological conditions.

2.1. Introduction:

The Nile Basin spans parts of 11 different countries in one of the most underdeveloped regions in the world. The transboundary nature of the Nile presents water-sharing challenges between upstream and downstream riparian nations (Waterbury et al. 1998). This is particularly true in the Eastern Nile basin, which is typically defined as the tributaries that arise in the Ethiopian Highlands—primarily the Blue Nile, Tekeze-Atbara, and Baro-Akobo-Sobat—together with the main stem Nile north of Khartoum (Figure 1). The Eastern Nile tributaries collectively contribute over 80% of flow in the main stem Nile. The Eastern Nile basin also exhibits strong hydrological connectivity, in that upstream climate variability and development directly impact downstream resources in a manner that is not observed in the White Nile system, where lakes and wetlands serve as a buffer between the Equatorial Lakes headwaters region and downstream water deficit areas in Sudan and Egypt (Blackmore & Whittington 2008). For this reason the utilization of Eastern Nile waters has long been a source of transboundary tension, most notably between Egypt, which claims historical rights to the majority of Nile River water, and Ethiopia, which has a strong interest in developing the Eastern Nile tributaries for hydropower and other uses.

While the diplomatic tensions between Egypt and Ethiopia have dominated the political and media discourse on Eastern Nile basin development (Cascao 2008, Igunza 2014, Hussein 2014, Gebreluel 2014), Sudan has the greatest potential to influence transboundary distribution of water resources. The 1959 Nile Waters Agreement grants Sudan the right to use 18.5 billion cubic meters (bcm) of Nile water per year. At present, however, Sudan uses less than this allocation; its actual water demand has been estimated

to be approximately 16.1 bcm per year (Jeuland 2010). This value could change in the future, both through internal development decisions and through external influences such as climate change and upstream infrastructure in Ethiopia. Where climate change has the potential to alter the magnitude of Blue Nile inflow and local evaporative demand, upstream infrastructure would be expected to regularize the timing of flows and to reduce silt load entering Sudan. Silt accumulates over time in the reservoir and reduces the volume of reservoir. This affects hydropower production, reduces the available water for irrigation, imposes dredging costs, and reduces flood control capabilities.

In this context, there is a need for analytical tools focused on Sudan's hydro-development options. In particular, it is important to understand how impending changes affecting the Sudanese portion of the Eastern Nile basin, including climate change and upstream development in Ethiopia, are likely to affect Sudan's use of its Nile River resources for hydropower and irrigation. The objective of this dissertation is to present an optimization model that illustrates the sensitivities of Sudan's Blue Nile and main stem Nile water resources infrastructure to changes in climate and upstream development.

2.1.1 The Blue Nile in Sudan

Approximately 60 bcm of water flows annually from the Blue Nile basin in Ethiopia to Sudan. Inter-seasonal variability is large, with flows peaking in August and September, and interannual variability is also considerable—gauged flow at Roseries (Figure 2.1) has an interannual variability equal to 25% of the mean flow. The basin is also undergoing climate change that has had a significant impact on temperature but, as

of yet, no clear directional impact on total annual precipitation or river discharge. In coming decades, climate change impacts on basin hydrology are expected to become more significant.

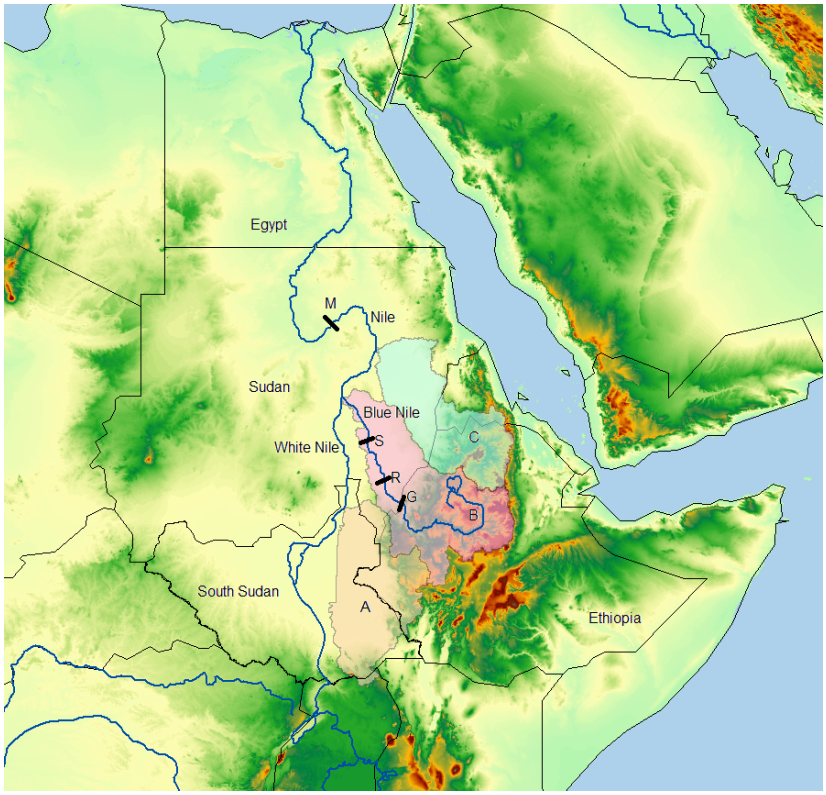

Figure 2.1: Map of the Nile and its tributaries A = Baro-Akobo-Sobat, B= Blue Nile, C = Tekese-Atbara Basins, S = Sennar Dam, R = Roseries Dam, M = Merowe Dam and G = GERD

The magnitude, seasonality, and even directionality of this change, however, are highly uncertain. Global Climate Models (GCM's) participating in the 5th Coupled Model Intercomparison Project (CMIP5; Taylor 2012) exhibit no consensus on projected change. A recent study of 10 CMIP5 models revealed projected precipitation change in the Blue Nile headwaters ranged from an increase of almost 40% by the mid 21st century relative to late 20th century to a decrease of approximately 40% at the same time period (Bhattacharjee and Zaitchik, 2015). Interestingly, some of the models with the most

widely diverging projections demonstrate reasonably good representation of current climate patterns and variability for commonly used model evaluation metrics (Bhattacharjee and Zaitchik, 2015). This range of uncertainty is evident in previous multimodel comparison studies as well, as past analysis have found 21st century change in Upper Blue Nile basin flows ranging from 133% to -35% and precipitation ranging from 55% to -9% (Yates and Strzepek 1998). Other studies of selected GCM's have found a smaller range of uncertainty, but no consensus on direction of change: Elshamy et al. (2008) examined 17 selected GCM's for the period 2081-2098 and found flow changes ranging from -15% to 14%, while Nawaz et al. (2010), analyzed the output of three GCM's and deduced that the mean annual Blue Nile runoff would change by +15%, 1% or -9% by the year 2025. Analysis conducted by Taye et al. (2010) projected future climate scenarios and ran them through two hydrologic models for two catchments representing source regions of the Blue and White Nile. Results illustrated a large range in the projected flows from the baseline for both basins. Changes in projected mean annual flows from the Blue Nile catchment range from approximately -80% to 70%.

In addition to climate change, proposed infrastructure projects will drastically alter the nature of downstream flows. There are currently no large structures along the main stem of the Blue Nile in Ethiopia, but the western portion of Ethiopia holds tremendous hydro-electric potential (Guariso et al 1987). The Ethiopian government has had plans to increase utilization of this energy source since at least 50 years ago, when the concept of a cascade of hydroelectric dams on the Blue Nile was first proposed (Bureau of Reclamation 1964, and Guariso et al 1987). The concept of a cascade of dams is still of interest to Ethiopia, but at present the country's development energies are

focused on construction of the Grand Ethiopian Renaissance dam (GERD), located at the border with Sudan (Figure 2.1). The GERD will be the Largest dam in Africa, holding back more than 60 billion cubic meters of water, and is expected to generate more than 5000 MW of electricity (Hammond 2013). The construction of this dam will affect many aspects of water sharing in the region and raises numerous questions about its effects on downstream riparian nations.

Sudan has one large dam on the main stem Nile—the 1250 MW capacity, 67 meter high Merowe dam, located 800 kilometers north of Khartoum near the fourth cataracts (Teodoru, 2006). In addition to Merowe, Sudan has two large dams along the Blue Nile reach, at Roseires and Sennar. Roseries was constructed in 1966 (Chesworth et al, 1990) with a capacity to generate 280 MW of electricity. Recent construction heightened the dam and increased the reservoir volume from 3.3 bcm to more than 7 bcm (McCartney et al. 2009). The Sennar dam was constructed in 1925 and holds back 900 million cubic meters of water (McCartney et al. 2009). Both dams were constructed to regulate flows that feed into multiple irrigation schemes, among them is the 800,000 hectare (ha) Geziera scheme. The Geziera was constructed by the governing British magistrate in 1925 as the largest single irrigation scheme in the world at the time (Bernal 1997). The dams also supply various schemes in Rahad and Suki as well as upstream and downstream of Sennar (McCartney et al. 2009). The Merowe dam (Figure 2.1) is located further downstream, in the cataracts of the main stem Nile in northern Sudan. This is a highly arid area and the dam's primary purpose is hydropower rather than irrigation. It was constructed in 2009 and now supplies the majority of Sudan's hydroelectric power.

All discussions of Nile flow and water resource development take place on the background of a complex and lengthy history of colonial and post-colonial era negotiations (Swain 1997). The most recent legally binding treaty involving Sudan is the 1959 Nile Waters Agreement, under which Sudan and Egypt agreed to divide the average flow of 84 bcm at the old Aswan dam between the two countries: 55.5 bcm to Egypt, 10 bcm to evaporation losses, and 18.5 bcm to Sudan. The treaty also granted Sudan permission to build a dam at Roseries. The agreement was limited to the two downstream nations and does not include any upstream riparian countries, and for this reason it is generally not recognized by the other countries on the Nile.

2.1.2 Hydroeconomic Modeling in the Nile basin

Hydroeconomic models integrate natural hydrologic dynamics, infrastructure, and management options in a framework of economic costs and benefits. They are particularly valued in complex water management problems because they provide a dynamic analysis of water resources and needs that guides basin managers and stakeholders towards an economically optimal management strategy in place of traditional, static systems based on water rights and fixed allocations (Harou et al., 2009). The core structure of most river basin hydroeconomic models is roughly similar: flows pass through a network of rivers and canals (or aquifers) and encounter nodes that represent resource infrastructure, such as reservoirs, abstraction sites, hydroelectric facilities, etc. But there is considerable diversity in the conceptual approach (simulation vs. optimization), representation of time (deterministic, stochastic, or dynamic), manner in which submodels are integrated to the hydroeconomic solution (modular vs. holistic), and, for optimization models, in the optimization objective function and algorithm

(Harou et al., 2009).

Not surprisingly, the Nile River basin has been a common and important target for hydroeconomic analyses. One relatively early effort was reported in Guariso et al. (1987), in which a linear optimization model was implemented to evaluate the effect of the long-discussed cascade of hydroelectric dams on the Ethiopian Blue Nile on overall benefit and on water economics in Sudan and Egypt. The optimization objectives of this model were to maximize hydropower production in Egypt, Sudan and Ethiopia, as well as downstream agricultural water supply. Simulations indicated that there was minimal tradeoff between the two competing objectives. Thus, Ethiopia's increased hydropower output would have a minor adverse effect on downstream riparian nations, but upstream flow regulation also had benefits for downstream riparian nations, including the fact that an increase in upstream flow regulation would decrease water levels in the highly evaporative downstream reservoirs, thus increasing total water availability for downstream riparian nations. This finding has been confirmed by subsequent modeling studies (e.g., Blackmore and Whittington 2008) and plays a role in studies that investigate the benefits of cooperation in the basin (Whittington 2004).

Another influential and relatively early optimization model for the Nile is the Nile Decision Support Tool (DST) which was developed by the Georgia Water Resources Institute. This model performs a basin wide hydrological and hydraulic simulation along with reservoir optimization capabilities and scenario assessment (Yao and Gerogakakos, Georgakakos 2007). The optimization model in DST utilizes the extended linear quadratic Gaussian (ELQG) control method in order to perform a stochastic multi-criteria optimization that aims to find the optimal reservoir operation (Georgakakos 1987, 1989).

A more recent basin-wide hydroeconomic optimization model, the Nile Economic Optimization Model (NEOM), was presented by Whittington et al. (2005) using GAMS software. This model was used to assess the economic implications of various infrastructural developments within the basin and aims to maximize for basin wide economic benefits due to irrigation and hydropower production. The authors quantify the economic benefit of cooperation by comparing the total benefits calculated from current allocation, with the total benefits derived from full communication and cooperation between various riparian nation states. They found that cumulative economic benefits for all players more than doubled the realized total benefit from $4.1 billion in the status quo scenario to more than $9 billion when all nations are fully cooperating.

Other recent modeling efforts have focused on a subset of the basin and investigated problems of dynamic and transient system management. In the Eastern Nile, Goor et al. (2010) present a dynamic reservoir optimization model that employs a Stochastic Dual Dynamic Optimization Program (SDDP). The model identifies the most economically efficient policies for large scale reservoirs (Goor et al. 2010). Block and Strzepek (2010) focus on the Ethiopian Blue Nile, implementing an Investment Model for Planning Ethiopian Nile Development (IMPEND) that calculates the economic benefit of proposed development under changing climatic conditions. IMPEND has the ability to model the transient filling stages of the dams, as well as the stochastic nature of the climate variables, allowing for a focus on the transient nature of the development process, an aspect of water management that is absent from most other hydroeconomic models of the basin. Block and Strzepek (2010, 2012) apply the model to climate change analysis and find that the omission of this transient period in models result in the

overestimation of total net benefits by more than $6 billion, as well as a significant change in the benefit to cost ratio of the project. Block and Strzepek (2010) also highlight changes in the hydrology that are neglected in models with no filling process: reservoir filling scenarios require that up to 170% more water be retained in Ethiopia over 30 years compared to scenarios where the reservoirs are assumed to already be filled.

More recently Jeuland (2010) and Jeuland and Whittington (2014) present hydroeconomic simulations that analyze decision making within the Nile basin under a changing climate. Jeuland (2010) presents a basin-wide hydroeconomic framework that integrates a stochastic flow generator, a hydrological simulation model and an economic model for the Nile. His analysis shows that varying specific economic and physical parameters simultaneously has a substantial impact on net present value. Jeuland and Whittington (2014) present long term planning hydropower investment options within Ethiopia under varying hydrological conditions. By using simulations, the authors are able to develop performance metrics for the different options, and show that results are dependent on the decision makers' risk preference.

The Sudan Hydroeconomic Optimization Model (SHOM) presented in this dissertation is intended to provide a complementary perspective on optimal water resource decision-making in the Eastern Nile. In contrast to earlier modeling efforts, we focus specifically on the Sudanese portion of the Blue Nile and the main stem Nile north of Khartoum. We do this because Sudan is a relatively understudied and a pivotal player in Nile water resource management. In addition, we use a non-linear optimization model (see section 2) that maximizes economic benefits and assesses trade-offs between hydropower production and irrigation within Sudan.

2.2. Methods:

2.2.1 The SHOM Optimization Model

The General Algebraic Modeling System (GAMS) is front-end software that can be used to solve non-linear multiobjective optimization problems by calling various solvers. By using the reduced gradient method in the CONOPT solver (Drud, 1992), the model seeks a stationary point while reducing the number of variables by conducting a variable selection processes. By curtailing the number of variables and linearizing the non-linear constraints via a Taylor series approximation, the algorithm simplifies the problem and solves for the non-linear objective (Drud, 1992).

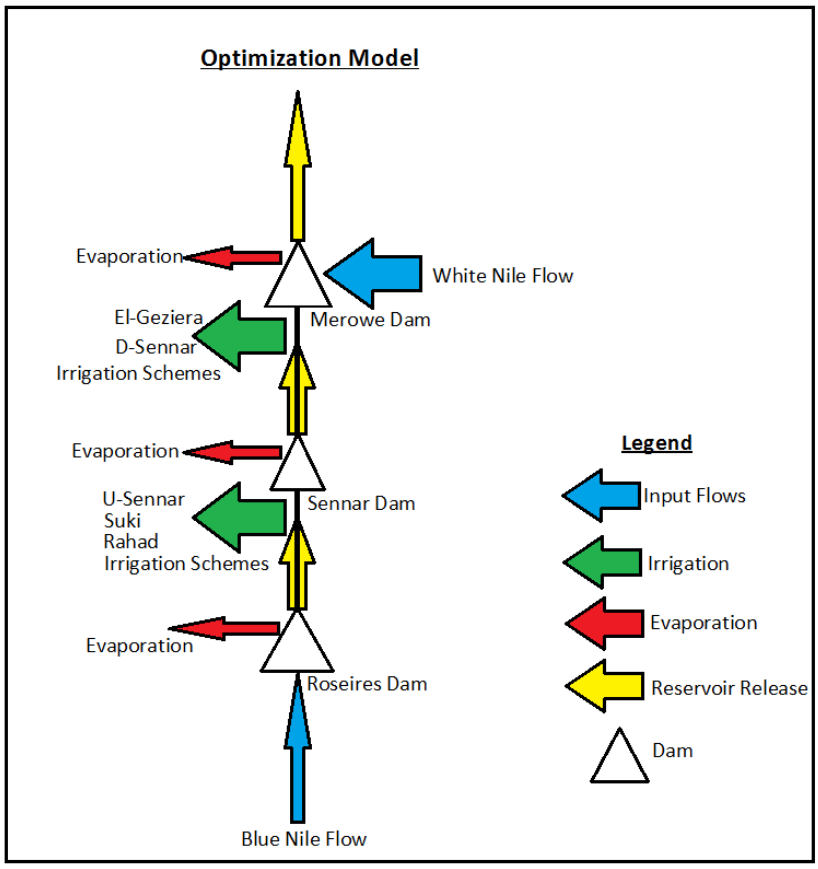

Figure 2.2: Schematic of the Optimization Model

SHOM runs on monthly time steps. In this implementation the simulation network includes 2 dams located on the Blue Nile reach (Roseires and Sennar), 1 dam on the main stem Nile (Merowe), and agriculture is represented by 5 irrigation schemes corresponding to existing developments along the Blue Nile (Figure 2.2). The combined storage volume of all dams is approximately 20 bcm, and the total irrigable area is 1.4 million ha. Tables 2.1 and 2.2 define all the parameters and variables in SHOM.

2.2.1.1 Objective Function:

The objective function of SHOM consists of two objectives which it seeks to maximize: agricultural and hydropower net benefits. Benefits refer to the total economic value attributed to each respective year summed over the twenty year run period. As noted by Whittington et al. (2005), the meaning of "value" takes more than one form. In this dissertation, the total net benefit attributed to the economic value of water is defined by the objective function and incorporates the benefits at each site location. Thus the total value of water is seen from the perspective of the producer (the State) and not from the perspective of the consumer. The objective function, illustrated below (Equation 2.1), represents the economic benefits from the agricultural and hydropower sectors. The total benefit attributed to hydropower production assumes infinite demand and is calculated as the total hydropower produced times the price per kilowatt hour. Initial dam infrastructural cost, cost of energy transmission and cost of dredging are not included in the objective function. Furthermore it is assumed in the sensitivity analysis presented in this dissertation that the price of electricity is fixed. Thus:

$$Objective = max \sum_{m,y} (D^y * bi_{m,y} + D^y * bh_{m,y}) \quad (2.1)$$

where, D^y= discount rate, $bi_{m,y}$ is the total benefits from Irrigation, $bh_{m,y}$ is the total benefits from hydropower, and all variables are indexed by month(m) and year(y).

2.2.1.2 Hydropower Constraints:

Total hydropower generation ($KWH_{l,m,y}$) is dependent on two variables (Equation 2.2), the amount of water passing through the turbines at any given time step ($rhe_{l,m,y}$), and the total height of water in the dam that forces water through the turbines ($h_{l,m,y}$) (Cohon 2003, Loucks et. al 1981).

$$\forall_{l,m,y},\ KWH_{l,m,y} = c * effh * n * rhe_{l,m,y} h_{l,m,y} \quad (2.2)$$

Production of hydropower is constrained by the dam's generation capacity; thus any additional release is categorized by the model as non-hydropower release. *effh* is the efficiency of the dams, which was assumed to be 0.85 in the model. There is also a conversion factor (c), c = 2.61×10^{-3}.

As shown in Equation 2.3, total hydropower benefits for each month in each year is dependent on the price of hydropower (P) and the sum of hydropower produced at all dam locations (l).

$$bh_{m,y} = \sum_l (P * KWH_{l,m,y}) \quad (2.3)$$

2.2.1.3 Irrigation Constraints:

The water used for irrigation ($i_{l,m,y}$) is dependent on the crop water requirement (i.e. the volume of water needed per unit area of crop cultivated), and the area irrigated during cropping season. Values of crop water requirement (Water) were drawn from a World Bank report (Plusquellec 1990). The area irrigated ($Area_{c,l,m,y}$) fluctuates

annually but remains constant during the cropping season (Equation 2.4). Therefore, the volume of water allocated for irrigation:

$$i_{l,m,y} = \sum_c (effi_c * Water_{c,l,m,y} * Area_{c,l,m,y}) \quad (2.4)$$

Efficiency of irrigation was assumed to be dependent on the crop type (Table 2.1) Elamin et al. (2011). (NB: The agricultural output in the objective function is irrigation fed; rain-fed agriculture was not considered). Therefore the total benefits due to irrigation for each m, at each y is:

$$bi_{m,y} = \sum_{c,l} (effi_c * v_c * Water_{c,l,m,y} * Area_{c,l,m,y}) \quad (2.5)$$

where vc is the marginal value of water for each crop (see section 2.2.2.1 for more details.)

Finally, per the 1959 Nile agreement Sudan's portion of withdrawals is limited to 18.5 bcm of water annually. Since our model is restricted to portions of the Blue Nile, we assume the maximum bounds to be 14.5 bcm (Equation 2.6). This approximation is based on the relative contribution of Blue Nile flows to the Nile system, and the recognition that the largest irrigation schemes in Sudan are located along the Blue Nile. Thus for a simulation of *Y* years the total water consumed by Sudan should be:

$$\sum_{l,m,y}(i_{l,m,y}) + \sum_{l,m,y}(e_{l,m,y}) \leq Y * 14.5\ bcm \quad (2.6)$$

A second constraint is included in the model to ensure Egypt's share and to prevent a large intake during drought years by ensuring Egypt's fractional share during those years (Equation 2.7):

$$\sum_{l,m}(i_{l,m,y}) + \sum_{l,m}(e_{l,m,y}) \leq 0.28 * \sum_m(R_y) \quad (2.7)$$

where R is the release at Merowe dam.

2.2.1.4 Continuity Constraints:

Storage at each dam location can be calculated using simple water balance. The storage at a particular time step is the total water contained in the reservoir in the previous time step plus the water entering each dam minus what comes out of the reservoir through upstream flow (Equation 2.8). The water entering is the upstream boundary flow or upstream total dam release ($q_{l,m,y}$ or $r_{l,m,y}$ respectively), the water leaving each dam node is the current dam release, the irrigated water and water loss due to evaporation.

$$\forall_{l,m,y},\ \ s_{l,m,y} = q_{l,m,y} + r_{(l-1),m,y} + s_{l,(m-1),y} - r_{l,m,y} - i_{l,m,y} - e_{l,m,y} \quad (2.8)$$

NB: $s_{l,(m-1),y}$ is the storage from the previous time step. When $m = 1$, the model uses the storage from $s_{l,12,(y-1)}$. Evaporation in m^3 / m^2 (Ev) is estimated using the Thornthwaite equation (Thornthwaite, 1948), thus the total evaporated volume: $e = Ev$ * Dam Surface Area. The storage at each time step must also be less than each dam's respective maximum volume (*Vmax*) (Equation 2.9).

$$s_{l,m,y} \leq Vmax \quad (2.9)$$

Lastly, all the decision variables calculated by the optimization model must satisfy non-negativity constraints (Equation 2.10):

$$s_{l,m,y}, rhe_{l,m,y}, i_{l,m,y} \geq 0. \quad (2.10)$$

Parameters	Value Range	Units	Notes
Discount Rate (D)	3% - 7%	-	5% used in the simulation analysis
Flows(q)			
High	20%		
Low	-20%	Million m^3	CI = Confidence Intervals
Smooth	3-month Average		
Bootstrapped Flows	5%, 50%, 95% CI		
Water Requirement(Water)			
Wheat	0.23 - 0.48		Value depends on Month
Cotton	0.48 - 0.73	m^3 / m^2	(Plusquellec 1990,
Sorghum	0.69 - 0.94		Ghezae 1998)
Groundnuts	0.89 - 1.14		
Efficiency			
Effh	0.85	-	Hydropower Efficiency
Irrigation			Irrigation Efficiency
Wheat	0.233	-	
Cotton	0.065	-	
Sorghum	0.333	-	
Groundnuts	0.312	-	
Power (P)	0.08	cents/KWh	
Evaporation[a]	0.08 - 0.3	m^3 / m^2	Evaporation is derived from the Thornthwaite equation (Thornthwaite, 1948). Range Depends on Month and location.
e	1.9 - 76.5	Million m^3	e = Ev*Dam Surface Area

Table 2.1: SHOM Parameters

Variables	Definition	Units	Notes
s^b	Storage	Million m^3	Storage volume is assumed to be cylindrical in the model
r	Release (r = rhe + nhe)	Million m^3	Release has two components, rhe = Hydropower release, nhe = non-hydropower release
i	Irrigation Volume	Million m^3	
Area	Area Irrigated	Million m^3	
bi	Irrigation Benefits	$	
KWH	Power Generated	KWh	Calculated from the hydropower equation. Function of hydropower release and head
bh	Hydropower Benefits	$	

Table 2.2: SHOM Variable definitions

2.2.2 Model Parameters:

2.2.2.1 *Marginal Value of Water for Irrigation*

Deriving the net benefits due to agriculture requires an intimate knowledge of both foreign and domestic agricultural economic markets. Calculating prices of output commodities relative to input production costs for future scenarios would require accurate price prediction of a non-linear, volatile market. Rather than attempt to analyze and project costs of agricultural inputs (e.g., water rates, fertilizer, land and labor) or to simplify tax rules and subsidies currently affecting agricultural prices in Sudan, we assign marginal water values for agriculture by assuming a horizontal demand curve for the marginal water values for each crop and that the average value of water equals the marginal value. The ratio of marginal water values for the crops was calculated using the producer price of the crop (P_c, FAO 2009), the yield (Y_c, Ghezae, 1998), and the crop water requirement (*water*, Plasquelle 1990). To explore the sensitivities of the model we perform simulations using 6 different sets of marginal water values, with each crop

assigned its own value (P1 – P6; Table 2.3). These values chosen are illustrative and are intended to assess the sensitivity of the model and are not meant to reflect the optimal estimate of current agricultural prices. Therefore the marginal crop values act as weights within the objective function to develop a tradeoff between the various objectives, as described in Section 2.3. For comparison, previous studies within the region have assumed a horizontal demand curve with an assigned marginal water value of 0.05$/m^3 for agriculture (Whittington et al. 2005, Arjoon et al. 2014).

	Marginal value of water ($/m3)					
	P1	P2	P3	P4	P5	P6
Cotton	0.287	0.118	0.036	0.008	0.001	0.00001
Wheat	0.062	0.025	0.008	0.002	0.000	0.000
Groundnut	0.083	0.034	0.011	0.002	0.000	0.000
Sorghum	0.017	0.007	0.002	0.000	0.000	0.000

Table 2.3: Marginal Values of Water for each Crop

2.2.2.2 Discount Rate (D^y)

Economic analyses of large-scale development projects need to discount anticipated future benefits relative to near-term costs and benefits forgone. Since the objective function and decision making in our model is solely based on economics, the discount rate can greatly influence the final value of the objective function of the model. To quantify this influence we performed simulations in which discount rate was varied from 3% to 7%, a range that has a considerable impact on the total value of the objective function, but not on the overall results. Discount rates may also affect the analysis of our deterministic hydroeconomic model by front-loading demands. In this model, this phenomenon is minimized by treaty constraints that limit water allocation for irrigation

(Equations 2.6 and 2.7). The same discount rate was applied to both objectives within the objective function. The results presented in Section 2.3 used a discount rate of 5% for all analyses.

2.2.2.3 Simulations

We apply SHOM to a set of hydrological and development scenarios to test sensitivities to changes in flow volume and timing in the Blue Nile as well as to investigate the influence that changing agricultural practices, electricity markets, and international agreements might have on optimal water allocations. A list of these scenarios is provided in Table 2.4.

Simulations	Description
High Flows	+20% Observed
Low Flows	-20% Observed
Smoothed Flows	3 month averaged
Smooth2crop	Smooth flow + 2 cropping season
SmoothPower	Smooth flow + 0.04 cents/KWh power price
Smooth2cropNA	Smooth flow + 2 cropping season + Removal of second 1959 agreement constraint
SmoothPower2crop	Smooth flow + 0.04 cents/KWh power price + 2 cropping season
SmoothPower2cropNA	Smooth flow + 0.04 cents/KWh power price+ 2 cropping season + Removal of second 1959 agreement constraint

Table 2.4: Description of the simulations used in SHOM

First, we examine sensitivity to changes in Blue Nile hydrology. As noted above, there is significant uncertainty in projections of future precipitation patterns—and hence future river flows—in the Blue Nile basin. For this reason we consider it important to test model sensitivity to substantial increases (+20%) "High flows" and decreases (-20%) "Low flows" in river flow, which is within the range of predictions of state of the art

global climate models for the first half of the 21st century. These simulations are compared to an "Observed Flow" simulation based on historic flow rates.

In addition, we are interested in how the model responds to temporal smoothing of inflow from Ethiopia, which might result from the construction of one or more upstream dams. For this reason we include a third flow scenario, "Smoothed Flows," in which the annual total flow is unchanged from present conditions but monthly flow values are averaged across three months, producing a smoothed hydrograph with less extreme wet season peaks and dry season troughs.

Changes in flows were restricted to the Blue Nile flows only; White Nile flows remained unchanged. This approach was adopted for multiple reasons. First, the White Nile originates in the Equatorial Lakes region, which is in a different climate zone. Thus it is unclear that an increase in Blue Nile flows would translate into an increase in White Nile flows. Second, the White Nile passes through the Equatorial lakes and Sudd wetland, so that its annual flow is more buffered than the Blue Nile. Lastly, majority of the water in Egypt originates from the Blue Nile region, so changes in White Nile flow under climate change would not impact the main stem Nile as significantly as changes in the Blue Nile.

Next, we consider how changing agricultural management practices due to upstream development might alter optimal allocations under a smoothed flow regime. Expected upstream development will increase water availability during the dry months, which will incentivize farmers to change their agricultural practices. This has already been observed on the Atbara River, just north of the Blue Nile, where construction of a dam in Ethiopia has led Sudanese farmers to transition from a one cropping season to a

multiple cropping season and to diversify crop types (Personal Communication, Professor Belay Simane, Addis Ababa University). For this reason we have included simulations to the smooth flows that add a second cropping season (Table 2.4 simulation "Smooth2crop").

Third, we examine sensitivity to electricity prices. The construction of a large upstream structure like the GERD would produce a large amount of hydropower itself, and in a connected electricity market this would drive down the price of electricity. The GERD, for example, is expected to generate electricity that can be sold to Sudan at a reduced price, about 4 cents a KWh (Hai 2013). To account for this dynamic in general terms, we include a model simulation "SmoothPower" in which flow is smoothed and the price of electricity is cut by half from 8 cents per KWh to 4 cents per KWh (see Table 2.4). We also consider how this change in power price might interact with a change in cropping practices in simulation "SmoothPower2Crop."

Finally, we introduce simulations in which there is upstream flow control, the opportunity for double cropping, and a relaxation of the downstream constraint. This relaxation, which we call "No Agreement" (NA), removes the requirement that Sudan provide adequate flow to Egypt in dry years—i.e., our second "treaty" constraint from section 2.2.1.3 (Equation 2.7). These simulations were performed for both high and low electricity prices: "Smooth2CropNA" and "SmoothPower2CropNA." Removing the second constraint allows us to examine the impact that downstream delivery requirements have on Sudan's optimal water allocations while keeping the total water use relatively similar to the baseline simulations, which facilitates comparisons between simulations.

All simulations in the sensitivity analysis were run for 20 years. To generate hydrological inputs for these simulations a 70 year record of monthly observed Blue Nile flows at Roseires was obtained from the Global Runoff Data Center (www.grdc.org). This record was randomly resampled to generate 1000 20-year timeseries of representative flow patterns. Interannual autocorrelation is insignificant (lag -1 autocorrelation is 0.165) for this hydrological timeseries dataset, thus the distortive effect of resampling is minimal. The mean flow for all 1000 bootstrapped timeseries were assembled and ranked, thus defining the 5% and 95% confidence levels of flows for the 20 year observed period. The model output was assessed using these confidence intervals.

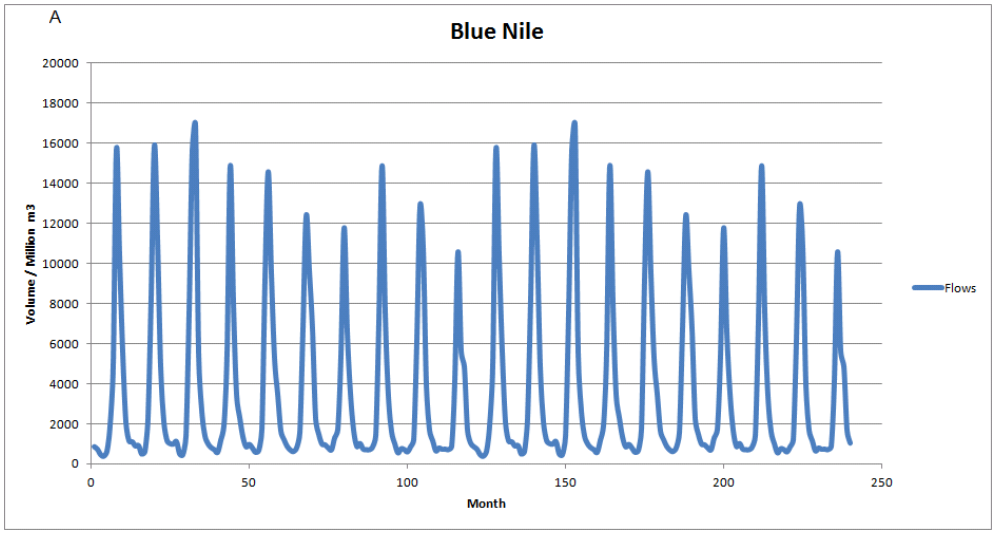

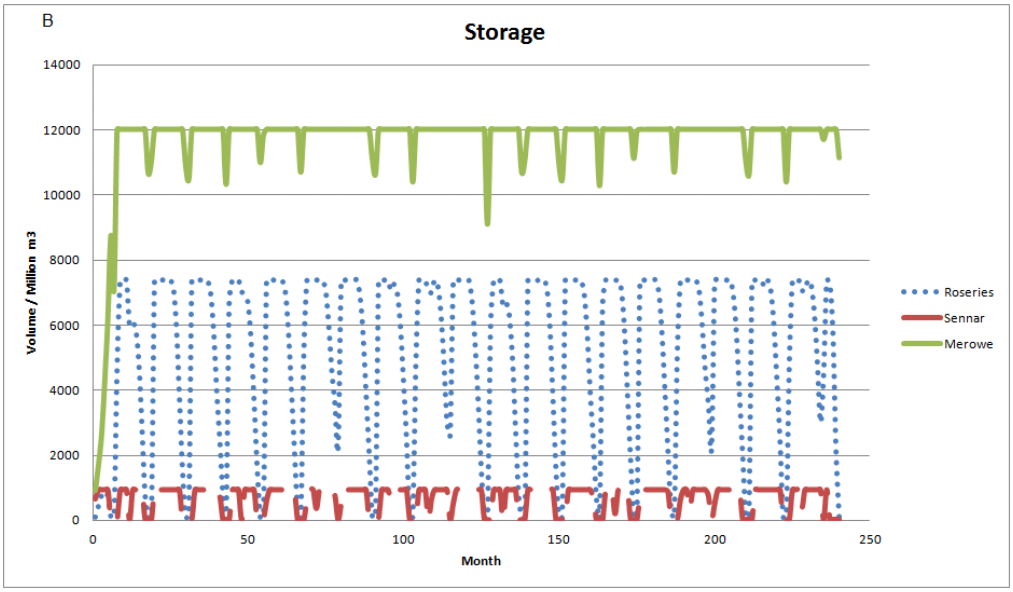

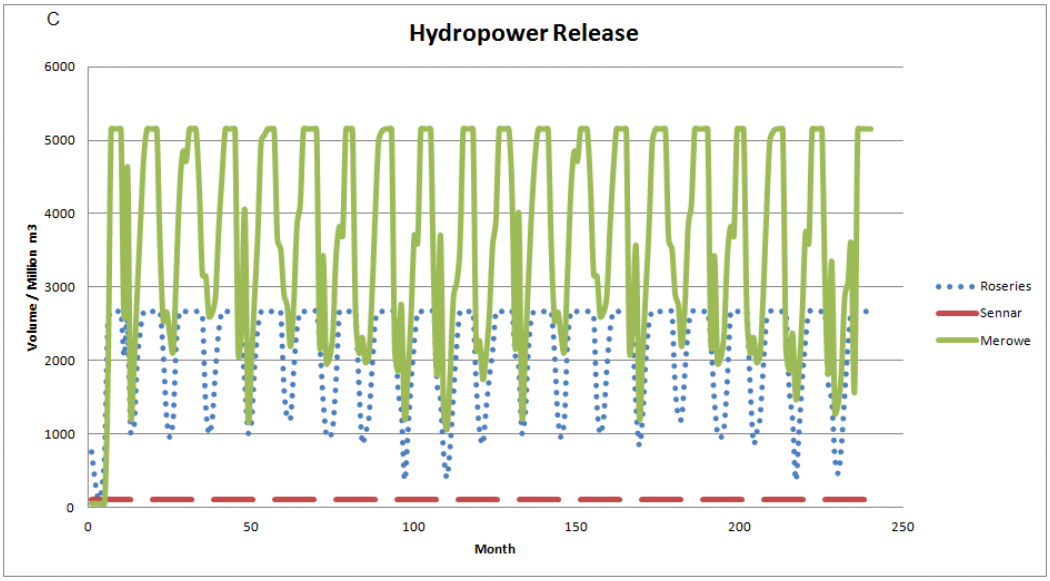

Figure 2.3: Annual cycle of (A) observed flow, (B) storage and (C) hydropower release at the three dams over the 20-year demonstration simulation

2.3. Results and Discussion:

2.3.1 Model Behavior

To demonstrate general model behavior we first examine a 20-year demonstration simulation that uses bootstrapped historical flows and the P5 set of marginal water values (see Table 2.3). Hydrologic fluxes and storages at the three dams in the simulation

(Roseires, Sennar, and Merowe) and for major irrigation areas are shown in Figures 2.3 and 2.4.

Figure 2.3A shows the observed 20 year flows for the Blue Nile at the Sudan-Ethiopia border. Fluctuations of flows are illustrative of the wet and dry seasonal pattern, and annual flows also vary significantly, from -26% to 26% of the mean. This record shows two distinct periods of below average annual flows (months 70-120 and months 190-240). The dam storage and release values reflect a response by the model to these periods of interseasonal dryness and wetness. The smaller dams (Roseries and Sennar) are emptied and filled annually (Figures 2.3B) with Merowe remaining relatively full year round in all years, with minor drops in its storage level during the dry months. Therefore there is no significant connection between the hydropower releases at Merowe and interannual variability. There is a significant connection between dry periods and hydropower release at Roseries. This is illustrated by lower hydropower releases during the periods of dry annual flows than during the wet periods (Figure 2.3C).

Figure 2.4 also shows results for the base case simulation, but as 20-year average seasonal cycles of storage, release, and withdrawals at each major dam and irrigation zone across the 1000 bootstrapped simulations. It is clear from Figure 2.4A that the large reservoir at Merowe is relatively insensitive to seasonal variability and to climatic variability represented by bootstrapping. This offers a more robust view of the sensitivity of optimal reservoir operation and water withdrawals to season and to potential patterns of variability given historical conditions.

Figure 2.4A shows that the dams along the Blue Nile (Sennar and Roseires), in contrast, are significantly sensitive to seasonal and interannual variability: in the months

preceding the wet season both Sennar and Roseires are emptied and then refilled during the rainy season, while Merowe is able to remain relatively full year round maximizing hydropower generation. This is in small part a product of the fact that Blue Nile flows are more strongly seasonal than main stem flows, which are slightly moderated by inflow from the White Nile. But the primary reason for the difference is the model's objective to maximize total benefit through the system. Maximizing hydropower output requires large hydropower release (Figure 2.4B), and adequate head through the turbines (see hydropower constraints section). Since Merowe is the largest hydroelectric facility, it is critical to hydropower optimization that it is active and that its reservoir is relatively full for as much of the year as possible. The model maximizes hydropower by maintaining Merowe at full capacity for most of the dry months at the expense of storage at Roseries and Sennar. Thus Roseries is emptied between January to May and a relatively full dam is maintained at Merowe for most of the dry season, maximizing total hydropower production. Since the Blue Nile has highly seasonal flows and Roseires and Sennar are relatively small dams, this comes at the cost of seasonally reduced reservoir storage and hydropower potential at those dams. In Figures 2.4A and B, the largest variability between simulations (biggest +/- bars) is observed during the months of emptying and filling (Feb-Aug), reflecting sensitivity to interannual climate variability.

Figure 2.4C shows total water withdrawal amounts during the cropping season upstream of Sennar dam, which would include the Rahad, Suki and Upstream Sennar irrigation schemes, and upstream of Merowe dam, which includes the Geziera and Downstream Sennar irrigation schemes. Since the larger schemes are situated upstream of Merowe and downstream of Sennar, the largest withdrawals are downstream of Sennar.

There were four crops modeled with different cropping cycles that overlapped during the season (Table 2.1), so the total agricultural water requirement varied on a monthly basis. Withdrawals, however, were maintained at between 1-2.5 bcm on average from July to October and drop to zero during the non-cropping period.

Currently, the influence of agriculture on dam management is limited due to two factors. First, though the crop calendar is somewhat different for each of the four crops, there is only one cropping season, which approximately coincides with the wet months, so agricultural productivity peaks when the water supply via Blue Nile peak flows is plentiful (Figure 2.4C) and the total annual withdrawals are limited by prevailing agricultural practices. Second, as shown in the tradeoff analysis below (Section 2.3.2), the 1959 Nile Waters Agreement constraints serves as a cap on water demands for scenarios with high marginal values of water for agriculture.

2.3.2 Tradeoff Analysis

Understanding the tradeoff between hydropower and irrigation is central to understanding how the model allocates water to the different objectives. Figure 2.5 shows results of simulations for three of the marginal values (P2, P4 and P5) represented in Table 2.3. The agricultural benefit is removed from the objective function and phrased as a constraint, and thus a tradeoff curve can be constructed that illustrates the hydropower-agriculture relationship for each set of agricultural marginal water values (Cohon 2003). For the case with higher marginal value of water for agriculture (P2), the gradient of the tradeoff curve is low. Thus the loss of one unit benefit of hydropower would result in a gain of more than one unit benefit of irrigation. In order to maximize total benefits, then,

the model would allocate more and more water to agricultural production until it hits a constraint. For the case with a low marginal value of water for agriculture (P5) the opposite is true: the model prioritizes moving water through the turbines at the expense of agriculture. For intermediate marginal water values (P4) there is an inflection point at which the gradient is equal to 1.0 (circled point in Figure 2.5). To the left of the point the gradient is less than 1.0, which would cause the model to shift towards agriculture, and to the right it is greater than 1.0, pushing the model back towards hydropower. Thus the inflection point is the optimum balance between agriculture and hydropower for that marginal value of water under given simulation conditions.

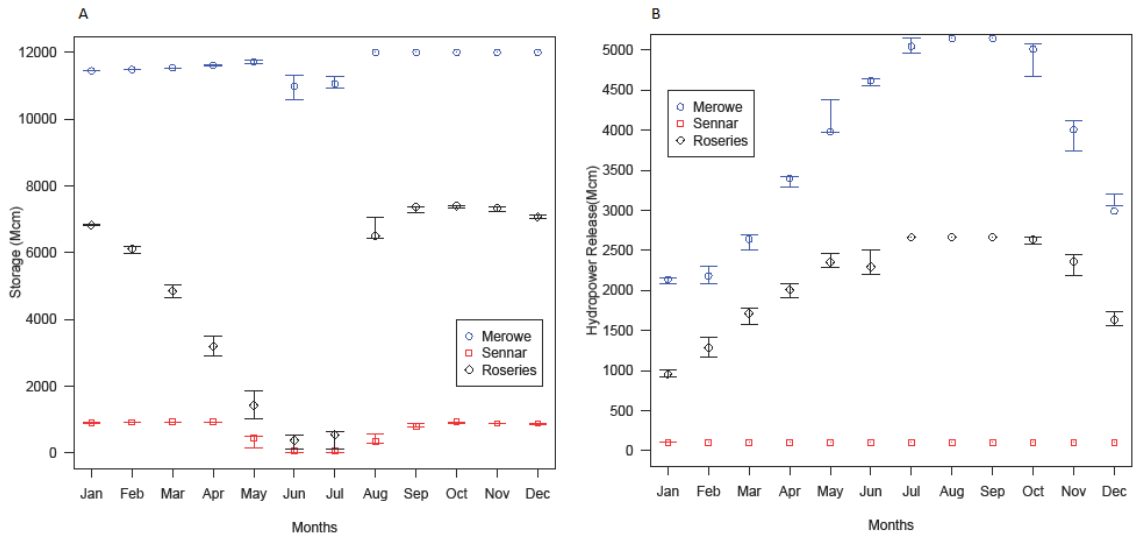

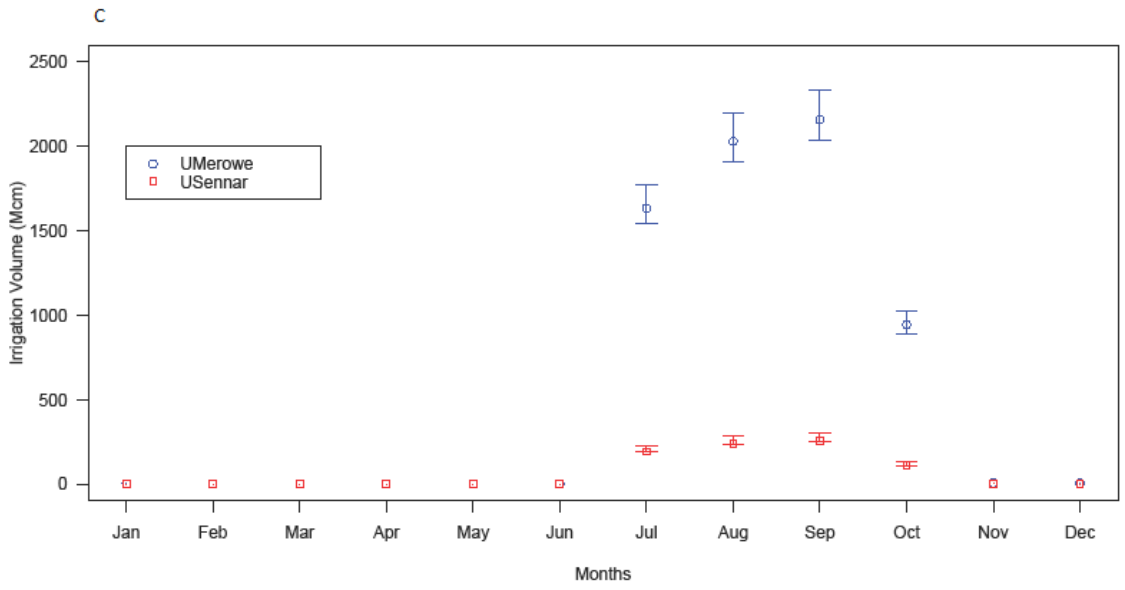

Figure 2.4: Annual cycle of (A) reservoir storage and (B) hydropower release at the three dams, and (C) irrigation withdrawals upstream of Sennar and upstream of Merowe in the base case simulation of bootstrapped historical flows and marginal values P4. Data points are the mean average value over the 20-year simulation and error bars represent the difference in output between the 5% and 95% confidence interval bootstrapped flow.

The implications of the optimal inflection point for total benefits are illustrated schematically in Figure 2.6. The blue line in Figure 2.6 represents a base case scenario with an optimum division between irrigation and hydropower indicated by the inflection point at gradient equal to one. The other lines are representative of scenarios in which changing conditions—altered flow regime, market modifications, policy decisions, or other external factors—shift the optimum in a manner that can change both the total value realized from the system and the division between irrigation and hydropower. A movement up and to the right on the chart is a win-win condition for Sudan in which both irrigation and hydropower benefits increase, while a move down and to the left is a lose-lose scenario. Movement up and to the left and down and to the right are trade-off scenarios in which hydropower benefit increases to the detriment of irrigation and vice versa. The interpretation of these "wins" and "losses" would, of course, differ for other

stakeholders. Egypt might view movement to the right on the chart—increasing irrigation withdrawals—as a potential threat to water resources in the absence of increased Nile river flow or the counterbalancing shared benefits.

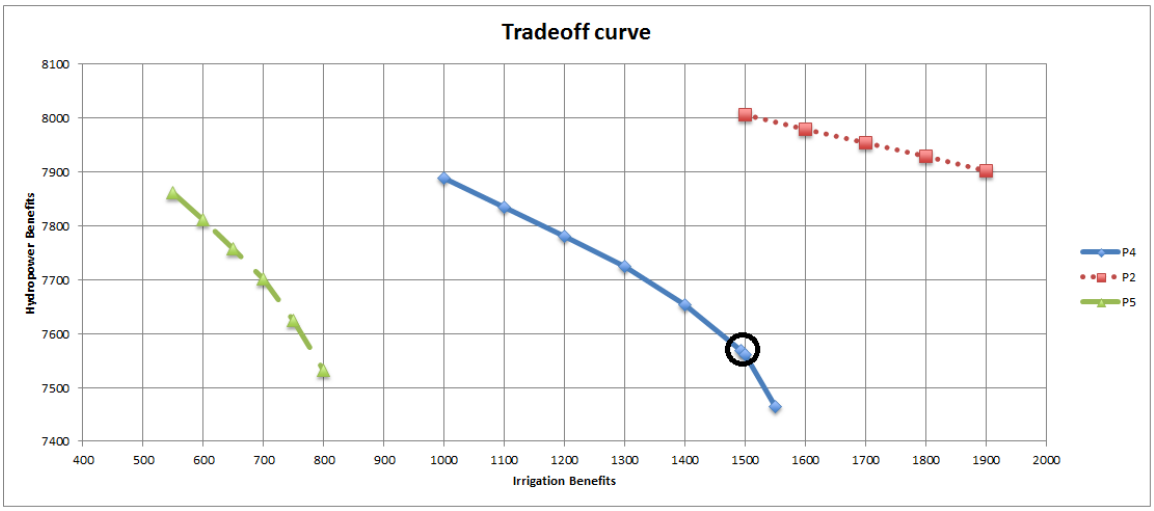

Figure 2.5: SHOM hydropower vs. irrigation benefit trade off curves for three different water values (P2, P4 and P5).

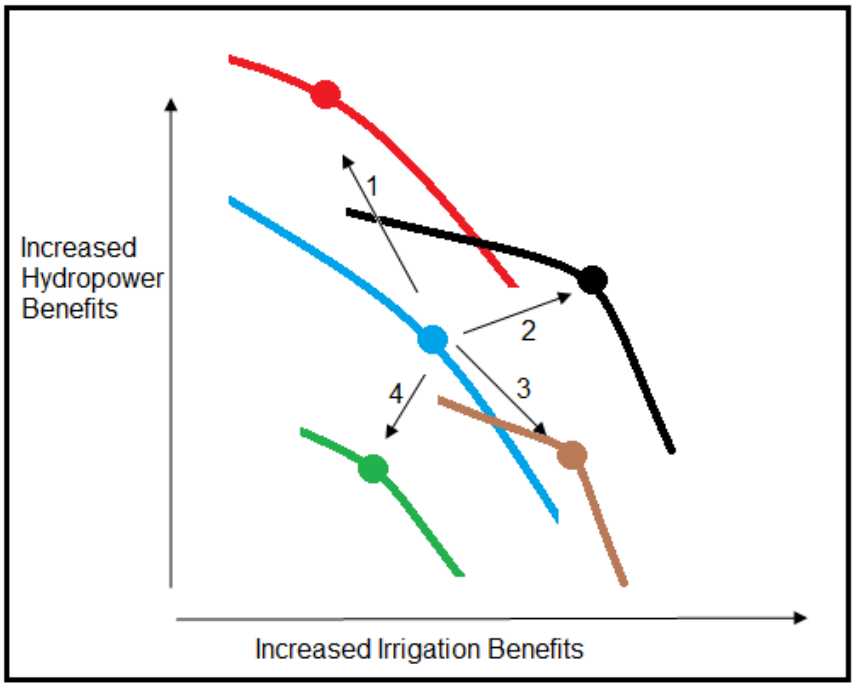

Figure 2.6: Schematic of the four possible ways in which changing conditions can shift the optimum model solution from a baseline set of solutions represented by the blue curve. Arrow 1 (shift to red curve) depicts a win-loss tradeoff where a loss in irrigation benefits is offset by an increased in hydropower benefits. Arrow 2 (shift to black curve)

depicts a win-win outcome, with a gain in both hydropower and irrigation. Similarly, arrows 3 and 4 can be characterized as loss-win and loss-loss, respectively.

With this framework in mind, we next consider simulations for one set of marginal water values (P4). These simulations allow us to ascertain the changing nature of the tradeoff curves for changes in mean flow consistent with the range of predicted climate change and for changes in flow timing representative of flow regulation from upstream development. P4 is used because it represents an intermediate set of profitability values; P3-P1 have high irrigation profitability and are limited by the 1959 constraints, while P5 and P6 push simulations strongly towards hydropower. Figure 2.7 shows the results of these simulations, with inflection points indicated as circles around the point at which the gradient crosses through 1.0. These circled data points are the optimal values for each scenario at which the model would converge for the given hydrologic inputs and parameter values.

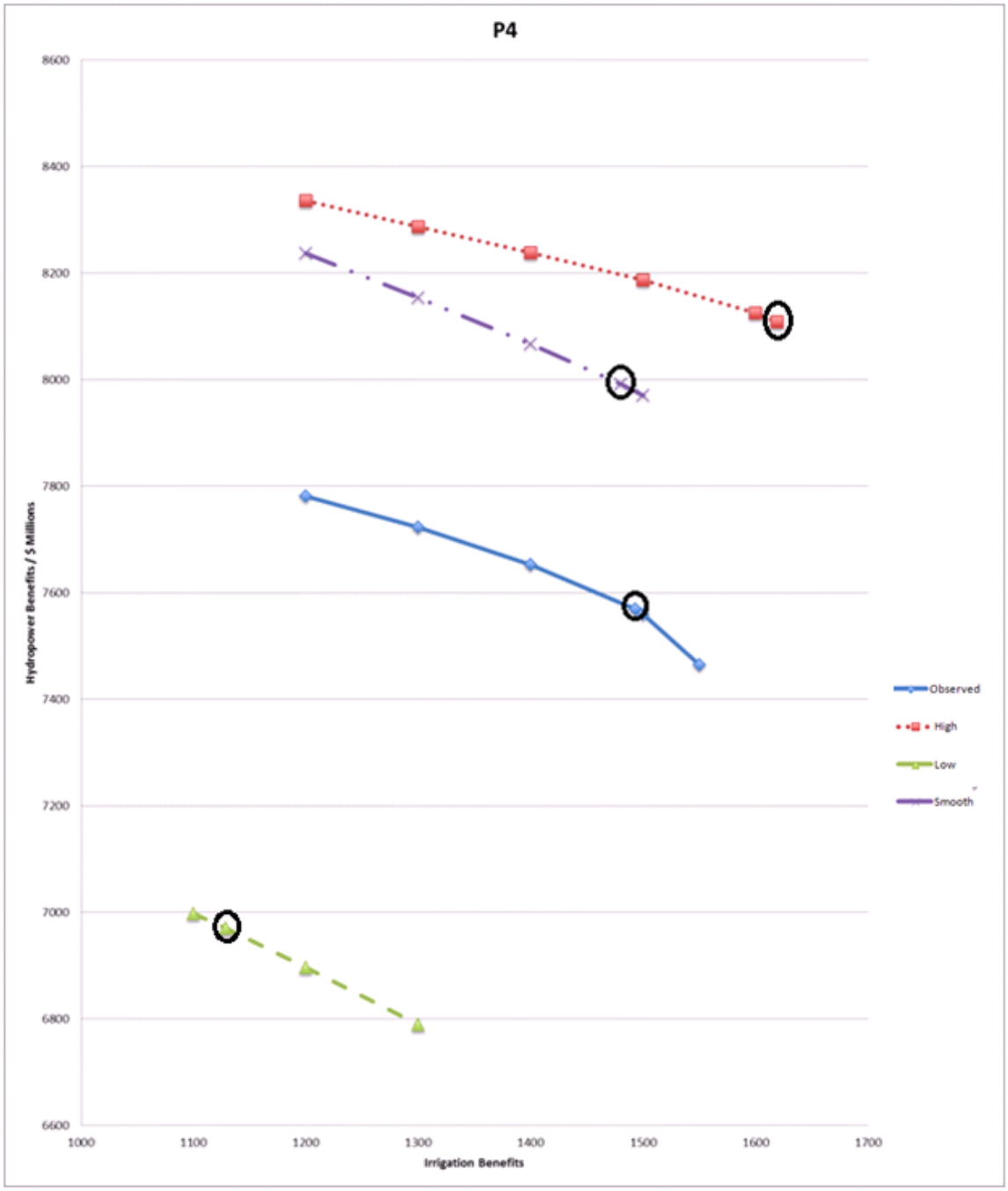

Figure 2.7: Results of SHOM simulations in which the agricultural benefits are phrased as constraints, and the hydropower benefits are calculated for a specific agricultural benefit. The circles highlight the optimal values for each scenario.

The relative position of these inflection points lies at the core of optimization-based hydro-economic analysis. When a change in hydrology (e.g., "high flow" versus

"observed flow") causes the inflection point to move to the right on the chart it suggests that this hydrologic change will push Sudan towards more irrigation. Similarly, if the inflection point moves up on the chart it suggests that the hydrologic change is pushing Sudan towards hydropower. These dynamics matter enormously for studies of how climate change or upstream development is likely to impact Sudan's water resource decision-making. Movement that is up and to the left or down and to the right is particularly interesting, as it suggests that Sudan's optimal development strategy involves a shift between hydropower and irrigation. In more general terms, a hydrologic shift that moves the optimal point up and to the left on Figure 2.6 could be thought of as a change that pushes Sudan towards a hydropower development pathway, while a shift that moves the point down and to the right pushes Sudan towards an irrigation development pathway relative to baseline simulation conditions.

Model sensitivity to reduced flow (-20%) is consistent with expectation. For the P4 water value set this low flow scenario results in a decrease in benefits from both irrigation and hydropower production (triangles and dashed line in Figure 2.7). Conversely, an increased flow (+20%) increases both agricultural production and hydropower production (squares and dotted line in Figure 2.7). Lastly, the smoothed flows show an increase in hydropower and almost no change in irrigation benefits. Stabilized flows increase water availability during the dry season and at the tail ends of the wet season, and thus there is more water available throughout the year for hydropower, increasing its benefits (x's and solid line in Figure 2.7).

Next, the sensitivity to agricultural value was analyzed by varying marginal value of water in agriculture (P1 – P6). Figure 2.8 shows the trade-off curve of Pareto optimal

values of hydropower and irrigation benefits for P1 – P6 (See Table 2.3). A solution point is Pareto optimal if there is no other feasible point that improves at least one objective function without exacerbating another objective function. As described above, a higher marginal value for agriculture assigns greater weight to agricultural production, which could be interpreted as a higher agricultural profit margin. First, we note that for all scenarios in Figure 2.8 the tradeoff curves flatten out at very high values of irrigation benefit. This flattening reflects the fact that at high marginal values the agricultural benefits are limited by the 1959 Nile Waters Agreement constraints. The trade-off curve approaches horizontal because the same amount of water is allowed to pass downstream through the turbines at Merowe while the calculated irrigation benefit per unit water continues to increase when marginal value is set to higher values.

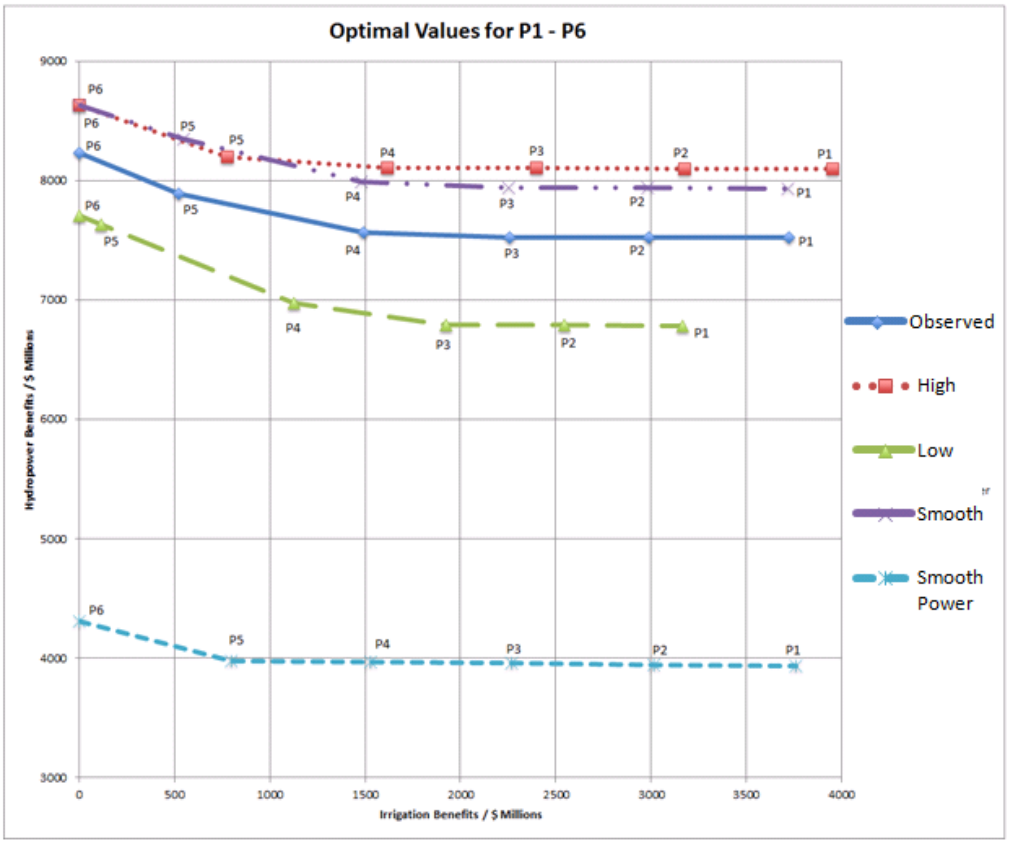

Figure 2.8: Hydropower vs. irrigation benefits in SHOM simulations. Points represent Pareto optima values for water value sets P1-P6.

Perhaps more interesting, Figure 8 can also be used to study how the marginal value of agricultural water affects the impact that a change in flow regime has on optimal water allocation. For the smoothed flow (upstream development) all marginal water value sets (P1-P6) show no significant increase/decrease in agriculture benefits, due in part to withdrawal restrictions imposed by the 1959 treaty and, perhaps, in part to the absence of a second cropping season in these simulations. All the P1-P6 marginal values, however, provide a win for Sudan: greater hydropower benefits. In other words, smoothed flows allow for more effective use of existing hydropower infrastructure.

The SmoothPower simulation (smoothed flow with a drop in the price of power) shows a policy shift from a hydropower-centric solution to a policy that increases agricultural production. Interestingly, this shift is relatively modest in all cases and is extremely small for simulations with high agricultural marginal water values (P1-P3). This is in large part reflects the limitation on Sudan's annual water withdrawals imposed by the model's downstream constraints, which guarantee flow to Egypt. For P1-P3 the Smooth Flow simulation already runs up against these constraints, preventing larger shifts to irrigation in SmoothPower.

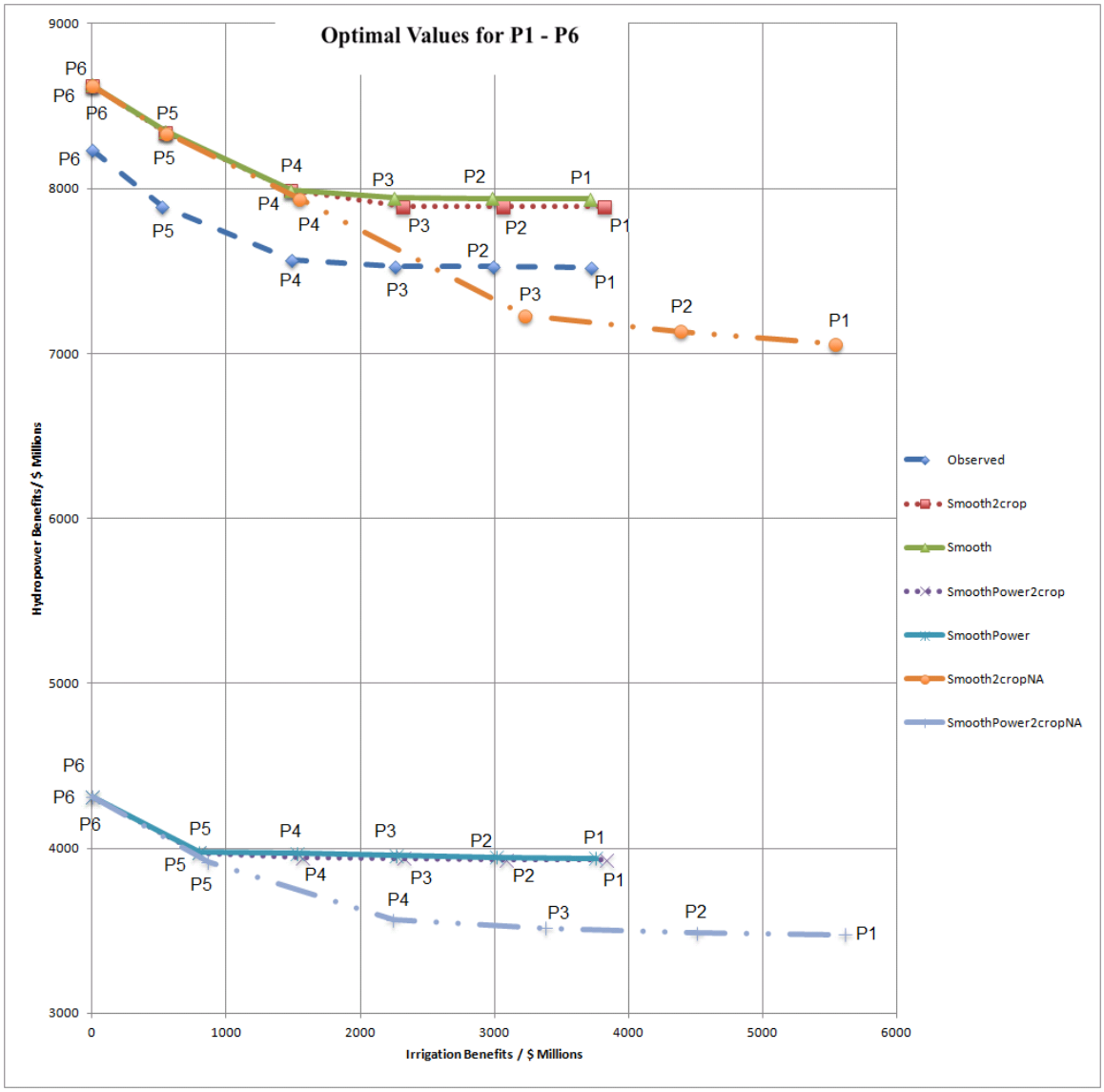

Figure 2.9: Hydropower vs. irrigation benefits illustrating adaptive management practices. Points represent Pareto optima values for water value sets P1-P6.

We note that all of these results, including the shift to agriculture in SmoothPower, are for existing cropping practices. Figure 2.9 considers a shift in management practices and introduces a second cropping season to the smoothed flow. An additional cropping season shows increases in irrigation benefits particularly if agricultural marginal water values are high (P1 – P3). Smooth2crop in Figure 2.9 introduces a second crop season to the smoothed flow, and SmoothPower2crop includes

this double cropping and an estimate of less expensive power due to upstream production sold to Sudan. The modest increases in irrigation benefits for these flows, particularly in scenarios of high irrigation profitability, illustrate Sudan's limitation due to the constraints in the model representative of the 1959 agreement. The second constraint guarantees at least three times more water passing Merowe downstream into Egypt that it does allow for irrigation at upstream schemes, thereby forcing Sudan toward a hydropower path and limiting its irrigation potential (see Irrigation constraints Section 2.2.2.1.3, Equation 2.7).

To test for the restrictive nature of the 1959 agreement in our simulations, we have included two additional runs that remove the second constraint of the 1959 agreement (Smooth2cropNA and SmoothPower2cropNA) but maintain Sudan's long term average water use at 14.5 bcm. SmoothPower2cropNA includes the reduction in power price due to upstream control and the removal of the second 1959 constraint. Both runs show a significant increase in irrigation benefits for cases P1 – P3 (Figure 2.9).

2.4. Conclusions:

This dissertation introduces a hydroeconomic model for Sudan (SHOM) that considers hydropower and irrigation benefits under conditions of existing infrastructure and practices. SHOM includes a nonlinear multiobjective optimization routine that allows us to study interactions between component objectives under a range of flow scenarios and valuation of agricultural returns. A number of our modeling results confirm or complement previous hydro-economic analyses—for example, the fact that upstream regulation can provide benefits to downstream riparians. Ajoon et al. (2014), for example,

shows that including the GERD in a SDDP hydroeconomic model resulted in an increase in hydropower generation in Sudan and Egypt. Other results are intuitive, such as the fact that under reduced flows there is a decline in hydropower and irrigation benefits. However, even in this simple sensitivity test the model returns some non-obvious results. While one might expect that smoothing the Blue Nile hydrograph through upstream regulation would inevitably lead to increased irrigation withdrawals, we find that doing so is only beneficial under select combinations of marginal values of water and if the upstream facility results in a drop in the price of electricity in Sudan. Otherwise the optimal development path is to increase hydropower production.

Another interesting result is the restrictive nature of the downstream flow constraint. The more that economic considerations (lowering of power prices and changes in agricultural practices) push Sudan towards irrigation, the more expensive these constraints—i.e., the restrictions imposed by a water sharing agreement—become to the country. The current requirement to deliver adequate flows to Egypt is not a severe constraint as long as agriculture is economically inefficient, irrigation is hampered by siltation and seasonal flow variability, and hydropower is an economic driver to send water downstream. But if these realities are shifted by an upstream facility that regulates flow, reduces sediment load, and provides inexpensive electricity, the treaty-enforced cap on water use will quickly become a constraint on Sudan's optimal hydro-development options.

The modeling results presented in this study contribute to current understanding of Nile hydroeconomics by presenting a focused analysis of Sudanese options, performed with a multiobjective optimization model capable of capturing nonlinear interactions.

There are, however, a number of important limitations that need to be addressed in future model development. First, the model does not include knowledge of current dam operating procedures or of stage-volume relationships for proposed dams (GERD) or for existing dams in recent years. Second, the model does not include the effects of siltation. A dam that controls siltation would affect the objective function by easing dam operation and significantly reducing dredging costs for canals that feed irrigation schemes. At the same time, reduced silt load would increase the need for fertilizer in downstream agricultural lands that currently benefit from natural nutrient input from silt-laden waters. Third, limitations in current agricultural and economic data make it difficult to estimate total agricultural benefits, so the marginal value of agricultural water essentially functions as a tuning parameter in SHOM that allows us to study general sensitivity to the value of agriculture. This could certainly be improved with access to more reliable and recent agricultural data, though the perceived value of agriculture and the support of this value through land and economic policies are always difficult to quantify.

The scope of SHOM is also a matter of ongoing evaluation. In focusing on hydropower and irrigation we adopt the framework of many earlier hydro-economic optimization models in the Nile and elsewhere. We recognize, however, that climate change and river development can have a broad range of impacts, many of which are difficult to quantify. These include ecological impacts, effects on fisheries, and burden placed on particular populations living within the basin. These important considerations must be accounted for in any application of hydroeconomic analysis to development decision making, and it would be valuable to find ways to broaden Nile basin hydroeconomic models to include a more diverse array of processes and outcome

variables. Lastly, we recognize that our use of a deterministic model presents a highly idealized scenario of a decision maker with perfect foresight. Deterministic models do not account for the uncertainties in some of the input parameters, therefore the results and decisions presented in this chapter will produce benefits that are higher than any real world scenario.

Future operation of SHOM may be within a value of information framework that aims to assess operational seasonal forecasts. A more in-depth study of the value of information of seasonal forecasts will require the conversion of SHOM from a deterministic model to a stochastic model in order to adjust to the stochastic nature of forecasts. In addition, we would add that our analysis was performed for a portion of the Blue Nile as well as the downstream main Nile stem within Sudan. Future development of the model should incorporate other major tributaries such as the White Nile and the Atbara. Inclusion of other Nile tributaries and their infrastructure in the model will present a more holistic approach to analyzing Sudan's water resources decision making.

The Nile River is a finite water resource shared by a number of emerging economies, and the long-standing tensions regarding its equitable use are only increasing as demand for food, water, and electricity rise across the region. On account of both history (i.e., the 1959 Nile Waters Agreement) and geography, the Republic of Sudan is a particularly critical player in determining the future of Nile development and related hydroeconomic development decisions in neighboring countries. The effect of climate change and upstream development, in turn, will be critically important in determining Sudan's long term optimal development path and associated policy decisions. Here we present a first analysis targeted specifically at Sudan's optimal irrigation and hydropower

development options under scenarios of changing Nile flows and upstream development. Results reinforce the understanding that Sudan has the potential to weigh in heavily on matters of regional water and food security depending on how it chooses to make use of the Blue Nile and main stem Nile as it flows through its territory. Further research is required to understand how these choices are affected by additional development, trade, and policy decisions within the basin, and how Sudan's own infrastructure and agricultural practices might evolve to optimize returns under evolving climatic and economic conditions.

3. Understanding and enhancing dynamical seasonal predictions through objective regionalization

Abstract

Improving seasonal forecasts in East Africa has great implications for food security and water resources planning in the region. Dynamically-based seasonal forecast systems have much to contribute to this effort, as they have demonstrated ability to represent and, to some extent, predict large scale atmospheric dynamics that drive interannual rainfall variability in East Africa. However, these global models often exhibit spatial biases in their placement of rainfall and rainfall anomalies within the region, which limits their direct applicability to forecast-based decision making. This dissertation introduces a method that uses objective climate regionalization to improve the utility of dynamically-based forecast system predictions for East Africa. By breaking up the study area into regions that are homogenous in interannual precipitation variability we show that models sometimes capture drivers of variability but misplace precipitation anomalies. These errors are evident in the pattern of homogenous regions in forecast systems relative to observation, indicating that forecasts can more meaningfully be applied at the scale of the analogous homogeneous climate region than as a direct forecast of the local grid cell. This regionalization approach was tested during the summer rain (July-August-September) months, and results show an improvement in the Max Plank Institute for Meteorology's Atmosphere-ocean General Circulation Model (AGCM) version 4.5 (ECHAM4.5) predictions for applicable areas of East Africa for the two test cases presented.

3.1. Introduction

East Africa (EA) is notoriously vulnerable to hydro-climatic extremes. Severe drought in the early 1980's affected large swaths of EA, resulting in crop failures that led to large migrations and widespread starvation. An estimated 16 million people were affected in Ethiopia and Sudan alone (Olsson 1993, FAO 2000). More recently, from 2011-2012 drought exacerbated food insecurity and left 8.8 million people in need of urgent humanitarian assistance. An estimated $1.3 billion was requested for a humanitarian response (UN-OCHR 2011). This drought affected multiple sectors, from agriculture and livestock to health and hygiene, and led to multiple countries declaring this drought a national disaster (UN-OCHR 2011). The occurrence of multiple hydro-climatic extremes that have impacted the lives of many within EA highlights the importance of understanding and improving seasonal forecasting in the region.

The generation of reliable forecasts at seasonal time scales has, however, proven to be a complex and elusive problem. In general, seasonal forecasts have presented a significant challenge relative to shorter term weather forecasts. Over the past 30 years, weather forecast skill has improved dramatically, in large part due to improved estimates of initial atmospheric conditions provided by satellite-derived observations and enhanced *in situ* observations (Goddard et al. 2001). Predictions on longer time scales (i.e., seasonal and interannual climate) do not benefit from these improved observations of initial atmospheric conditions, as the memory of the atmosphere is not adequate to inform forecasts beyond one or two weeks. Instead, dynamical forecasts on these longer time horizon forecasts rely on the initial state of climate system components that have longer

memory (e.g., sea surface temperature, and soil and vegetation conditions on land) and on realistic simulation of gradually evolving atmospheric circulations and surface states. Seasonal forecasts have improved, at least in some regions across the globe, as observations of these memory components of the climate system have improved and as forecast systems have gone to higher resolution, more complete physics, and more advanced data assimilation algorithms (Goddard et. al 2001). In EA, however, the forecasting challenge is particularly acute on account of complex synoptic and mesoscale conditions, non-linear interactions between large scale climate modes, and sub-seasonal variability in teleconnections and precipitation processes (Nicholson 2000).

The evaluation of seasonal forecast skill is a challenge in its own right. The seasonal forecasting community utilizes several methods of skill scores in order to gauge the accuracy of these different methods (Goddard et al. 2001). Model skill is determined by a retrospective model evaluation, where model results are compared with observational data. Due to inherent biases and errors within the dynamical models there is a need for statistical processing of model outputs. One method for rectifying systematic model errors is to represent the forecast outputs as a percentage of ensemble forecasts that lie within an assigned category. Traditionally, these categorical forecast outputs are evaluated using categorical evaluation metrics such as Rank Probability Skill Score (RPSS), Likelihood Skill Score (LSS) and Generalized Relative Operating Characteristics (GROC) (Barnston 2010).

A second important decision in forecast evaluation, but one that generally receives less attention, is the spatial basis applied when evaluating a model. Because dynamical forecasts produce gridded output, it is common practice to extract predictions

at a specific location from the closest model grid cell. A potentially more forgiving approach is to evaluate models at a coarse regional scale for a box or geographical unit of interest. These Grid-to-Grid (GtG) and box area averaging methods are currently being used by the climate forecasting community to form seasonal forecast predictions (Jury 2014, Batte and Deque, 2011, Barnston 2010).

Both the GtG and box area averaging however, do not adequately account for spatial biases. GtG unduly penalizes the model for small spatial inaccuracies even when the overall forecast anomalies are correct. General area averaging implicitly assumes spatial matching between model and observations and also can introduce error by combining regions that have different responses to large scale drivers. Several researchers are attempting to address this issue. Koster et al. (2008), for example, apply observed spatial correlation structures to translate model-generated forecasts skill from locations of high skill to locations of low skill. This transformation approach is shown to improve forecast accuracy.

Other research in precipitation prediction has illustrated the importance of isolating regions of similar variance through objective regionalization techniques in order to adequately describe the nature of large scale influence on the area of interest (Nicholson and Dezfuli 2013, and Dezfuli and Nicholson 2013). This method of regionalization divides areas into smaller homogenous regions based on the variance of a particular variable. Chamberlin and Phillippon (2001) use principle components analysis (PCA) in order to analyze the regional and seasonal structure of their interannual precipitation variability across EA. Performing a PCA allowed the region to be divided into two subregions with contrasting variability: Ethiopia to the northwest and Uganda-

Kenya to the south east. More recent studies have also attempt to separate EA into different areas before performing seasonal predictions. Nicholson (2014), shows two relatively distinct areas within EA by delineating based on the seasonal cycle of precipitation. The first region has rainfall peaking in the summer months and covers Sudan and north-west Ethiopia while the "equatorial" region covers the horn of Africa region and has its peak rainfall in March-April-May (MAM), and in October-November-December (OND).

3.1.1. Dynamics of the East African Summer Rains

Local topography, regional winds and large-scale drivers greatly influence precipitation variability in EA. Many studies have presented in-depth analyses of the various mechanisms that drive variability, often with the intention of improving predictability (Conway 2000, Chamberlin and Phillippon 2001, Gissila et al. 2004, Segele and Lamb 2005, Block and Rajagopalan 2007 and Diro et al. 2011). Berhane et al. (2014) performed a broad study of the various teleconnections that influence Ethiopian highland precipitation during the summer months. They found that teleconnection strength of various large scale drivers varies during the June-July-August-September rainy season, with the latter months generally showing stronger associations with large scale modes of variability in the Pacific and Indian Oceans. In the early rainy season teleconnections are generally weaker, but there is a tendency towards associations with variability to the west, including the Atlantic Ocean, rather than the Pacific and Indian Oceans to the east.

This lack of large-scale driver consistency in precipitation throughout the rainy season

presents challenges of physical process and timing of influence to dynamical model predictions. The influence of multiple mechanisms within a similar area adds to the complexity of accurately predicting seasonal precipitation using dynamical models. Global dynamics related pressure systems in the Atlantic, Mediterranean, and the Pacific, propagating waves associated with the subseasonal Madden-Julien Oscillation (MJO), and mesoscale winds responding to both remote and local variability have all been shown to influence precipitation (e.g., Nicholson 1996, Berhane 2015). The inability to properly capture one or more of these processes can lead to inaccurate prediction in the amount and location of seasonal precipitation.

In this study, we examine the performance of global dynamically-based seasonal forecast systems in EA. In contrast to other studies, we begin with an objective regionalization of EA based on interannual precipitation variability (the primary target of seasonal forecasts) for each month of the rainy season. The regionalization is performed on observations and, independently, on each forecast system. The purposes of this study are: (1) to distinguish regions that have distinct patterns of variability (presumably, differing sensitivities to large scale climate modes), and (2) to identify systematic differences between the regionalization of observation and models, which would indicate the presence of spatial biases in the modeling systems. Once these biases are identified it is possible to adjust for them through evaluation based on analogous region matching (ARM) in place of standard spatial match assumption (SMA) methods like grid-to-grid or box averaging. In adjusting for spatial biases, the ARM method evaluates models on the basis of their own spatial structures of variability providing the possibility of drawing useful predictions even from a model with significant spatial biases.

3.2. Methods

3.2.1. Data and Models

The extent of the analysis region spans from 25^0N to 12^0S and 20^0E to 54^0E. Observed precipitation data used in this analysis was from version 2 of the Climate Hazards Infra-Red Precipitation with Station data (CHIRPS) at 0.05 x 0.05 degree resolution, for the period from 1981 to 2010 (Funk et al. 2015). Observed SST anomalies used to identify teleconnections were extracted from the Kaplan Extended SST version 2 dataset, which is produced at 5 x 5 degree resolution (Reynolds et al. 1994, Parker et al. 1994, Kaplan et al. 1998). These data were obtained from the NOAA/OAR/ESRL PSD, Boulder Colorado USA (http://www.esri.noaa.gov/psd/).

Two models were used in this analysis: the Coupled Forecasting System version 2 (CFSv2) and the Max Plank Institute for Meteorology's Atmosphere-ocean General Circulation Model (AGCM) version 4.5 (ECHAM4.5). Both precipitation and SST model data were extracted from the National Multi Model Ensemble (NMME) hindcast monthly dataset (Kirtman et. al 2014) distributed via the International Research Institute (IRI) data library. Data were available at 1 x 1 resolution for the period from 1982 to 2010. CFSv2 was initialized 24 times to produce 24 different realizations for each separate month, while ECHAM4.5 was initialized 12 times, producing 12 realizations. These two models were selected from NMME simply as examples for the regionalization method; there was no *a priori* reason for choosing these models over others, though both are leading forecast systems that have been applied in previous studies of the region (Jury, 2014).

3.2.2. Regionalization

Regionalization is the division of a large area into smaller regions based on the characteristics of a specific variable or set of variables. The basis of any objective regionalization is a statistical clustering algorithm that defines regions on the basis of internal homogeneity and/or metrics of difference from other clusters. Numerous algorithms are in use for climate studies (Badr et al. 2015). In this application we apply Ward's Minimum Variance Method because of its widespread use and its tendency to generate regions with high internal homogeneity. The method clusters data points with variance lower than an allotted threshold value, and aggregates the points in order to maximize the correlation of the data set points within a designated region. Regions that are homogenous with respect to interannual precipitation variability are expected to be relatively uniform in their response to large scale variability and therefore serve as a good target for seasonal prediction. We apply Ward's Method using the Hierarchical Climate Regionalization (HiClimR) package for R (Badr et al., 2014) described in Badr et al. (2015) . HiClimR includes a range of agglomerative hierarchical clustering methods and provides pre- and post-processing tools relevant for climate applications.

For this application, preprocessing was performed to mask noise and to focus the analysis on areas in which summertime is the primary rainy season. Some areas within the limits of the project area do not experience a rainy season in JAS, but rather have a biannual rainy season in March-April-May (MAM), and in October-November-December (OND). These grid cells were masked because JAS precipitation is not of primary importance for seasonal forecasts in these areas.

Pre-processing was performed in four steps: First, in order to analyze precipitation trends in the JAS season, only data points that experience a significant increase in precipitation for those months were selected for regionalization. Points that registered a more than 7% increase in the monthly average precipitation for the months of JAS relative to all other months were used. This 7% threshold value is subjective; a 10% increase masks large parts of the EA region, while a 5% increase retains data points in locations where the MAM and OND rains dominate.

Second, any data points in the desert within the project area that receive less than 200 mm of rainfall annually were discarded. This is done to prevent an anomalous rainfall event from affecting the regionalization process. Third, the spatial resolution of the CHIRPS dataset was reduced from 0.05 x 0.05 degrees to 1 x 1 degrees to be consistent with the resolution of the seasonal forecasting models used in this analysis. This reduction also reduces the noise level within the observational dataset. Fourth, principal component analysis was applied to remove noise from the dataset. The first three principal components were retained. These four steps improved the homogeneity of the regionalization and made the regions created more statistically robust.

We note that regionalization for both observations and models was performed on a relatively short 28 year record (1982-2010). To ensure that regionalization results were not dominated by outliers (which could be error in the observed data) we performed regionalization 28 times, leaving one year out in each iteration. This leave-one out repetition had little impact on forecast system regionalization, which was relatively smooth and consistent, but we did see variability in the CHIRPS-based regionalization.

For the final regionalization we combine all 28 regionalizations and assign each grid cell to its most frequently assigned region.

3.2.3. Spatial Match Assumption (SMA) Evaluation

For the first evaluation, we adopt the standard practice of evaluating model performance without adjusting for spatial model biases. This standard approach makes a spatial match assumption (SMA)—that each grid cell in the model should predict the collocated grid cell in observation (GtG). Since we are interested in evaluating regional averages, we apply this SMA method at the scale of CHIRPS regions: both observed and forecast precipitation are aggregated using the CHIRPS regions, and model skill is assessed on this scale.

3.2.4. Analogous Region Matching (ARM) Evaluation

For our second method of evaluation we relax the spatial match assumption by evaluating forecast predictions on the basis of their own regionalization rather than the CHIRPS regionalization. The motivation for this approach is the recognition that GtG differences between observed and model regions are partially due to erroneous placement of climate phenomenon captured by the model. Often, the model will capture the predictive phenomenon of interest but misplace the precipitation anomaly, in which case regionalization reveals the spatial bias of the model and can serve as a basis for making predictions based on the relevant similarities between model and observation.

3.2.5. Model Skill Assessment

The model's predictions for each year in the 1982-2010 hindcast archive are ranked and placed into terciles. For each year, the fraction of model realizations that falls within the lowest third of all realizations in the full study period are denoted as the probability of a 'Below Normal' forecast. Similarly, the fraction of forecasts that fall within the second and third terciles are placed in the 'Normal' and 'Above Normal' terciles respectively. For example, each month's prediction in ECHAM4.5 consists of 12 realizations. Each of these realizations is ranked against the full population of 336 realizations for the study period (12 realizations for the remaining 28 years). The fraction of the 12 realizations that fall within the first third of the ranked realizations (have values in the range of the driest 112 realizations) becomes the probability of a "Below Average" forecast. Forecasts are demarcated into terciles of below average, average and above average probability forecasts to represent the fraction of realizations that fall within the dry, middle, and wet thirds of total ranked realizations respectively. Each year's forecast tercile probabilities are calculated using both the SMA and the ARM evaluation methods. We assess both methods by comparing their respective forecasts to observations. For this we utilize the Rank Probability Score (RPS) for category forecasts.

3.2.6. Rank Probability score (RPS)

RPS assigns a squared error based on the accuracy of the forecast. The value of the RPS depends on the value of forecast and whether the observation occurs at the category (Equation 3.1; Wilks 2011). F_i denotes the forecast probability, Ob_i denotes the probability of the observation, n is the category (1, 2 or 3) and I is the total number of

categories. Ob_i can either be 0 or 1, thus an event either occurs or doesn't in that category. A high RPS indicates a forecast of low accuracy.

$$RPS = \sum_{n=1}^{I} (\sum_{i=1}^{n} F_i - \sum_{i=1}^{n} Ob_i)^2 \quad (3.1)$$

The RPS depends on proximity of the forecast probabilities to the actual observation. A forecast with a high probability two categories away from the observation will have a lower RPS than a forecast with a high probability one category away. Therefore, a forecast can perform worse than a scenario with no prior information (a climatological forecast with no prior information will assign a probability of 0.333 across all terciles (Barnston 2010)).

Comparison of the forecasts to a scenario containing no prior information can be determined by the Rank Probability Skill Score (RPSS). The RPSS depends on the average RPS over all the forecasting years (RPS_{av}), and the average RPS with no prior information (RPS_{clim}).

$$RPSS = 1 - \frac{RPS_{ave}}{RPS_{c\lim}} \quad (3.2)$$

The RPSS varies from negative values to 1, with 1 being a perfect forecast, and a negative value indicating that the climatological forecast RPS_{clim} outperforms RPS_{av}.

3.3. Results and Discussion

3.3.1. Regionalization

Climate regionalization algorithms provide objective metrics that serve as a basis for dividing a large region of interest into coherent subregions. The final decision on the

optimal number of regions, however, is context dependent: there is a tradeoff between increasing intra-regional homogeneity (which we want to maximize) but increasing inter-regional correlation (which we want to minimize) as one moves from defining a few small regions to defining highly granular regions. This tradeoff is evident in the dendrograms shown in Figure 3.1A-C: as one moves from top to bottom on the dendrogram the homogeneity of regions increases but the correlation between regions also increases. For the purposes of this study we are interested in relatively large regions that have low inter-regional correlation and are therefore likely to represent differing sensitivities to large scale climate variability on a scale that GCM-based forecast systems are likely to resolve. Figure 3.1 shows the application of regionalization to CFSv2. Applying a threshold value that provides an acceptable balance between intra- and inter-regional correlation yields the maps shown in Figure 3.1D-F, with three regions in July and two regions in August and September.

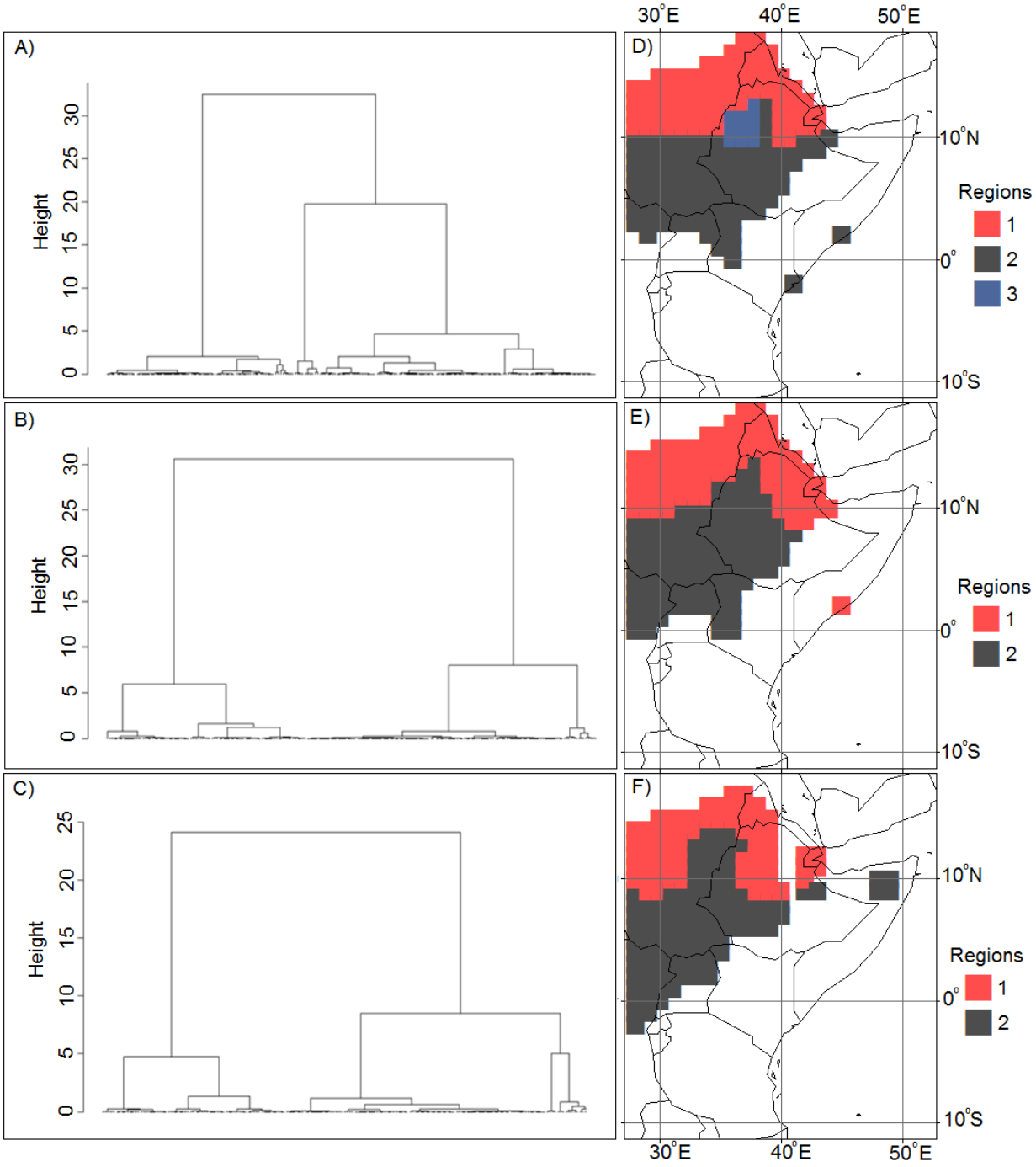

Figure 3.1: (A-C): CFSv2 regionalization dendograms for (A) July, (B) August, and (C) September; (D-F): Homogenous regions created using CFSv2 precipitation forecasts for (D) July, (E) August, and (F) and September.

Figure 3.2 shows the same regionalization process applied to ECHAM4.5.

Differences between CFSv2 and ECHAM4.5 are immediately visible: for ECHAM4.5 the

regionalization statistics point to three distinct regions in July, August, and September. The spatial pattern of these regions is quite distinct from CFSv2 regions, as ECHAM4.5 tends towards an East vs. West division in the southern portion of the regionalized area (ECHAM4.5 region 2 vs. region 3), which is not evident in CFSv2. The extent of the ECHAM4.5 regions are also quite different from CFSv2, in large part because ECHAM4.5 puts more rain in the eastern Horn of Africa than CFSv2 does in this season, such that ECHAM4.5 passes our precipitation threshold tests.

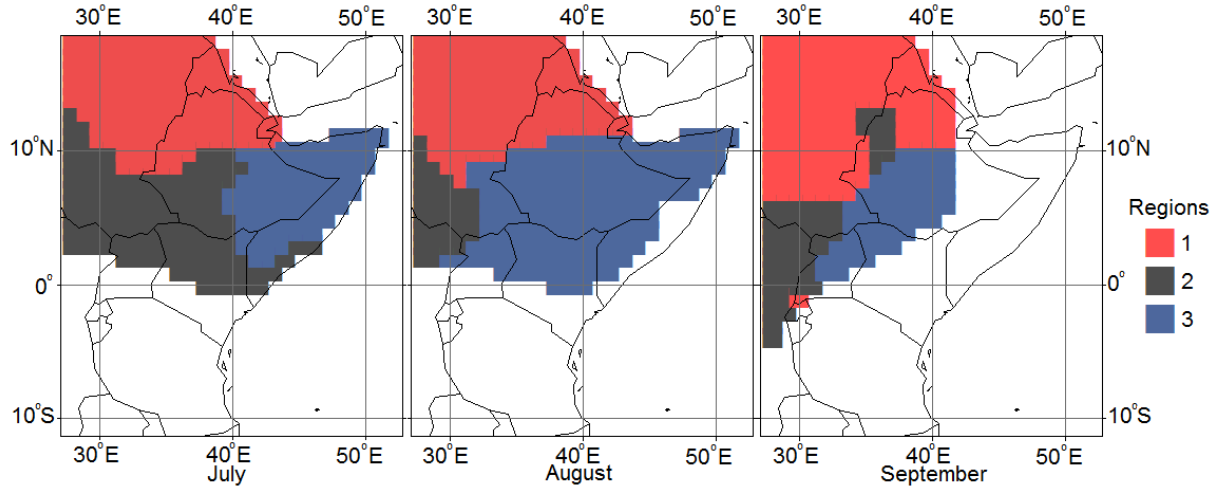

Figure 3.2: Regions created using ECHAM4.5 Forecasts

Regionalization based on CHIRPS precipitation observations shows more noise than the model-based regionalizations (Figure 3.3). This is to be expected, since models typically smooth variability. But the magnitude of spatial heterogeneity seen in the CHIRPS regionalization is quite high (especially in August), indicative of the highly localized variability and/or challenge in measurement known to exist in the East African highlands. Nevertheless, the regions do generally divide into a northern region (Region 1) and a southeastern region (Region 3), with a third region that moves between months, but lies in the southwest in August and September (Region 2).

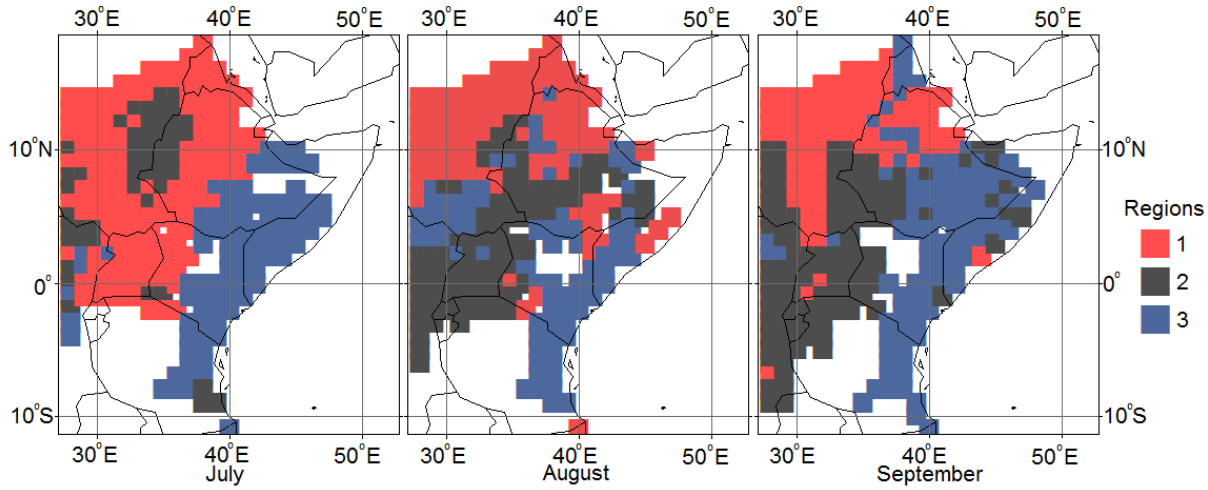

Figure 3.3: Regions created using CHIRPS observed precipitation

Table 3.1 provides a statistical summary of all regions shown in Figures 3.1-3.3 in terms of intraregional correlation and inter-regional correlation. These statistics demonstrate the tradeoffs inherent in picking regions. For example, CFSv2 Region 1 and Region 2 show high interregional correlation in all months and could potentially be combined into a single region. Doing so, however, would result in a heterogeneous region that might include areas that have differing response to the large scale dynamics captured by the model. For all three datasets (CHIRPS, ECHAM4.5, and CFSv2) in all months the intraregional correlation for all regions exceeds the interregional correlation between any regions.

July	**CHIRPS**	**CFSv2**	**ECHAM4.5**
Inter	**Corr**	**Corr**	**Corr**
1&2	0.44	0.63	0.13
1&3	-0.33	-0.23	0.27
2&3	0.12	-0.60	0.20
Intra	**CHIRPS**	**CFSv2**	**ECHAM4.5**
1	0.65	0.84	0.67
2	0.50	0.90	0.87
3	0.57	0.79	0.84
August	**CHIRPS**	**CFSv2**	**ECHAM4.5**
Inter	**Corr**	**Corr**	**Corr**
1&2	0.35	0.66	-0.32
1&3	0.23		0.07
2&3	0.10		-0.16
Intra	**CHIRPS**	**CFSv2**	**ECHAM4.5**
1	0.59	0.88	0.86
2	0.42	0.87	0.89
3	0.63		0.79
September	**CHIRPS**	**CFSv2**	**ECHAM4.5**
Inter	**Corr**	**Corr**	**Corr**
1&2	0.12	0.67	0.23
1&3	0.19		0.00
2&3	0.05		-0.13
Intra	**CHIRPS**	**CFSv2**	**ECHAM4.5**
1	0.52	0.86	0.65
2	0.47	0.88	0.84
3	0.45		0.93

Table 3.1: Inter-regional and intra-regional correlations for all the regions in Figures 3.1-3.3.

Regionalization applied to CFSv2 and ECHAM4.5 (see Figure 3.2 and 3.3) yields three regions for both models in the month of July. In August and September ECHAM has three separable regions while CFSv2 has only two. Correlations within regions and

between regions show large intraregional correlations and low interregional correlation for ECHAM4.5, consistent with homogenous regions (Table 3.1).

3.3.2. SMA and ARM

SMA model evaluation is consistent with commonly used evaluation and application techniques. It is simpler than ARM to implement, as it does not require that each model be regionalized, and easier to explain. For these reasons SMA is a preferable approach provided that model and observation show reasonably similar spatial patterns of variability.

To determine when this condition applies, we calculate correlations between the CHIRPS mean time series for each CHIRPS-defined region in each month and the CFSv2 and ECHAM4.5 mean time series for each region defined for those models (Table 3.2). These values can then be compared against the region maps presented in Figures 3.1-3.3. Whenever there is significant correlation between regions in Table 3.2 that are associated with geographically similar areas in Figures 3.1-3.3 we conclude that SMA is a reasonable approach for evaluating model performance in that region. For example, the August CHIRPS Region 1 (Figure 3.3) is spatially similar to August CFSv2 Region 1 (Figure 3.1), and the two show statistically significant correlation, so we conclude that SMA is adequate for evaluating CFSv2 in CHIRPS Region 1 for that month—CFSv2 is properly localizing the drivers of precipitation variability. Unfortunately, this approach is not satisfied in all scenarios. For example, there is extremely high correlation between July CHIRPS Region 1 and July ECHAM4.5 Region 3 (0.65), but the two have almost no spatial overlap (Figure 3.4). Less than 5% of CHIRPS region 1 overlaps with ECHAM4.5

Region 3. August is similar, with less than 26% of CHIRPS region 1 falling within ECHAM4.5 region 3.

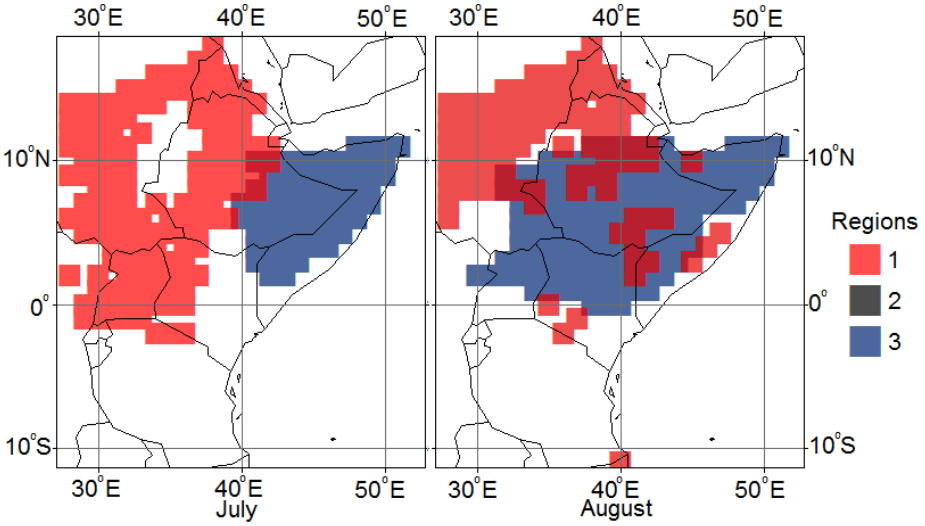

Figure 3.4: Location of ECHAM4.5's Region 3 (blue) that is used to predict observed CHIRPS Region 1 (red) for July and August.

		CFSv2			ECHAM4.5		
Month	CHIRPS	Reg1	Reg2	Reg3	Reg1	Reg2	Reg3
JULY	Reg1	**0.38**	**0.38**	-0.39	0.00	**0.38**	**0.65**
	Reg2	0.22	0.03	0.03	0.18	0.09	0.11
	Reg3	0.07	0.13	0.05	0.01	0.13	0.20
August	Reg1	**0.39**	0.18		-0.27	-0.25	**0.35**
	Reg2	0.24	0.25		0.13	-0.01	0.33
	Reg3	0.27	0.16		-0.10	-0.25	0.13
September	Reg1	**0.41**	0.13		-0.07	-0.31	0.09
	Reg2	0.26	0.28		-0.28	-0.33	0.11
	Reg3	0.19	0.15		0.10	0.05	0.15

Table 3.2: Correlations of the time series for each of the CHIRPS regions with the CFSv2 and ECHAM4.5 regions. Bold values show correlations at the 90% significance threshold.

These correlations between spatially mismatched regions suggest that ECHAM4.5 does capture a large scale driver of precipitation variability for East Africa, but that the model does not localize this phenomenon in the correct area within East Africa. For these

situations SMA is not an appropriate approach for model evaluation or application, as it fails to recognize potential value in the forecast—the correlation between CHIRPS Region 1 and ECHAM4.5 Region 3 would be entirely lost. To capture this phenomenon, we apply ARM for any case where there is less than a third (33.3%) overlap between the most highly correlated CHIRPS and model regions.

	CHIRPS Regions		
CFSv2	**Reg1**	**Reg2**	**Reg3**
July	SMA	None	None
August	SMA	None	None
September	SMA	None	None
ECHAM4.5	**Reg1**	**Reg2**	**Reg3**
July	ARM	None	None
August	ARM	None	None
September	None	None	None

Table 3.3: Prediction Method for the CHIRPS regions using CFSv2 and ECHAM4.5.

Table 3.3 shows the result of this analysis for both models in all months. There are some regions for which models fail to show significant correlation with observations regardless of whether SMA or ARM is applied. For several other combinations, however, ARM identifies significant correlations where SMA does not, suggesting that applying the ARM method could produce skillful predictions for areas where traditional SMA approaches fail to identify any significant predictive skill. Indeed, for ECHAM4.5 we find that ARM is the only way to identify significant correlations with observations at our scale of analysis.

Comparing the RPS_{av} for ARM to that of SMA, the ARM RPS_{av} is lower for both July and August (Table 3.4). A list of all the RPS for each month using both ARM and SMA is presented in Appendix B. ARM outperforms SMA in 17 of the 29 years and 23

of the 29 years in predicting the month of July and August, respectively, when using the ECHAM4.5 forecast. The differences between yearly RPS values for ARM and SMA are marginally statistically significant for July (pairwise two-tailed t-test $p = 0.08$) and highly significant for August ($p = 0.003$). RPSS values also show the value of ARM relative to SMA for these months (Table 3.4). Indeed, the RPSS for SMA shows negative values for both months, indicating a lower forecasting performance than having no prior information.

	Average RPS		RPSS		
	SMA	ARM	SMA	ARM	NS
July	0.49	0.36	-0.09	0.20	18
Aug	0.59	0.33	-0.28	0.28	23

Table 3.4: Shows the average RPS for ARM and SMA. Number of Successes (NS) is the number of times ARM outperforms SMA over the 29-year time span of the analysis. See Appendix B for further illustration of the yearly model performance.

3.3.3. Large-scale Drivers

Understanding the improved performance of the ARM requires an understanding of the dynamics at play within the region. Correlations of observed CHIRPS precipitation for August region 1 with observed SSTs (Figure 3.5A) show a strong anti-correlation with the central tropical Pacific Ocean, in addition to a positive correlation in the western pacific over the maritime continent. In a broad sense these patterns are consistent in the maps of ECHAM4.5 SSTs correlation with ECHAM4.5 precipitation using both SMA (Figure 5B) and ARM (Figures 3.5C). However, there is much greater similarity between observation (Figure 3.5A) and ARM (Figure 3.5C) correlation maps than there is between observation and SMA (Figure 3.5B). This is particularly clear in the Indian Ocean, where ARM captures the positive correlation between precipitation and SSTs in the Indian

ocean off the coast of south east India, while SMA does not. Figure 3.5B also shows a large anti-correlation with Mediterranean SSTs, which directly opposes the relationship with observed SST's. ARM shows no significant correlations at the 90% significance threshold, but correlations in the Eastern Mediterranean are positive, matching the general tendency of observation (not shown). These correlation patterns are also consistent with CFSv2 using SMA (Figure 3.5D), further illustrating the spatial bias within ECHAM4.5 and the need for spatial correction within ECHAM4.5's precipitation outputs. These similarities in SST correlations show that ARM method in ECHAM4.5 more accurately captures large scale dynamics that influence precipitation within the observed Region 1.

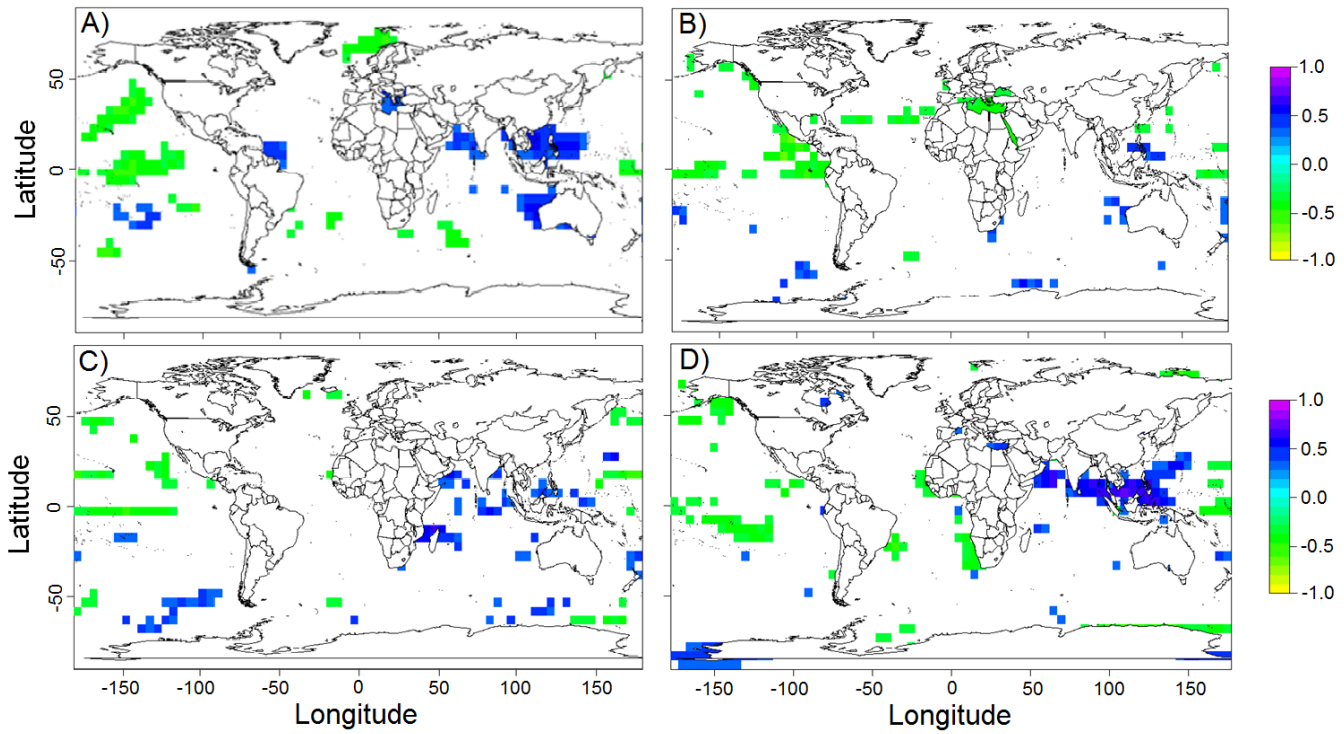

Figure 3.5: correlation of August precipitation with global gridded SST. All correlations are calculated as Spearman linear correlations and are masked at α=0.1. (A) Observed Region 1 CHIRPS precipitation correlation with observed SST; (B) ECHAM4.5 precipitation within observed Region 1 correlation with ECHAM4.5 SST (i.e., SMA

method); (C) ECHAM4.5 precipitation in ECHAM4.5 Region 3 with ECHAM4.5 SST (i.e., ARM approach for observed Region 1); (D) CFSv2 precipitation in CFSv2 Region 1 with CFSv2 SST (i.e., SMA approach).

The ARM result for ECHAM4.5 in August is reinforced if one looks at observed correlations between CHIRPS and SST when CHIRPS is averaged for ECHAM4.5 region 3 (i.e., the eastern Horn of Africa). These correlations are shown in Figure 3.6, and it is evident that there is no significant association between rainfall in this region and the tropical Pacific. The fact that ECHAM4.5 region 3 precipitation does show correlation with SST in the tropical Pacific is further evidence that the model has shifted the true teleconnection eastward within the Horn of Africa, resulting in correlations between the Eastern Horn and the Pacific that are in fact, more representative of northwest Ethiopia and Sudan—i.e., observed region 1.

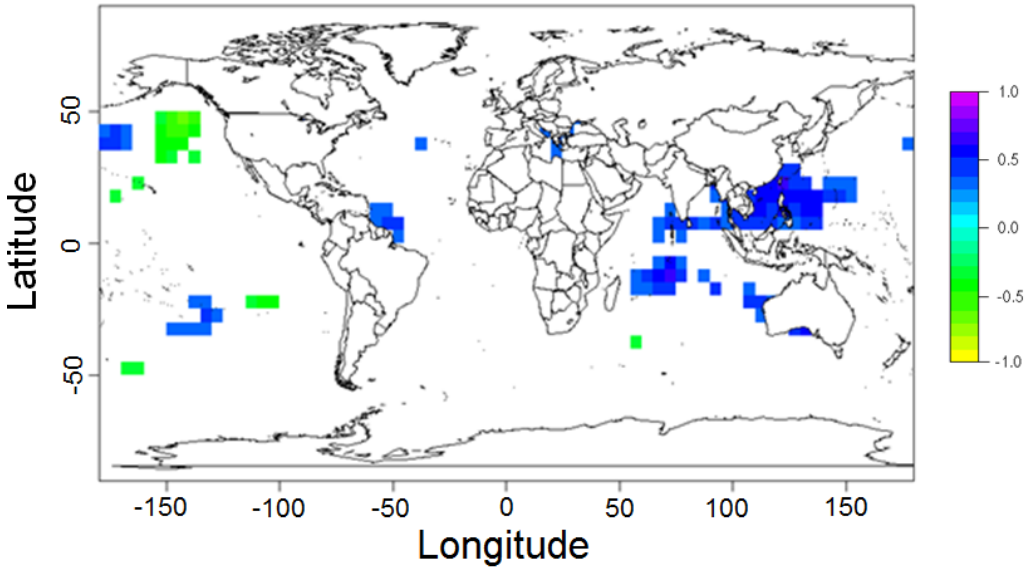

Figure 3.6: Correlation of August CHIRPS precipitation averaged over ECHAM4.5 Region 3 with observed SSTs.

3.4. Conclusions

Multiple studies have shown the challenging nature of seasonal precipitation prediction over EA. The region contains steep precipitation gradients, is topographically complex, and is influenced by different large scale climate dynamics in different seasons. Accurate seasonal forecast systems must capture the interplay of local, regional and global dynamics that determine the temporal variability and spatial placement of rain within the region. The motivation for this chapter is the recognition that dynamical forecast systems that capture large scale dynamics can still fail to place precipitation variability correctly within the region. This results in low skill scores when models are evaluated or applied on the basis of traditional methods, which effectively make a spatial matching assumption of zero spatial bias. When the evaluation or application of the forecast is mediated by an objective regionalization that identifies analogous regions in model and observation it is possible to extract meaningful information from a forecast system that would otherwise be discarded as unskillful.

We found that this approach can be quite important for summertime EA precipitation. Objective regionalization for each of the summer months shows that two commonly used dynamical forecast systems (ECHAM4.5 and CFSv2) regionalize quite differently from one another and also show distinct differences from regionalization based on observed precipitation. Differences between observation and model regions indicate spatial biases within the models. We address this through analogous region mapping (ARM), which corrects acknowledges and adjusts for spatial bias. When compared to evaluation based on a spatial match assumption (SMA), which is similar to the traditional grid to grid approach, we find cases where ARM allows for significant

improvement. This was most clear for ECHAM4.5; at the peak of the summer rainy season, the ARM method shows an improvement of the RPSS skill score from -0.09 to 0.20, and -0.28 to 0.28 for the months of July and August, respectively, for a region that includes portions of the Eastern Nile basin and parts of northern Ethiopia that are currently being affected by a significant El Nino associated drought.

The RPSS results as well as the correlation maps presented in this chapter show the ability of objective regionalization to improve the predictive utility of dynamic models. Ultimately, one would expect that analyses like these will contribute to continued model improvement to the point that spatial bias in dynamically-based seasonal forecast systems becomes negligible. That level of model performance, however, is far from the current reality. For the foreseeable future it will be necessary to apply spatial correction methods like the regionalization approach presented in this chapter in order to maximize the information contained in seasonal forecast systems.

4. Value versus Accuracy: application of seasonal forecasts to a hydroeconomic optimization model

Abstract:

The variable nature of precipitation in East Africa (EA) contributes to the climate vulnerability and food insecurity of the region. Seasonal forecasts have the potential to support resilience-building strategies, but only if they are reliable and relevant according to metrics that are meaningful for decision makers. Here, we assess the value of information (VOI) of candidate statistical and dynamical seasonal forecast models for the EA region using the Sudanese Hydroeconomic Optimization Model (SHOM) as an example of forecast-based management. SHOM combines hydrologic, agronomic and economic inputs to determine the optimal allocation of water between storage, hydropower, and irrigation to maximize economic benefits along the Sudanese Blue Nile. For each forecast model, we assess both the hydrological accuracy of the forecast in predicting Blue Nile flow and the VOI of the forecast when it is applied to drive SHOM. A rank of each model's forecasting skill score along and VOI relative to climatology is analyzed in order compare the performance of each forecast. Synthetic forecasts with idealized error characteristics are also analyzed to aid interpretation of model results. Results show that: (1) the relationship between forecast accuracy and VOI to SHOM is complex; (2) forecasts have the potential to add more value during dry periods than wet periods; and (3) forecasts that overestimate flows are particularly damaging to achieving high value of information in SHOM.

4.1. Introduction

Past research in the field of forecasting has improved seasonal prediction, particularly in vulnerable communities with success. Advancements in the understanding of the physics of precipitation, as well as the large-scale phenomenon that drives rainfall, has improved seasonal predictive accuracy. The need to adequately disseminate short term climate information to decision makers is vital. The Famine Early Warning Systems Network (FEWS) is an example of issued seasonal forecasts deployed internationally, providing climate diagnostics to multiple countries covering 3 continents. With the advent of climate change, and an exponential increase in population within the developing world, the need for accurate, timely seasonal forecasts will become more essential. It is therefore important to analyze and comprehend aspects of the seasonal forecast that are valued by the decision makers in order to improve the efficacy of the information provided. This chapter presents a modeling framework that aims to assess the value of information (VOI) provided by a suite of state of the art seasonal forecasts to water resources decision makers along the Sudanese Blue Nile.

4.1.1 Seasonal Climate Forecasts

There are two general approaches to seasonal forecasting currently employed by the climate community: statistical and dynamical. Statistical models capture and express dominant large-scale modes, and local variables that drive the intended response variable. Variable selection is usually done with some knowledge of the different prevailing weather and climate processes that influence precipitation within the region. Multiple statistical techniques have been used to forecast for seasonal precipitation. Within Africa

there are a myriad of statistical methods used to capture temperature and rainfall at synoptic scales. These time and regionally sensitive methods include linear parametric models (Diro et al. 2011, Nicholson 2014, Ntale et al. 2003, Korecha and Barnston 2007), as well as other complex non-linear machine learning and tree based methods (Mwale and Gan 2005, Badr et. al 2014). Comparison across models has also been conducted for various seasons within different parts of Africa. Badr et al. (2014) performed a comprehensive statistical analysis for the Sahel rainy season using a wide range of statistical models. Likewise, Mwale and Gan (2005), also make comparisons between models, their analysis included two model types: a Canonical Correlation Analysis model (CCA) and an Artificial Neural Network with a Genetic Algorithm (ANN_GA), predictive comparisons were made for the September-October-November (SON) rains in EA. Traditional statistical models have also been incorporated with other computing algorithms to improve predictions (Ntale et al., 2003) by optimizing the predictor selection and weighing process.

Other more process based methods exists. Dynamical models run with multiple realizations initialized under different conditions calculate predictions by resolving physically based equations that mimic the earth system. Most dynamical models are two-tiered coupled ocean atmosphere models forced by boundary layer conditions (Goddard et al. 2001, Barnston et al 2010). Performance of dynamical models is spatially restricted, within specific regions, the inability of models to resolve local topography contributes to prediction inaccuracies and spatial biases that need to be identified and addressed. For this, dynamical forecast outputs must undergo a post processing statistical correction of their climate diagnostics. Past studies have assessed dynamical model performance

globally (Goddard et al. 2001, Barnston et al 2010) and regionally (Batte and Deque 2011, Jury 2014). Some analysis integrated multiple models while taking the ensemble average (Weisheimer et al 2009, Doblas-Reyes et al. 2009, Bette and Deque 2011, Shukla et al. 2014) Use of the multimodel mean ensemble to derive predictions and assess the forecasting skill has shown to be more accurate that stand alone model predictions. Model comparison between different specific sets of dynamical models has been conducted in past research (Bette and Deque 2011, Satti 2016), however comparison between different types (statistical versus dynamical) of models is rare. This chapter will use the findings from one statistical model, and offer a comparison with the predictions of two dynamical models over the Blue Nile north of the Sudan-Ethiopian border. Results of the predictions will be used to determine the value of each forecast via a VOI study.

4.1.2 Hydroeconomic Models

Performing a VOI study on a forecast requires the integration of a forecast valuation model. Economic optimization models that integrate natural hydrologic, agronomic and economic inputs can utilize climate inputs and assign a value to the input information. Studies utilizing mutliobjective hydroeconomics address multiple large scale management and policy issues.

Hydroeconomic models apply the fundamentals of economics to water management, and view water as a commodity that can vary in value based on demand and quantity (Harou et al. 2009). This is a departure from traditional static, descriptive methods of water resources management and engineering models. Hydroeconomic optimization models are prescriptive, with economic return used to optimize water resources under various

strategies. Multiple hydroeconomic optimization approaches exist to tackle different management questions and basin characterizations. The nature of model inputs (stochastic versus deterministic) or modeling approach (dynamic versus static) influences the optimization algorithm used (Labadie). Guariso and Whittington (1987) use hydroeconomic optimization of agriculture and energy to assess regional transboundary issues of cooperation in future large scale planning. The objective function of such models focused primarily on two sectors, agriculture and hydropower production. Other studies focused not only regionally, but looked at incorporating the whole Nile basin. The Nile decision support tool constructed by the Georgia water resources institute does a basin-wide hydrological and hydraulic simulation along with reservoir optimization and scenario assessment (Yao and Gerogakakos 2003, Georgakakos 2007). More recent hydroeconomic studies have utilized more updated infrastructure in their studies (Goor et al. 2010, Arjoon 2014), such as the inclusion of the Grand Ethiopian Renaissance Dam (GERD) along the Sudan/Ethiopian border. Other studies have developed a framework that has looked at the stochastic nature of climate change on transboundary planning. Jeuland (2010) performed a holistic simulation incorporating a complex network that looked at various feedbacks integrating the fields of climate, hydrology and economics. Other studies are more regionally focused; the Investment Model for Planning and Ethiopian Nile Development (IMPEND) was created to assess hydropower and irrigation strategies along the Nile during transient periods of dam construction and filling (Block 2011). Other studies using IMPEND alter the model to include the stochastic nature of climate variables, allowing for a focus on changing climate, value of forecasting (Block 2011). Inclusion of these hydroeconomic models as assessment tools to gauge the value

of forecasts to a particular end user has featured in various VOI studies over the last 30 years.

4.1.3 Value of Information Studies

The need to properly assess the seasonal predictions is instrumental in understanding the value the forecasts provided to the end users. The applicability of seasonal forecasts in the decision making process underlines the importance of accurate forecasts. The assessment of forecasts within the climate community has been largely determined by the error attributed to the forecast predictions. This method of evaluation is prominently featured in multiple forecasting literature and is seen as an assessment of forecast quality (Katz and Murphy 1997). This approach, however removes the potential user from the assessment. Inclusion of the forecasts users in the assessment incorporates a specific decision makers utility. Historically forecasting frameworks that integrate seasonal forecasts with decision making models have been built to help assess the added value incurred by forecasting. A comparison of both complementary value and accuracy assessments within the same modeling framework is needed to better understand aspects of the forecast most beneficial to their end users.

Earlier studies that assess the value of a forecast traditionally use decision theory. Bayerlee and Anderson 1969 derive the maximum expected amount of profit in wheat production given changes in the distribution function of seasonal precipitation using Bayesian decision tree analysis. Multiple other VOI analysis also use Bayesian framework for model evaluation of agricultural production (Katz et al. 1982, Wilks and Murphy 1985, Mjelde et al 1988). Different studies focus on the forecast of specific

variables, such as precipitation, temperature, soil moisture etc. or a combination of different variables at multiple lead times. Majority of the economic value of forecasts studies undertaken over the last three decades feature mainly VOI studies in agriculture. Findings from various VOI studies outline the important characteristics of seasonal forecasts like the lag time, and the accuracy are highly dependent on the nature of the decisions being made (Mjede 1988, Meza et al. 2008). Some studies have shown that the ability of seasonal forecasts to capture extremes is very important in adding value to the forecast (Shafiee-Jood 2014), and this has implications in other sectors like biofuels and crop insurance. Past agricultural VOI studies have focused on more developed regions of the world (Mjede 1988, Petersen and Fraser 2001, etc.)The future of value forecast in agriculture lies in applying the most rigorous quantitative studies of both climate modeling and economic modeling to the most vulnerable developing communities. VOI studies have been featured in other sectors, studies in reservoir management and electricity production benefits from the forecasted information seasonal predictions have been undertaken. VOI studies specifically targeting dam operations have been conducted in multiple regions including, among others, the Columbia River basin (Hamlet et al. 2014), Northern California (Georgakakos 2012) and the Ethiopian Blue Nile (Block 2011), the region directly upstream of the SHOM analysis domain. In examining VOI of forecasts for the Blue Nile, Block (2011) used a stochastic implementation of IMPEND to assess the role of forecasting in hydropower operations. A range of forecasted flows were analyzed to determine the aspects of forecasts that decreased value to decision-makers. From the analysis Block (2011) was able to tailor a forecast that added value to Ethiopian Blue Nile hydropower operations. The VOI analysis presented in this chapter

addresses similar questions, with a focus on the downstream, Sudanese portion of the Blue Nile basin. Focusing on a downstream management region offers a different perspective on how forecasts might be used by decision makers as infrastructure changes within Sudan and upstream in Ethiopia.

4.2. Methodology

4.2.1 SHOM

The SHOM optimization (See Chapter 2 for model details) model is built using the General Algebraic Modeling System (GAMS) with the CONOPT nonlinear solver (Drud 1992). The purpose of SHOM is to evaluate the optimal allocation of water resources between hydropower and irrigation—the two dominant economic applications of Blue Nile flows—along the Sudanese Blue Nile in order to assess the effects of potential infrastructure developments, management strategies, and policy mandates on water resources and economic output of the river system. Though designed to address development in Sudan, SHOM does include the Ethiopian GERD on account of its tremendous anticipated impact on hydrology of the river system and electricity markets in the region. Hence, the model includes four major dams in total: the GERD, the Roseires and Sennar dams on the Sudanese Blue Nile, and the Merowe Dam on the main stem of the Nile in Sudan (Figure 4.1). Merowe is not formally located on the Blue Nile, but the majority of flows to Merowe come from the Blue Nile.

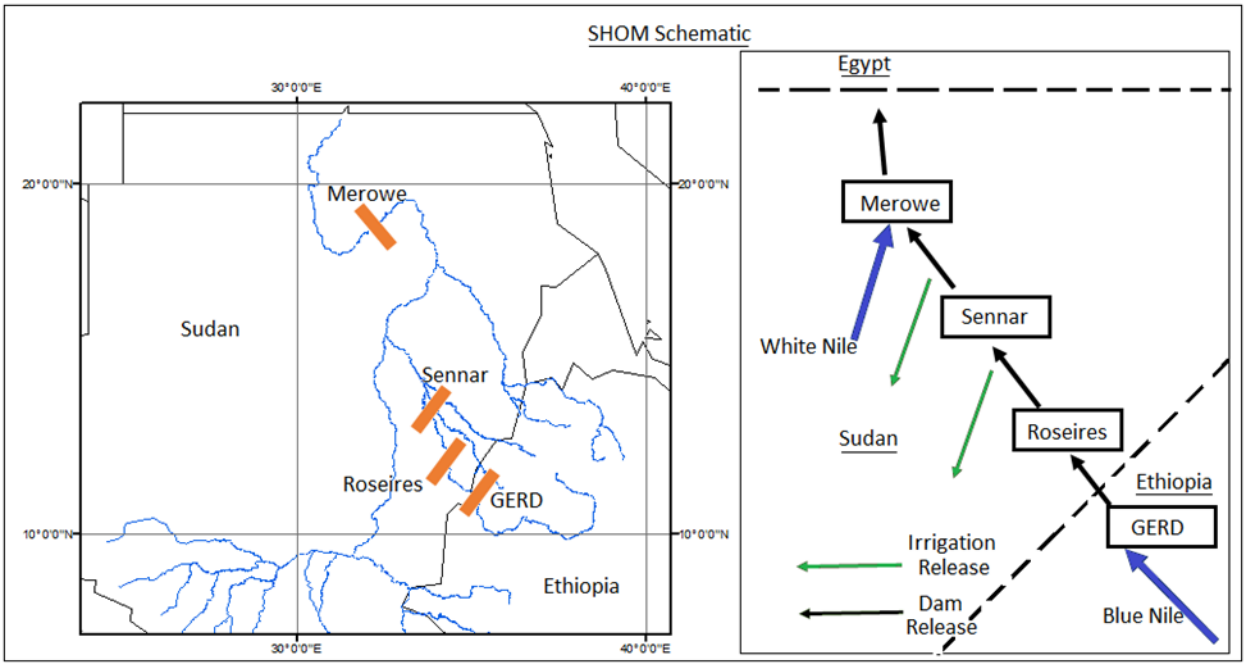

Figure 4.1: SHOM Schematic showing dam locations and releases that contribute to the Objective function.

The objective function of SHOM aims to maximize the economic value of hydropower and irrigation. This is done using agronomic and economic inputs, as well as river flows that feed into the model as upstream boundary conditions (see Satti et al 2015 for details). Originally, SHOM was implemented as a deterministic model that runs on monthly time-steps with continuous access to all input information. In other words, the model had perfect foresight when calculating the optimal decision variables. In order to adequately evaluate the performance of seasonal forecasts on decision-making, specific aspects of SHOM needed to be revised.

Four major revisions were made to SHOM in this chapter to allow for forecast evaluation and assessment (Appendix C). First, the deterministic nature of the model was altered to account for the stochastic nature of incoming upstream ensemble flow forecasts. Conversion of SHOM from a deterministic optimization model to an implicit stochastic model required looping and running multiple flow sequences.

Second, the model's access to information on future flow conditions was removed. This was done by adjusting the model to run on annual basis, blinded to future conditions, rather than allowing it to optimize for the entire simulation period at once.

Third, the continuity equations in SHOM that are representative of the state storage variable were adjusted. In order to account for the differences between decisions made under forecasted flows, the volume of water stored in reservoirs at each time step was updated by the difference between the forecasted flows and the actual flows. This means that the reservoir storage is increased or decreased to reflect the error in the forecast, which makes decision making under forecasted flows less than optimal. Additionally, a penalty function was administered when the difference between the forecasted and actual flows were larger than the size of the reservoir. This penalty is intended to indicate lost benefits due to error in the forecast leading to spill over (in the case of underestimation of flows) or cession of hydropower production due to an emptying of the reservoir (in the case of overestimation of flows).

4.2.2 Dam Combinations

Three dam combinations were introduced to SHOM (Table 4.1) to represent current (Original) and future (3dam, 4dam) developments. The 4dam scenario represents the soon-to-be realized condition of having an operating GERD on the Ethiopia-Sudan border, along with the existing Sudanese dams. 3dam scenario differs from the 4dam by excluding Merowe downstream along the main stem. 3dam aims to assess VOI of seasonal forecasting on the Blue Nile only, and thus removes the buffering effects of the steadier White Nile River and large reservoir at Merowe from the economic benefits calculations.

Name	Combinations
Original	Roseires+Sennar+Merowe
3dam	GERD+Roseires+Sennar
4dam	GERD+Roseires+Sennar+Merowe

Table 4.1: Shows the dam combinations used in the analysis

Addition of the GERD included implantation of rudimentary operation rules to maintain the realistic nature of operating a large hydropower dam. Implementation of yearly model benefit maximization without any attention given to the conditions in the following years may lead the model to empty the dam during the dry months. Operation rules are derived to rectify this and improve water management by running the dam long term and developing a linear relationship between release and water availability, improvements can be made to conserve water during dry spells. This adds to the realism of the model and improves overall benefits. In this project reservoir operating rules were implemented in the last month of each year. Addition of reservoir rules to every dry month will significantly decreases the sensitivity of the model to variability in upstream flow. Details of Reservoir operations are highlighted in Appendix C.

4.2.3 Synthetic Forecasts

A set of synthetic hydrological forecasts were applied to SHOM to evaluate model sensitivity to differing seasonal forecasts. The synthetic forecasts were derived from the 70-year Blue Nile gauge record at Roseires, near the Ethiopia-Sudan border. The data were used to generate a continuous distribution function (CDF, figure 4.2) of annual wet season (JJAS) flows. Nine synthetic forecasts were then generated to test the sensitivity of SHOM to forecast characteristics (Table 4.2). The first (*Match*) is a high performing forecast with no systematic error: we simply found the best gamma distribution

parameters to fit the CDF of observed flow. *S.Dhi* and *S.Dlo* represent forecasts that overestimate and underestimate the frequency of extremes, respectively. They are both 100% accurate in the direction of the anomaly—there are no "missed" forecasts—but they are skewed relative to *Match*.

Next, we alter the accuracy rates of the forecasts to assess the effects of the forecasting model's hit and miss rates on the overall value of information. *0.5lo* uses the *Match* distribution but includes a 50% miss rate for predicting high flows—half of all above average flows (defined as CDF probability > 0.7) are incorrectly predicted as below average (CDF probability < 0.3). Similarly *0.5hi* uses the *Match* distribution but includes a 50% miss rate, predicting below average flows as above average. To better characterize sensitivity to miss rate, we also include *0.75lo* and *0.75hi* forecasts that have a 25% miss rate. These synthetic forecasts are all compared to a *mean* forecast that samples randomly from the historical record and a *mean0.9* forecast that applies a 10% low bias to the *mean* forecast in order to test sensitivity to systematic forecast bias.

The distributions were randomly sampled for a 20-year period 10,000 times. Random sampling from the distribution on an annual basis is appropriate given the low autocorrelation at multiple lags. Each year contained the total flows that need to be disaggregated to derive the flows for each month in the rainy season. For dry season months the climatological flows were used, as these months are difficult to forecast and represent only 32% of total interannual variability.

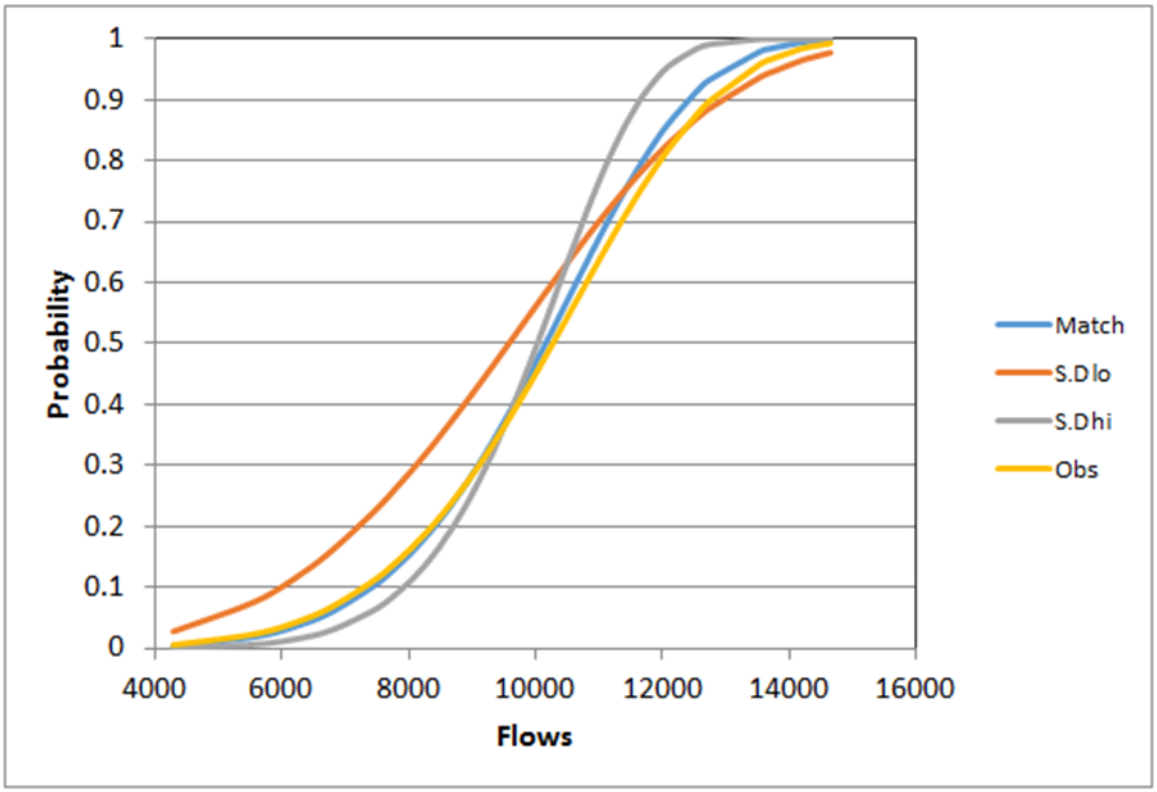

Figure 4.2: Cumulative Distribution function of the three test forecasts. Match (blue) represents a forecast with the same distribution as observations; S.Dlo (orange) has higher probability of extreme events occurring; S.Dhi (grey) has lower probability of extreme events occurring.

Simulation	Description
Match	Forecast with same distribution as observations
S.Dlo	Forecast with larger probability of extreme events
S.Dhi	Forecast with lower probability of extreme events
0.5lo	Match Forecast with 0.5 of the above average flows predicted as below average
0.5hi	Match Forecast with 0.5 of the below average flows predicted as above average
0.75lo	Match Forecast with 0.25 of the above average flows predicted as below average
0.75hi	Match Forecast with 0.5 of the below average flows predicted as above average
mean	Climatological flows
mean0.9	Underestimation of mean with 90% of climatological flows

Table 4.2: Description of Scenarios for the sensitivity analysis

4.2.4 Statistical and Dynamically-based Hindcasts

4.2.4.1 Precipitation

We apply both statistical and dynamically-based prediction models to evaluate forecast skill and value of information in SHOM. Our statistical model is a generalized linear model (GLM) that uses large-scale climate indices, pressure fields, and sea surface temperature to predict rainfall in the Ethiopian Blue Nile at monthly time scales. Predictions are made for each month of the rainy season, June-September (JJAS), with one-month lead for each month (details provided in Appendix D). GLM is a linear regression technique that generalizes the ordinary least squares model with a link function that mediates the linear relationship between predictors and the response variable.

To generate an ensemble forecast for seasonal precipitation predictions, the GLM was run using a k-fold random holdout analysis method on 60 years of data (1950-2010) drawn from the CenTrends 1900-2014 gridded monthly precipitation dataset for East Africa (Funk et al 2015). The model was run 100 times leaving out 20% of the data for validation purposes with the remaining 80% of the data used to train the model. This ensemble was used to provide an uncertainty estimate for GLM predictions—i.e., the estimate is the uncertainty for this GLM when applied to available data, and is not a full uncertainty estimate for all possible statistical models. The GLM was compared with other non-linear machine learning models (Appendix D) and was found to perform as well as or better than other regression techniques.

We draw dynamically-based forecasts from the National Multi Model Ensemble (NMME) hindcast monthly dataset (Kirtman et. al 2014) distributed via the International

Research Institute (IRI) data library. Two models were used in this analysis, the Coupled Forecasting System version 2 (CFSv2) and the Max Plank Institute for Meteorology's AGCM version 4.5 (ECHAM4.5). Precipitation and SST data for each model were available at 1^0 x 1^0 resolution for the period 1982-2010. The NMME hindcast archive includes 24 CFSv2 and 12 ECHAM4.5 realizations for each month, where each ensemble member has a different initialization time. These two models were selected from NMME simply as examples; there was no *a priori* reason for choosing these models over others, though both are leading forecast systems that have been applied in previous studies of the region (Shukla et al. 2014, Jury, 2014, Satti 2016).

4.2.4.2 Converting Precipitation to Streamflow

We derive streamflow estimates from monthly precipitation using statistical models, which can perform as well as process-based hydrologic models in the simulation of interannual streamflow variability in this region (Shortridge et al., 2016). As described in Appendix D, we compare multiple regression techniques using 70 years of streamflow data (1912-1982) recorded at Roseires and distributed by the Global Runoff Data Center (GRDC), paired with CenTrends precipitation estimates. Models were generated independently for each month in the rainy season (JJAS), which collectively account for ~80% of annual Blue Nile flow. Models are evaluated for out-of-sample predictive skill using k-fold random holdout cross validation. We find that Bayesian Additive Regression Tree (BART) and GLM perform best. We choose to proceed with GLM as the preferred model on account of its simpler nature, lower RMSE and higher average correlation in the predictions.

The streamflow GLMs for JJAS were then applied to estimate monthly Blue Nile flow at the SHOM upstream boundary for the period 1982-2010. For this period we generate a "perfect" forecast that uses precipitation values extracted from the Climate Hazards Group InfraRed Precipitation with Stations (CHIRPS) dataset (Funk et al. 2015) and hindcasts derived from our statistical forecast model and from CLMv2 and ECHAM4.5 precipitation (see Appendix D for details). We note that CHIRPS and CenTrends are both produced by the Climate Hazards Group and are aligned with a common Climate Hazards Group Precipitation Climatology (CHPclim) baseline. Thus the two precipitation datasets used in this study are as consistent as possible, with CenTrends offering a long data record of monthly precipitation estimates and CHIRPS offering high resolution, daily estimates that are regularly updated. As with our synthetic forecasts, we use climatological mean flows for the October-May low flow period for all cases. Understanding SHOMs allocation of benefits during anomalously dry and wet years is important when assessing forecast characteristics that add the most value to decision maker. To this end, we assess the performance of the forecast models during unprecedented dry/wet flow sequences by assessing each forecast's value for a scenario in which the 10 consecutive driest/wettest years in the 28 year period of analysis occur consecutively; i.e., a decade long drought/pluvial period. We note that this test does not necessarily reflect how an actual forecast system would perform during a decade long anomaly, since extended climate excursions on that scale would likely be driven by mechanisms that are systematically different from those that drive observed interannual variability. The purpose of the test is simply to assess how the value of forecasts of a

given accuracy changes under such hydrologically extreme conditions. A summary of the flow sequences used in this chapter is provided in Table 4.3.

Flow sequence	Duration	Description
Perfect	28 years	Flows generated from the Hydrology Model using Observed precipitation
Forecasted	28 years	Flows generated from the Hydrology Model using forecasted precipitation (GLM, CFSv2, or ECHAM4.5) during the wet season (JJAS). Climatological mean was used for the remaining months
Mean	28 years	Climatological Mean of 28 year perfect flows
Dry	10 years	The same as "Forecasted" flow sequences, but using only the 10 lowest flow years (drawn from the Perfect sequence) arranged consecutively
Wet	10 years	The same as "Forecasted" flow sequences, but using only the 10 highest flow years (drawn from the Perfect sequence) arranged consecutively

Table 4.3: Description of the flow sequences used in the analysis

We also note that the sequences of flow predictions are derived for each forecasted month at a 1 month lead, while water allocations determined by SHOM are made on an annual basis. This could lead us to underestimate relative VOI of any forecast system that has significant skill at leads greater than one month. The approach taken here is adopted as a proof of concept method that can be applied consistently across model types while preserving month to month variability. This allows us to explore the effects of monthly overprediction and underprediction on decision making.

4.2.5 Value versus Accuracy

SHOM maximizes total hydropower and irrigation benefits by assigning an economic value to energy and crop production assuming infinite demand. The value in this study is from the perspective of a producer (the State), and not a consumer. An increase in the overall benefits attributed to use of forecasted flows over climatological flows (flows

with no prior information) is the value of information (or added value) provided by the forecast.

Accuracy of a forecast is measured as a deviation from the Perfect flow value. The metric used in this study to represent the accuracy of forecasted flows is the Root Mean Square Error (RMSE) value (Wilks 2011).

4.3. Results and Discussions

4.3.1 Synthetic Forecasts

The flow sequences described in Table 2 were input to the updated version of SHOM to evaluate the added value of the ensemble forecast flows. Figure 4.3 compares the accuracy (RMSE) and the hydroeconomic value of each forecast. Box plots show the minimum and maximum values as well as the 25%, 50% and 75% CI values. Interestingly, there is no linear relationship between value and accuracy. While the most accurate forecasts in terms of RMSE (*Observed* and *match*) provide the highest value, moderately accurate forecasts like *0.75hi* yield lower median value than some high RMSE forecasts, including *0.5lo* and *mean0.9*. Forecast *0.5lo* is significantly less accurate (higher RMSE) than *0.75hi*, but its median value is higher.

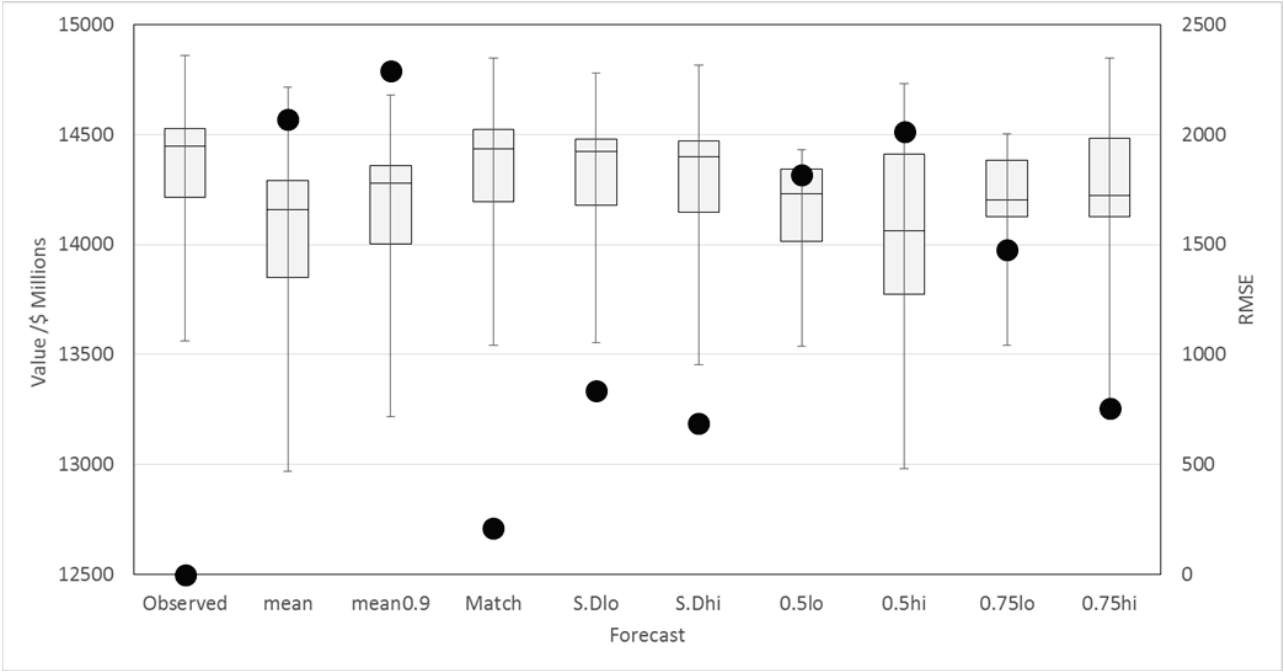

Figure 4.3: Accuracy and value of the synthetic forecasts (Table 4.1). Black dots are the root mean square error of the generated flows; box plots represent the value of information of the forecasted flows.

This nonlinearity reflects the fact that a forecast's ability to capture extreme events, particularly a drought, can add disproportionate value to a forecast. This becomes clear when one examines the value of forecasts for *dry* versus *wet* flow sequences (Figure 4.4). In all cases, the value of a forecast relative to the null (*mean*) forecast is greater under dry conditions than wet conditions. Hence, underestimation of drought severity (e.g, *S.Dhi*) or poor prediction performance in capturing drought processes (e.g., the *0.5hi* and *0.75hi* forecasts) is particularly damaging to overall value of a forecast system. Errors in predicting high flows (e.g., *0.75lo* and *0.5lo*) or systematic underestimation of flows (*mean0.9*) are less problematic. Indeed, systematic low bias in a null forecast (*mean0.9*) led to some value relative to *mean* because a *mean* forecast incurs loss of value in dry years while *mean0.9* loses relatively less in wet years. Explanation of this phenomenon is further described in Section 4.3.2, below.

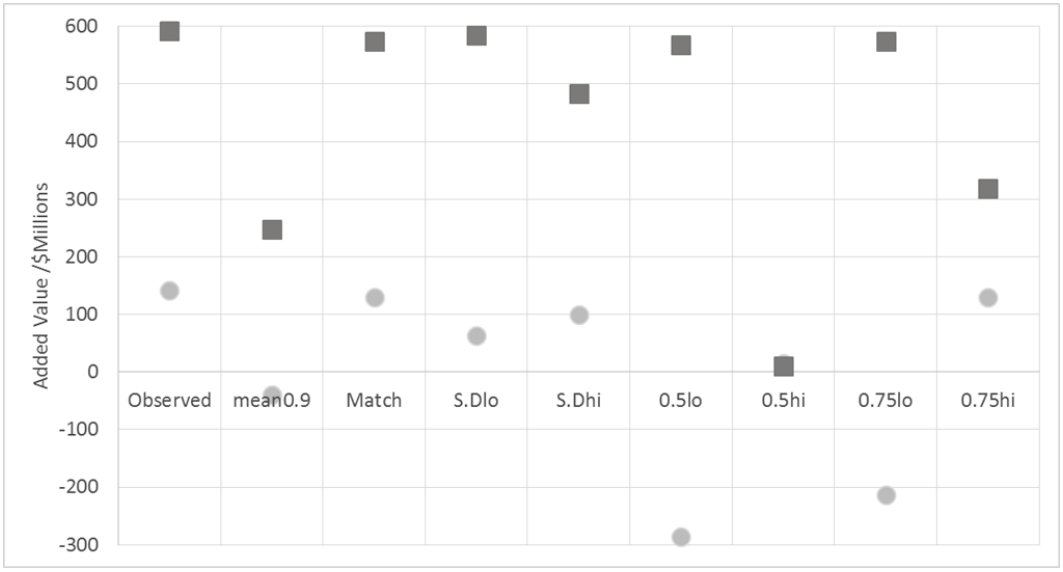

Figure 4.4: Added Value of the driest (squares) and wettest (dots) flow sequences for each forecast. Added value is the difference between the forecast value and the value with no prior information (mean).

4.3.2 Statistical and Dynamically-based Hindcasts

Comparisons between the statistical model and the two operational dynamically-based seasonal prediction systems (CFSv2 and ECHAM4.5) are shown in Figure 4.5. The error bars show the range of the values calculated for SHOM for all model realizations. The model applies a penalty when predictions err by a volume that is larger than the capacity of the upstream reservoir. Dynamical models, particularly ECHAM4.5, frequently produce errors larger than Roseries's capacity, but they rarely produce errors larger than the GERD's capacity. Thus the increase in upstream reservoir capacity reduced the frequency of penalty for dynamically-based forecasts and increased their average value.

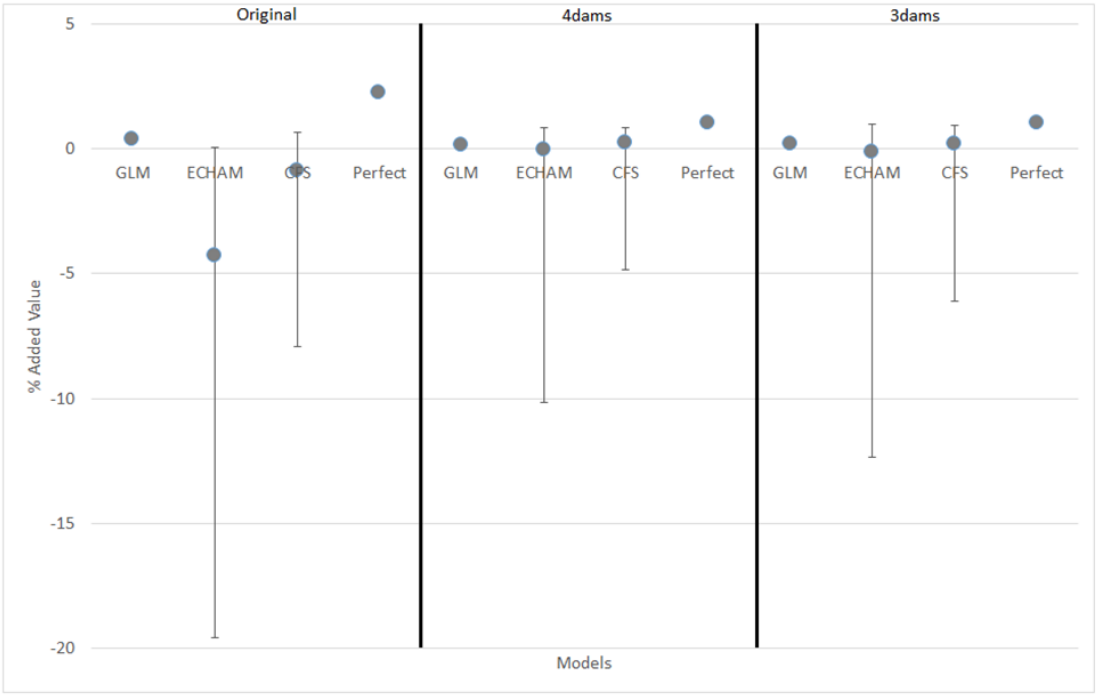

Figure 4.5: Comparison of the SHOM value of the ensemble forecasted flows for each model under different dam combination scenarios (table 4.2).

The general behavior of the forecasts is shown in Figure 4.6. Recall that each forecast method—GLM, ECHAM4.5, and CFSv2—yields an ensemble of Blue Nile flow predictions for each forecast period. The ensemble mean will, averaged over time, have relatively low bias, while a prediction sequence composed of the high flow or low flow ensemble endmembers will have relatively high bias. Thus, the RMSE of the ensemble mean forecast (black dots in Figure 4.6) is always lower than the RMSE of the high (black +) or low (black -) flow sequence for each forecast method. This is easier to see for ECHAM4.5 and CFSv2 than for the GLM, simply because the ensemble spread is larger. The same is not true for forecast value (red symbols in Figure 4.6). Here, we see that systematic over-prediction (high endmembers; red + symbols) results in extremely low value, while under-prediction is less costly in the *original* dam configuration and can even out-perform the ensemble mean for the *3dams* and *4dams* configurations. The

reason for this is the same as was described for the relatively high value of synthetic forecasts *0.5lo*, *0.75lo*, and *mean0.9*. Under-predicting flows leads to conservative management, which is sub-optimal but does not incur any large risks, while over-predicting can lead to costly management errors. These errors are represented by a penalty function (Appendix C equation 5) in SHOM, which serves as a proxy for the significant political and economic damage that could arise from drawing reservoirs down to a point where they cannot support hydropower generation or irrigation withdrawals. Since the ensemble mean over-predicts more often than the low endmember does, it can actually end up providing lower value over time even though its RMSE is substantially better.

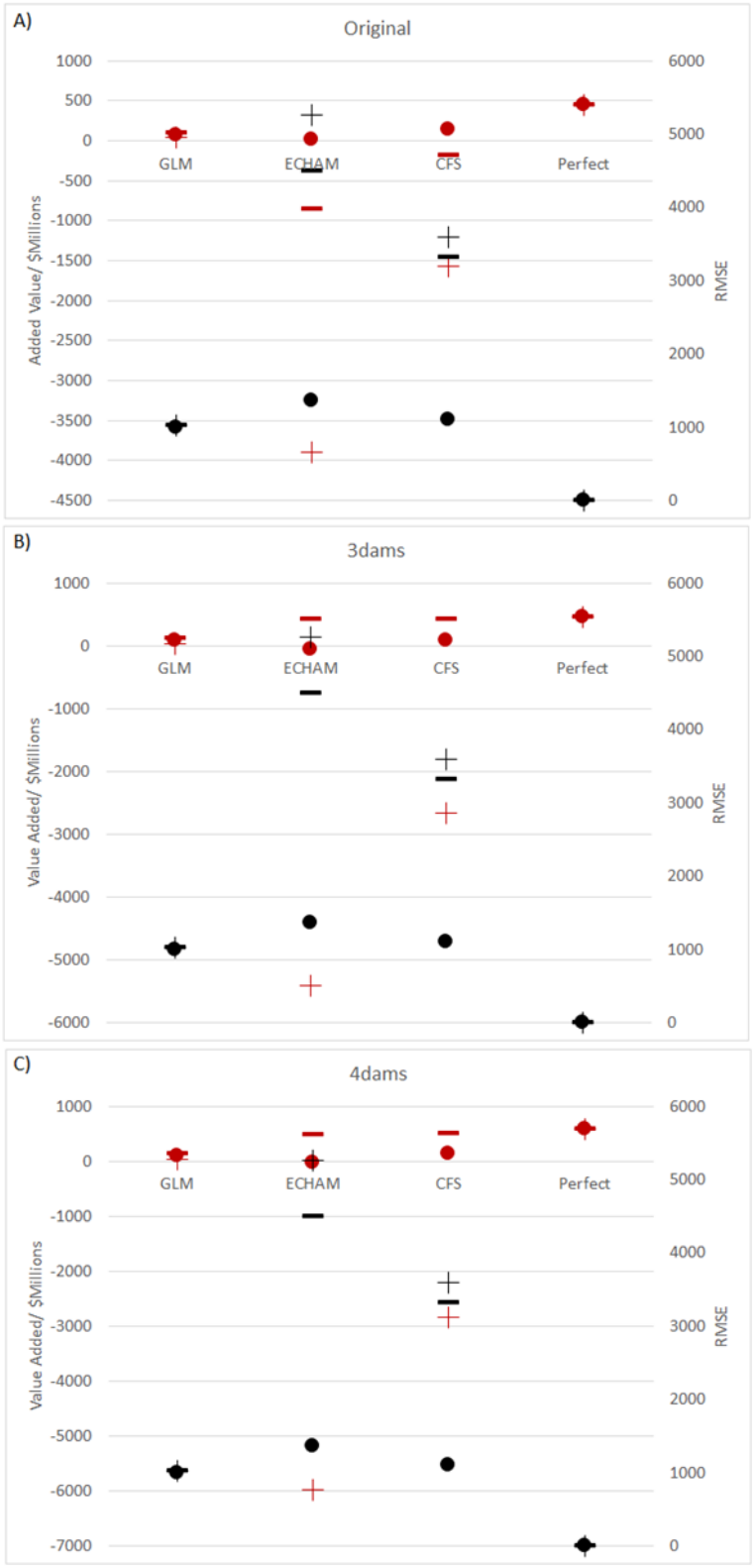

Figure 4.6: A comparison of RMSE (black) and value (red) for each forecast method in the (a) original, (b) 3dams, and (c) 4dams configurations. The ensemble mean (•), minimum (-) and maximum (+) are shown for each forecast method.

To explore this phenomenon, we examine river flow and hydropower production for a sample year in which the low ensemble endmember outperformed the ensemble mean (Figure 4.7). The mean river flow forecast (grey solid line) over-predicts flows in the year, leading to reduced hydropower benefits (grey dashed line), while the ensemble minimum flow forecast (orange solid line) does not suffer from this error, and produces substantially more hydropower benefits. Past studies (Block 2011) have shown overestimation by forecasts can be detrimental to their value. Over prediction causes excess release in the preceding months in anticipation of larger flows. This leads to lower hydraulic head and less available water for release in subsequent months, leading to a reduction in hydropower generation.

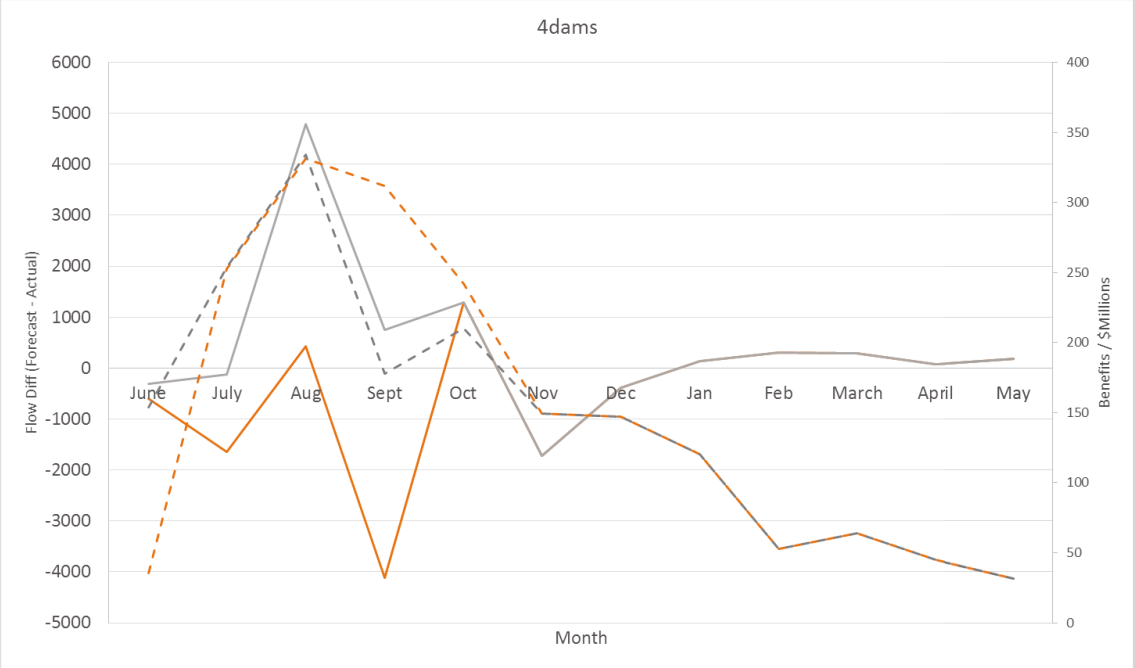

Figure 4.7: 4dams difference in incoming flow (Actual flow – forecasted flow, solid lines, primary axis) and hydropower benefits (dashed lines, secondary axis) for the minimum ECHAM ensemble flow (orange) and the mean ECHAM ensemble flow (grey). Results show underestimating flows produces larger hydropower benefits.

We note, however, that low endmember forecasts only offer higher value than the ensemble mean for the dam configurations that include the GERD (3dams and 4dams). In the original dam configuration (Roseires, Sennar, and Merowe, but no GERD) the ensemble mean has the highest value. This result reflects the fact that the presence of a large upstream reservoir favors conservative management: in a system with small upstream reservoirs, conservative release can lead to spillover when reservoir capacity is exceeded, but in a system in which the upstream facility has large reservoir capacity there is less risk of exceeding capacity and losing potential hydropower production due to spillover.

This pattern is clear in an indicative example year drawn from simulations for the original dam configuration (Figure 4.8). In this year the ensemble mean forecast significantly outperforms the minimum forecast in terms of total value, and this occurs because under-prediction of flows results in a spillover event that foregoes hydropower income and incurs a penalty in SHOM (Aug in Figure 4.8) because of foregone opportunity and the potential risks of spillover events (e.g., downstream floods).

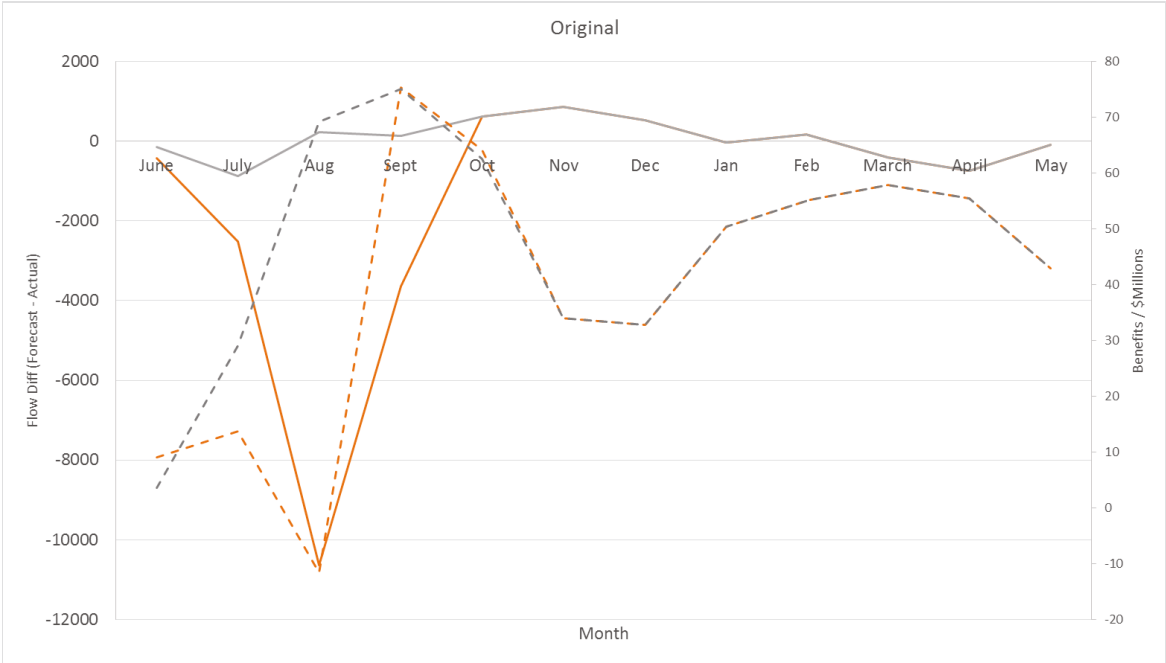

Figure 4.8: Original dam set-up. Graph shows difference in incoming flow (solid lines, primary axis) and hydropower benefits (dashed lines, secondary axis) for the minimum ECHAM ensemble flow (orange) and the mean ECHAM ensemble flow (grey).

Finally, we consider how dam configuration influences the value of forecasts under periods of extended hydrological extremes: the *wet* and *dry* flow sequences described in Section 4.2.4. *Dry* is a 10-year run composed of the ten driest years in the 30 year time span, and wet runs are composed of the predictions for the 10 consecutive wettest years. The first conclusion from these experiments is that forecasts are more valuable during an extended dry period than an extended wet period (Figure 4.9). This follows naturally from previous results that show forecasts are more valuable when water is limited. Indeed, for the *wet* flow sequence even the perfect forecast offers little value under either the original or the 4dams configuration, and actual forecasts have zero or negative value. For the *dry* flow sequence forecasts do add substantial value, with the exception of the

high end ensemble members of the dynamically-based forecast models, which show negative value due to over-prediction penalties.

The second finding from the *dry* and *wet* simulations is that the addition of the GERD to the system (Figure 4.9b) enhances the value of conservative prediction during extended hydrological extremes, much as it did under normal hydrological conditions. The effect is greater for *dry*, but it is present in *wet* as well. For the original dam configuration the differences between the mean and minimum forecasts is negligible during the dry years, with the wet showing greater benefits for the mean realization in the dynamical models on account of spillover penalties incurred by the ensemble minimum forecast. Results for the GLM are generally consistent with this pattern but are much less dramatic on account of the smaller ensemble spread.

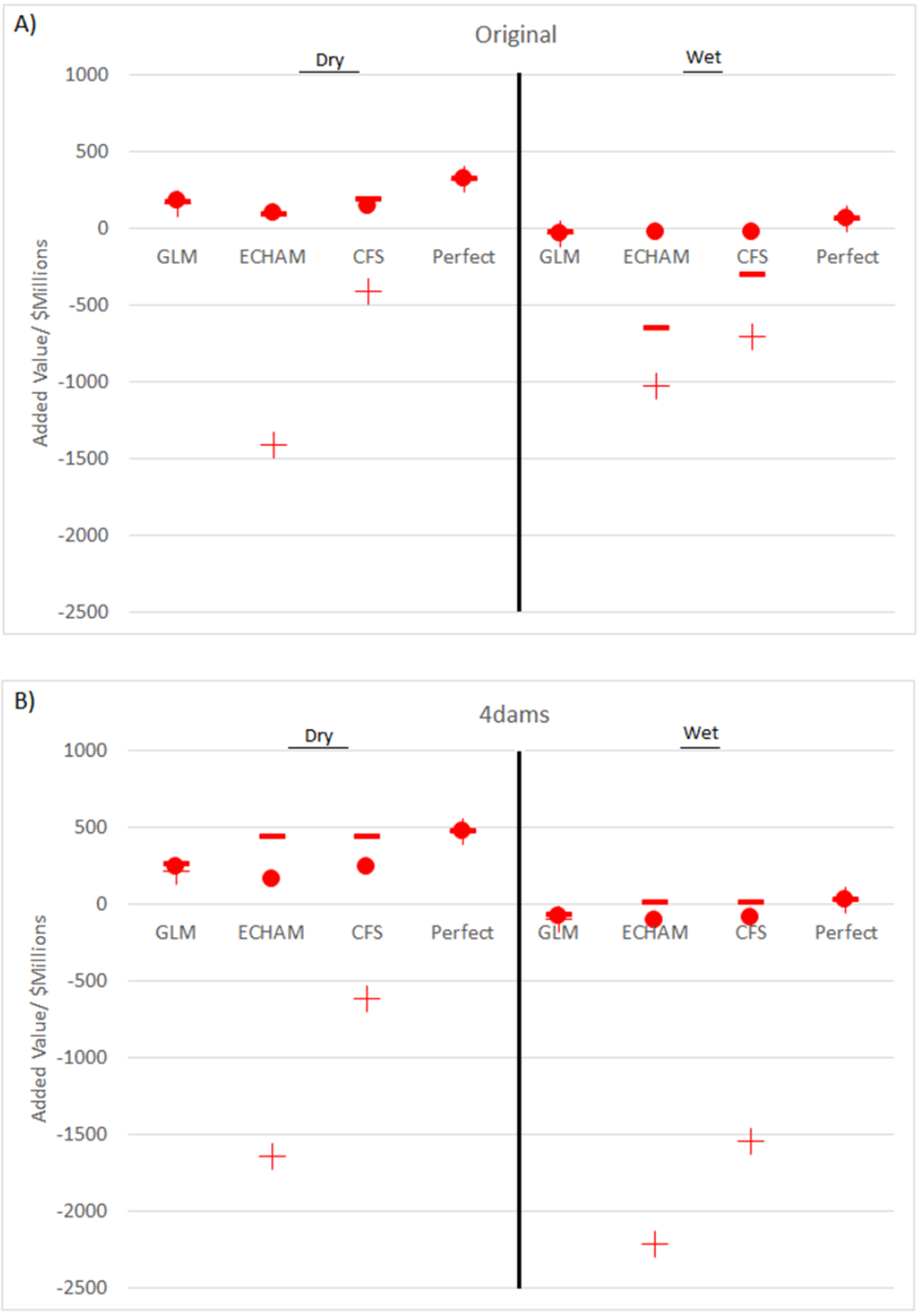

Figure 4.9: Minimum flow realization (-), maximum flow realization (+) and mean (•) for A) the original SHOM dam configuration and B) the 4 dam scenario. All scenarios include the dry and wet flow sequences.

4.4. Conclusions

Overall forecast accuracy cannot be used to gauge the added value, rather forecasts performance depends on the water infrastructure set-up including dam specifications and locations in relation to irrigation schemes within the region.

Additionally a forecasts predictive capacity hinges on its ability to underestimate flows more frequently than overestimating flows regardless of the overall model error. Consistent gross overestimation of flows by the maximum realization forecast of dynamical models, as well as significant underestimation of flows by the minimum realization forecast provide large uncertainty in the potential VOI. The conservative nature of underestimation plays a large role in the large value of information of dam management. Implementation of reservoir operation rules throughout the dry months of the analysis would buffer the model and reduce the added value of minimum realization flows.

Furthermore, the performance of the different models under the extreme dry and wet periods (Figure 4.9) allows forecasters to tailor predictions to the needs of the decision maker. For example, the most valuable forecast in extreme dry and wet conditions varies depending on the dam configuration. Given the current optimization object function, minimum realization flows become more valuable with the addition of the GERD (Table 4.4), thus the forecast information they provide would allow for the decision maker to shift from the mean forecast to the minimum realization forecast when the GERD comes online.

Interpretation of the results of this chapter is highly dependent on the tradeoff between objectives in the objective function. SHOM maximizes the benefits of two objectives;

hydropower and irrigation. In this analysis irrigation benefits remained relatively consistent for all model flow sequences due to two factors: (1) for all model runs, the marginal value of water was kept constant, (2) the irrigation area constraints, as well as withdrawal limitations dictated by the 1959 Nile agreement, greatly limited the irrigation contribution in this analysis.

We emphasize several limitations in the current study that can be addressed in future work. As noted, there is an inconsistency between the 1-month forecast lead time and the one year optimization window for SHOM, and that this inconsistency could lead to conservative error in estimates of forecast VOI. Second, the absence of flood control objectives in SHOM leads to an objective function that rewards underestimation, as there is no catastrophic penalty for running reservoirs high and thus risking large releases in an unexpectedly wet month. The analysis presented here also ignores the influence that dam scenarios have on regional power prices, and it lumps benefits between Sudan and Ethiopia rather than treating the GERD and the Sudanese dams as separate (and possibly competing) optimization problems. Each of these limitations represents a research path that could further advance our understanding of forecast VOI in rapidly developing transboundary basins like the Blue Nile.

	Min Realization	Mean	Max Realization
Original	Low Value Low Accuracy	High Value High Accuracy	Low Value Low Accuracy
With GERD	High Value Low Accuracy	High Value High Accuracy	Low Value Low Accuracy

Table 4.4: Illustrates the value-accuracy relationship of the minimum, mean and maximum flow sequences with, and without the GERD.

5. Conclusions

The preceeding chapters introduce a multiobjective hydroeconomic model for the Sudanese Blue Nile (SHOM) in the GAMS package. Chapter 2 details various aspects of the model set up and performs a sensitivity analysis in order to gage model sensitivity to various upstream climate conditions and economic changes to value of water for irrigation. Multiple conclusions can be drawn from this chapter, firstly construction of an upstream structure that regulates and smoothens flows would lead to an increase in irrigation withdrawals. This is beneficial most when the marginal value of water for irrigation is relatively high compared to the price of energy. Secondly, given the current set up of SHOM, there is an increase in overall benefits with increased upstream flow. Lastly, the withdrawal restrictions put in place by the 1959 water agreement between Sudan and Egypt becomes more expensive as the price of energy decreases due to the construction of the GERD. The drop in power price, as well as the availability of water during the dry season incentivizes the need for a second cropping season which increases the irrigation benefits in the objective function. It is important to note that the results presented in chapter 2 are constrained by the lack of agricultural and energy data that would adequately describe the hydropower and irrigation benefits. Issues of siltation that have long plagued dam management in Sudan have been neglected in this analysis. Lastly optimization performed in this section assumes perfect foresight which can be improved by reducing the foresight to the models monthly time-step.

Chapter 3 analyzed spatial biases in dynamical models using regionalization. Use of objective regionalization in chapter 3 shows that dynamical models do have a spatial bias, and dividing the project area into homogenous regions can identify regions of spatial

bias. Secondly, correcting for the spatial mismatch of forecast outputs can improve forecasting skill. Chapter 3 introduces an analogous regional matching (ARM) technique that performs a cross correlation of all the regions and uses predictions from highly correlated regions to forecast precipitation for those model regions. In addition correction of forecasts for ECHAM4.5 showed that forecast skill improved for summertime precipitation in EA with summer rainy season, the ARM method shows an improvement of the RPSS skill score from -0.09 to 0.20, and -0.28 to 0.28 for the months of July and August, respectively, for a region that includes portions of the Eastern Nile basin.

In Chapter 4, SHOM is used to perform a VOI on three different seasonal forecasts. Results show that the SHOM objective function that heavily penalizes overprediction of flows, and rewards the conservative nature of underpredicted flows. The addition of the GERD upstream further illustrates this point, with the minimum realization of forecasted flows outperforming both the mean of all forecasted flows, and the maximum realization flows. Additionally, there is a no consistent relationship between accuracy of the forecasts using RMSE and the total benefits accrued by SHOM. Forecasts that underestimate flows tend to have a large error associated with them, but they generally seem to exhibit high value as well. Lastly, the forecasting sensitivity analysis shows that SHOM is more sensitive to forecast accuracy rather than nature of the forecast distribution function.

5.1 Future Work

There are multiple avenues to further improve the studies presented in this dissertation. The optimization model presented, and altered for the VOI study makes many

assumptions. The objective function within SHOM assumes benefits are seen from the perspective of the state. Within a transboundary framework there may be multiple actors, who may, or may not choose to cooperate with one another. The current set-up assumes full cooperation and shared benefits with Ethiopia. This is not a realistic assumption. There has been past work on the Nile looking at forecast VOI using hydroeconomic optimization (IMPEND) along the Blue Nile focused on Ethiopia upstream of SHOM. Integrating SHOM with IMPEND can give a more holistic representation of water resources VOI using optimization for a larger portion of the Blue Nile can raise interesting questions about the value of forecasts with and without cooperation.

Within the forecasting method developed in chapter 3, one improvement in improving dynamical forecasts using ARM, is to automate the process to randomly correct for models within NMME. The current process demand an intensive analysis that requires regionalization, cross correlation between regions, determining the range of spatial overlap, and then forecast correction. The creation of a robust algorithm to automatically perform the required steps for multiple models will have great implications for improving forecast outlooks.

References

Arjoon D., Mohamed Y., Goor Q., Tilmant A. 2014: Hydro-economic risk assessment in the eastern Nile River basin, *Water Resources and Economics* 8 (2014): 16-31.

Awulachew, S., Rebelo, L., and Molden, D., 2010: The Nile Basin: tapping the unmet agricultural potential of Nile waters, Water Int., 35, 623–654, 2010.

Badr, H. S., Zaitchik, B. F., & Guikema, S. D. 2014: Application of Statistical Models to the Prediction of Seasonal Rainfall Anomalies over the Sahel.*Journal of Applied Meteorology and Climatology*, *53*(3), 614-636.

Badr, H. S., B. F. Zaitchik, and A. K. Dezfuli, 2014: HiClimR: Hierarchical climate regionalization. *Comprehensive R Archive Network (CRAN)*. [Available online at http://cran.r-project.org/package=HiClimR.]

Badr, H., Zaitchik, B., and Dezfuli, A. 2015: A tool for hierarchical climate regionalization. *Earth Science Informatics* 8.4 949-958.

Barnston, A. G., Li, S., Mason, S. J., DeWitt, D. G., Goddard, L., and Gong, X. 2010: Verification of the first 11 years of IRI's seasonal climate forecasts. *Journal of Applied Meteorology and Climatology*, *49*(3), 493-520.

Batté, L., and Déqué, M. 2011: Seasonal predictions of precipitation over Africa using coupled ocean-atmosphere general circulation models: skill of the ENSEMBLES project multimodel ensemble forecasts. *Tellus A*, ***63*(2)**, 283-299.

Berhane, F, Benjamin Z, and Dezfuli, A. 2014: Subseasonal analysis of precipitation variability in the Blue Nile river basin. *Journal of Climate* **27.1**: 325-344.

Bernal, V. 1997: Colonial moral economy and the discipline of development: the Gezira scheme and modern Sudan, *Cult. Anthropol.*, 12, 447–479.

Beyene, T., Lettenmaier, D., and Kabat, P. 2010: Hydrologic impacts of climate change on the Nile River Basin: implications of the 2007 IPCC scenarios, *Clim. Change*, 100, 433–461.

Bhattacharjee, P.S. and Zaitchik, B.F., 2015: Perspectives on CMIP5 model performance in the Nile River headwaters regions. *International Journal of Climatology*, *35*(14), pp.4262-4275.

Blackmore, D. and Whittington, D. 2008: Opportunities for cooperative water resources development 20 on the eastern Nile: risks and rewards, Report to the Eastern Nile Council of Ministers, Nile Basin Initiative, Entebbe.

Block, P. and Strzepek, K. 2010: Economic analysis of large-scale upstream river basin development on the Blue Nile in Ethiopia considering transient conditions, climate

variability, and climate change, *J. Water Res. Pl.*-ASCE, 136, 156–166.

Block, P. and Strzepek, K. 2012: Power ahead: meeting Ethiopia's energy needs under a changing climate review of development, *Economics,* 16, 476–488.

Block, P., Assis Souza Filho, F., Sun, L., and Kwon, H. 2009: A streamflow forecasting framework using multiple climate and hydrological models, *J. Am. Water Resour. Assoc.*, 45, 828–843.

Block, P., 2011: Tailoring seasonal climate forecasts for hydropower operations. *Hydrology and Earth System Sciences*, *15*(4), pp.1355-1368.

Bureau of Reclamation, US Department of Interior: Land and Water Resources of the Blue Nile Basin 1964: Ethiopia, Main Report and Appendices I–V, Government Printing Office, Washington DC.

Byerlee, D. R., & Anderson, J. R. 1969: Value of predictors of uncontrolled factors in response functions. *Australian Journal of Agricultural Economics*,*13*(2), 118-127.

Cascao, A. 2008: Ethiopia – challenges to Egyptian hegemony in the Nile Basin, *Water Pol.,* 10, 13–28.

Camberlin, P., and Philippon, N. 2002: The East African March-May rainy season: Associated atmospheric dynamics and predictability over the 1968-97 period. *Journal of Climate* **15.9** 1002-1019.

Chesworth, P. M., Howell, P. P., and Allan, J. A. 1990: The History of Water Use in Sudan and Egypt in the Nile, Resource Evaluation, Resource Management, Hydropolitics and Legal Issues, Centre of Near and Middle Eastern Studies, 40–58.

Chipman, H.A., George, E.I. and McCulloch, R.E., 2010. BART: Bayesian additive regression trees. *The Annals of Applied Statistics*, pp.266-298.

Cohon, J. 2005: Multiobjective Programming and Planning, Dover Publications, Mineola, NY, 2003. Conway, D.: From headwater tributaries to international river: observing and adapting to climate variability and change in the Nile basin, *Global Environ. Change*, 15, 99–114.

Conway, D. 2000: The climate and hydrology of the Upper Blue Nile River. *The Geographical Journal*, ***166*****(1)**, 49-62.

Diro, G. T., Grimes, D. I. F., and Black, E. 2011: Teleconnections between Ethiopian summer rainfall and sea surface temperature: part II. Seasonal forecasting. *Climate Dynamics*, ***37*****(1-2)**, 121-131.

Dezfuli, A, and Nicholson, S. 2013: The relationship of rainfall variability in western equatorial Africa to the tropical oceans and atmospheric circulation. Part II: The boreal autumn. *Journal of Climate* **26.1** 66-84.

Doblas-Reyes, F. J., Weisheimer, A., Déqué, M., Keenlyside, N., McVean, M., Murphy, J. M., ... & Palmer, T. N. (2009). Addressing model uncertainty in seasonal and annual dynamical ensemble forecasts. *Quarterly Journal of the Royal Meteorological Society*, *135*(643), 1538-1559.

Drud, A. S. 1992: CONOPT – a large scale GRG code, *ORSA J. Computing*, 6, 207–216

Elamin, A., Saeed, A., Boush, A. 2011: Water Use efficiencies of Gezira, Rahad and New Halfa irrigated schemes under Sudan dryland condition, Sudan *J. Des. Res.* 3(1): 62-72.

Elshamy, M. E., Seierstad, I. A., and Sorteberg, A. 2009: Impacts of climate change on Blue Nile flows using bias-corrected GCM scenarios, *Hydrol. Earth Syst. Sci.*, 13, 551–565, doi:10.5194/hess-13-551-2009.

Food and Agricultural Organization, FAO, 2000: The elimination of food insecurity in the Horn of Africa. A concerted government and UN agency action. Final Report. http://www.fao.org/docrep/003/x8406e/x8406e00.htm

Food and Agricultural Organization: FAOSTAT, available at: http://faostat.fao.org/site/703/default.aspx#ancor (last access: August 2013), 2009.

Funk, C. et al. 2015: The climate hazards infrared precipitation with stations—a new environmental record for monitoring extremes. *Scientific data* **2**, doi:10.1038/sdata.2015.6.

Gissila, T., Black, E., Grimes, D. I. F., and Slingo, J. M. 2004: Seasonal forecasting of the Ethiopian summer rains. *International Journal of Climatology*, ***24*(11),** 1345-1358.

Gamal, K. A. E. M. 2009: Impact of Policy and Institutional Changes on Livelihood of Farmers in Gezira Scheme of Sudan, M.S. Thesis, University of Gezira, Sudan.

Gebreluel, G. 2014: Ethiopia's Grand Renaissance Dam: ending Africa's oldest geopolitical rivalry?, Wash. Quart., 37, 25–37.

Georgakakos, A. 1987: New method for the real-time operation of reservoir systems, *Water Resour. Res.,* 23, 1376–1390.

Georgakakos, A. 1989: Extended linear quadratic gaussian control: further extensions, *Water Resour. Res.,* 25, 191–201.

Georgakakos, A. 2007: Topics on System Analysis and Integrated Water Resources Management, chap. 6, edited by: Castelletti, A. and Soncini-Sessa, R., Elsevier, Amsterdam.

Georgakakos, A. P., Yao, H., Kistenmacher, M., Georgakakos, K. P., Graham, N. E.,

Cheng, F. Y., Spencer C., & Shamir, E. 2012: Value of adaptive water resources management in Northern California under climatic variability and change: reservoir management. *Journal of Hydrology*, *412*, 34-46.

Ghezae, N. 1998: Irrigation Water Management. A Performance Study of the Rahad Scheme in Sudan, 1977–1996, Ph.D. thesis, Uppsala University Library, Uppsala, Sweden.

Gleick, P. 1986: Methods for evaluating the regional hydrologic impacts of global climate changes, *J. Hydrol*., 88, 97–116.

Goddard, L., Mason, S. J., Zebiak, S. E., Ropelewski, C. F., Basher, R., & Cane, M. A. 2001: Current approaches to seasonal to interannual climate predictions. *International Journal of Climatology*, ***21*****(9),** 1111-1152.

Goor, Q., Kelman, R., and Tilmant, A. 2010: Optimal multipurpose-multireservoir operation model with variable productivity of hydropower plants, *J. Water Res. Pl.*-ASCE, 137, 258–267.

Guariso, G., Haynes K., Whittington D., Younis M, Energy, agriculture, and water: a multiobjective programming analysis of the operations of the Aswan High Dam, *Environment and planning*. 12(4) Pg 369-379.

Guariso, G. and Whittington, D. 1987: Implications of Ethiopian water development for Egypt and Sudan, *Int. J. Water Resour*. D, 3, 105–114.

Hai, H.: Sudan, Ethiopia. 2013: Close Relations in All Fields, Sudan Vision, available at: http://news.sudanvisiondaily.com/details.html?rsnpid=229800. (last access: 10 January 2015).

Hamlet, A. F., Huppert, D., & Lettenmaier, D. P. 2002: Economic value of long-lead streamflow forecasts for Columbia River hydropower. *Journal of Water Resources Planning and Management*, *128*(2), 91-101.

Hammond, M. 2013: The Grand Ethiopian Renaissance Dan and the Blue Nile: Implications for transboundary water governance, GWF Discussion Paper 1307, Global Water Forum, Canberra, Australia, available at: http://www.globalwaterforum.org/2013/02/18/the-?grand-? ethiopian-?renaissance-?dam-?and-?the-?blue-?nile-?implications-?for-?transboundary-? water-?governance/ (last access: 4 August 2014).

Harou, J., Pulido-Velazquez, M., Rosenberg, D., Medellín-Azuara, J., Lund, J., and Howitt, R. 2009: Hydro-economic models: concepts, design, applications, and future prospects, *J. Hydrol.,* 375, 627–643.

Hussien, H. 2014: Egypt and Ethiopia Spar Over the Nile, Opinion Piece, Al- jazeera America, available at: http://america.aljazeera.com/opinions/2014/2/ egypt-disputes-

ethiopiarenaissancedam.html (last access: 4 August 2014).

Igunza, E.: Will Ethiopia's Grand Rennaissance Dam Dry the Nile in Egypt, British Broadcasting Corporation, available at: http://www.bbc.com/news/world-africa-26679225, last access: 4 August 2014.

Jury, M. 2014: Evaluation of Coupled Model Forecasts of Ethiopian Highlands Summer Climate." *Advances in Meteorology*, http://dx.doi.org/10.1155/2014/894318.

Kalnay, E., Kanamitsu, M., Kistler, R., Collins, W., Deaven, D., Gandin, L., Iredell, M., Saha, S., White, G., Woollen, J. and Zhu, Y., 1996. The NCEP/NCAR 40-year reanalysis project. *Bulletin of the American meteorological Society*, *77*(3), pp.437-471.

Kaplan, A., Cane, M. A., Kushnir, Y., Clement, A. C., Blumenthal, M. B., & Rajagopalan, B. 1998: Analyses of global sea surface temperature 1856–1991. *Journal of Geophysical Research: Oceans*, *103*(C9), 18567-18589.

Katz, R. W., Murphy, A. H., & Winkler, R. L. 1982: Assessing the value of frost forecasts to orchardists: a dynamic decision-making approach. *Journal of Applied Meteorology*, *21*(4), 518-531.

Katz, R. W., & Murphy, A. H. 1997: Economic value of weather and climate forecasts. Cambridge University Press.

Kirtman, Ben P., et al. 2014 : The North American Multimodel Ensemble: Phase-1 seasonal-to-interannual prediction; Phase-2 toward developing intraseasonal prediction. *Bull. Amer. Meteor. Soc.*, **95**, 585–601. doi: http://dx.doi.org/10.1175/BAMS-D-12-00050.1.

Korecha, D., & Barnston, A. G. 2007: Predictability of June-September rainfall in Ethiopia. *Monthly weather review*, *135*(2), 628-650.

Koster, R. D., Bell, T. L., Reichle, R. H., Suarez, M. J., & Schubert, S. D. 2008: Using observed spatial correlation structures to increase the skill of subseasonal forecasts. *Monthly Weather Review*, *136*(6), 1923-1930.

Knott, D. and Hewett, R. 1994: Water resources planning in the Sudan, in: The Nile, Sharing a Scarce Resource, A Historical and Technical Review of Water Management and of Economic and Legal Issues, edited by: Howell, P. P. and Allan, J. A., Cambridge University Press, Cambridge, 205–216.

Loucks, D. P., Stedinger, J. R., and Douglas, H. 1981: Water Resource Systems Planning and Analysis, Prentice-Hall, Englewood Cliffs, NJ.

Lyon, B., & DeWitt, D. G. 2012: A recent and abrupt decline in the East African long rains. *Geophysical Research Letters*, ***39***(2).

McCartney, M, and Girma, M. 2012: Evaluating the downstream implications of planned water resource development in the Ethiopian portion of the Blue Nile River. *Water Int.,* 37(4), 362-379.

McCartney, M., Ibrahim, Y. A., Sileshi, Y., and Awulachew, S. B. 2009: Application of the Water Eval- uation and Planning (WEAP) Model to simulate current and future water demand in the Blue Nile, in: Improved water and land management in the Ethiopian highlands: its impact on downstream stakeholders dependent on the Blue Nile, Intermediate Results Dissemina- tion Workshop held at the International Livestock Research Institute (ILRI), Addis Ababa, Ethiopia, 5–6 February 2009, edited by: Awulachew, S. B., Erkossa, T., Smakhtin, V., and Fernando, A., International Water Management Institute, Colombo, Sri Lanka, 78.

Mwale, D., & Gan, T. Y. 2005: Wavelet analysis of variability, teleconnectivity, and predictability of the September-November East African rainfall. *Journal of applied meteorology*, *44*(2), 256-269.

Nawaz, R., Bellerby, T., Sayed, M., and Elshamy, M. 2010: Blue Nile runoff sensitivity to climate change, Open Hydrol. J., 4, 137–151.

Nicholson, S. E 2000: The nature of rainfall variability over Africa on time scales of decades to millennia. *Global and planetary change* **26.1**: 137-158.

Nicholson, S E. 2014: The predictability of rainfall over the Greater Horn of Africa. Part I: Prediction of seasonal rainfall. *Journal of Hydrometeorology* **15.3** (2014): 1011-1027.

Nicholson, S. E. 2015: The Predictability of Rainfall over the Greater Horn of Africa. Part II: Prediction of Monthly Rainfall during the Long Rains. *Journal of Hydrometeorology*, ***16*****(5)**, 2001-2012.

Ntale, H. K., Gan, T. Y., & Mwale, D. 2003: Prediction of East African seasonal rainfall using simplex canonical correlation analysis. *Journal of climate*, *16*(12), 2105-2112.

Petersen, E. H., & Fraser, R. W. 2001: An assessment of the value of seasonal forecasting technology for Western Australian farmers. *Agricultural Systems*, *70*(1), 259-274.

Plusquellec, H. 1990: The Gezira Irrigation Scheme in Sudan, Objectives, Design, and Performance, World Bank, Technical Paper 120, Washington DC.

Professor Belay Simane, Addis Ababa University personal communication.

Olsson, L. 1993: On the causes of famine: drought, desertification and market failure in the Sudan. *Ambio*, 395-403.

Parker, D. E., Jones, P. D., Folland, C. K., & Bevan, A. 1994: Interdecadal changes of surface temperature since the late nineteenth century. *Journal of Geophysical Research: Atmospheres*, ***99*****(D7)**, 14373-14399.

Reynolds, R. W., & Smith, T. M. 1994: Improved global sea surface temperature analyses using optimum interpolation. *Journal of climate*, **7(6),** 929-948.

Satti, S., Zaitchik, B., & Siddiqui, S. 2015: The question of Sudan: a hydro-economic optimization model for the Sudanese Blue Nile. *Hydrology and Earth System Sciences*, *19*(5), 2275-2293.

Satti S., Zaitchik B., Badr H., Tadesse T., 2016: Understanding and enhancing dynamical seasonal predictions through objective regionalization, *Journal of Applied Meterology and Climatology* (In review).

Shafiee-Jood, M., Cai, X., Chen, L., Liang, X. Z., & Kumar, P. 2014: Assessing the value of seasonal climate forecast information through an end-to-end forecasting framework: Application to US 2012 drought in central Illinois. *Water Resources Research*, *50*(8), 6592-6609.

Segele, Z. T., & Lamb, P. J. 2005: Characterization and variability of Kiremt rainy season over Ethiopia. *Meteorology and Atmospheric Physics*, ***89*(1-4),** 153-180.

Soliman, E., Sayed, M., and Jeuland, M. 2009: Impact assessment of future climate change for the Blue Nile basin, using a RCM nested in a GCM, Nile Basin. *Water Eng. Sci. Magazine*, 2, 15–30.

Swain, A. 1997: Ethiopia, the Sudan, and Egypt: the Nile River dispute, J. Mod. Afr. Stud., 35, 675– 694.

Taye, M. T., Ntegeka, V., Ogiramoi, N. P., and Willems, P. 2011: Assessment of climate change impact on hydrological extremes in two source regions of the Nile River Basin, *Hydrol. Earth Syst. Sci.*, 15, 209–222, doi:10.5194/hess-15-209-2011.

Taylor, K., Stoffer, R., and Meehl, G. 2012: An overview of CMIP5 and the experiment design, *B. Am. Meteorol. Soc.*, 93, 485–498.

Teodoru, C., Wüest, A., and Wehrli, B. 2006: Independent review of the environmental impact assessment for the Merowe Dam project (Nile River, Sudan). Eawag aquatic research, Kastanienbaum, Switzerland.

Thornthwaite, C. W. 1948: An approach toward a rational classification of climate, *Geogr. Rev.*, 38, 55–94.

United Arab Republic and Sudan Agreement (With Annexes) For The Full Utilization of the Nile Waters, signed at Cairo on 8 November 1959, in force: 12 December 1959, 6519 U.N.T.S., 63, available at: http://www.internationalwaterlaw.org/documents/regionaldocs/uar_sudan. html, last access: 10 August 2014.

United Nations Office for the Coordination of Humanitarian Affairs, OCHR, (2011), Eastern African Drought Humanitarian Report. No. 3.

Waterbury, J. and Whittington, D. 1998: Playing chicken on the Nile? the implications of microdam development in the ethiopian highlands and Egypt's New Valley Project, Nat. Resour. Forum, 22, 155–163.

Whittington, D. 2004: Visions of Nile basin development, *Water Pol*., 6, 1–24.

Whittington, D., Wu, X., and Sadoff, C. 2005: Water resources management in the Nile basin: the economic value of cooperation, *Water Pol*., 7, 227–252.

Wilks, D. S., & Murphy, A. H. 1985: The value of seasonal precipitation forecasts in a haying/pasturing problem in Western Oregon. *Monthly weather review*, *113*(10), 1738-1745.

Wilks, D. S. 2001: A skill score based on economic value for probability forecasts". *Meteorological Applications*, ***8*(02),** 209-219.

Wilks, D. S. Statistical methods in the atmospheric sciences. Vol. 100. Academic press, 2011.

Yao, H. and Georgakakos, A. P. 2003: Nile Decision Support Tool River Simulation and Management, Georgia Water Resources Institute, Georgia Tech, Atlanta, USA.

Yates, D. and Strzepek, K. 1998: Modeling the Nile basin under climate change, *J. Hydrol. Eng*., 3, 98–108.

Appendix A:

SHOM MODEL:

Objective Function:

$$Objective = max \sum_{m,y}(D^y * bi_{m,y} + D^y * P_{m,y}\, bh_{m,y}) \quad (1)$$

Constraints:

Hydropower:

$$\forall_{l,m,y},\ KWH_{l,m,y} = c * n * effh * rhe_{l,m,y} * h_{l,m,y} \quad (2)$$

$$bh_{m,y} = \sum_l (P * KWH_{l,m,y}) \quad (3)$$

$$\forall_{l,m,y},\ r_{l,m,y} = rhe_{l,m,y} + nhe_{l,m,y} \quad (9)$$

$r_{l,m,y}$ = total release, $rhe_{l,m,y}$ =hydropower release, $nhe_{l,m,y}$ = non-hydropower release

$$\forall_{l,m,y},\ rhe_{l,m,y} \leq Q_{dc} \quad (11)$$

where Q_{dc} is the flow capacity through the turbines.

Irri*gation:*

$$i_{l,m,y} = \sum_c (effi_c * Water_{c,l,m,y} * Area_{c,l,m,y}) \quad (4)$$

$$bi_{m,y} = \sum_{c,l} (effi_c * v_c * Water_{c,l,m,y} * Area_{c,l,m,y}) \quad (5)$$

$$\sum_{l,m,y}(i_{l,m,y}) + \sum_{l,m,y}(e_{l,m,y}) \leq Y * 14.5\ bcm \quad (6)$$

$$\sum_{l,m}(i_{l,m,y}) + \sum_{l,m}(e_{l,m,y}) \leq 0.28 * \sum_m (R_y) \quad (7)$$

$$\sum_{c,l} Area_{c,l,m,y} \leq 1.4 million\ ha \quad (12)$$

Continuity:

$$\forall_{m,y},\ s_{l,m,y} = q_{l,m,y} + r_{(l-1),m,y} + s_{l,(m-1),y} - r_{l,m,y} - i_{l,m,y} - e_{l,m,y} \quad (8)$$

$$s_{l,m,y} \leq Vmax \quad (9)$$

Non Negativity Constraints: $s_{l,m,y}, rhe_{l,m,y}, nhe_{l,m,y}, r_{l,m,y}, i_{l,m,y}, Area_{c,l,m,y} \geq 0$ (10)

Appendix B

	RPS				NS	
Run	July SMA	July ARM	Aug SMA	Aug ARM	July	Aug
1	0.47	0.67	0.44	0.17	0	1
2	0.94	0.87	0.09	0.57	1	0
3	1.03	0.59	1.03	0.56	1	1
4	0.34	0.24	1.53	0.51	1	1
5	0.17	0.45	1.17	0.40	0	1
6	0.06	0.07	0.24	0.40	0	0
7	0.45	0.45	0.18	0.34	0	0
8	0.14	0.40	0.28	0.25	0	1
9	0.17	0.26	0.40	0.18	0	1
10	0.20	0.09	0.31	0.67	1	0
11	1.14	0.59	0.06	0.37	1	0
12	0.69	0.45	0.63	0.36	1	1
13	0.63	0.31	0.28	0.36	1	0
14	0.81	0.45	0.51	0.26	1	1
15	0.17	0.28	0.28	0.17	0	1
16	0.57	0.37	0.40	0.06	1	1
17	0.37	0.12	0.45	0.14	1	1
18	0.17	0.74	0.40	0.40	0	1
19	0.34	0.18	1.09	0.26	1	1
20	1.09	0.67	1.28	0.94	1	1
21	0.37	0.47	0.67	0.56	0	1
22	0.28	0.14	0.87	0.40	1	1
23	1.14	0.25	0.94	0.37	1	1
24	0.45	0.20	0.28	0.24	1	1
25	0.03	0.31	0.59	0.06	0	1
26	0.69	0.11	0.95	0.07	1	1
27	0.74	0.03	0.81	0.03	1	1
28	0.11	0.51	0.14	0.07	0	1
29	0.47	0.14	0.87	0.51	1	1
	0.49	**0.36**	**0.59**	**0.33**	**18**	**23**

Appendix C
UPDATES TO SHOM MODEL:

New Objective Function:

$$Objective = max \sum_m (bi_m + bh_m) \quad (1)$$

New Continuity:

$$\forall_{l,m},\ s_{l,m} = F_{l,m} + Ur_{(l-1),m} + T_{l,(m-1)} - r_{l,m} - i_{l,m} - e_{l,m} \quad (2)$$

Where, $F_{l,m}$ is forecasted flows, $s_{l,m}$ is forecasted storage, $Ur_{(l-1),m}$ is the upstream releases, $T_{l,m}$ is the actual storage, $r_{l,m}$ is the dam release, $i_{l,m}$ is the irrigation release and$e_{l,m}$ is the evaporation

$$T_{l,m} = s_{l,m} + q_{l,m} - F_{l,m} - er_{l,m} \quad (3)$$

$q_{l,m}$ is the actual flow, and when $er_{l,m}$ is positive, it is the emergency release due to forecasting error, and when $er_{l,m}$ is negative it is the amount of water held back due to forecasting error.

$$Ur_{l,m} = r_{l,m} + er_{l,m} \quad (4)$$

Non Negativity Constraints: $s_{l,m}, r_{l,m}, T_{l,m}, i_{l,m,} \geq 0$

Penalty:

$$Pen_{l,m} = P * [c * n * effh * hmax_{l,m} * abs(er_{l,m})] \quad (5)$$

effh is the efficiency of the dams, which was assumed to be 0.85 in the model. There is a conversion factor (c), c = 2.61×10^{-3}. P = 5 times the price of Hydroelectricity in the model.

GERD Reservoir Operating Rule (ROR) for last month in annual run:

$$r_{1,12} = (s_{1,12} + q_{1,12}) * 0.9659 - 60709 \quad (6)$$

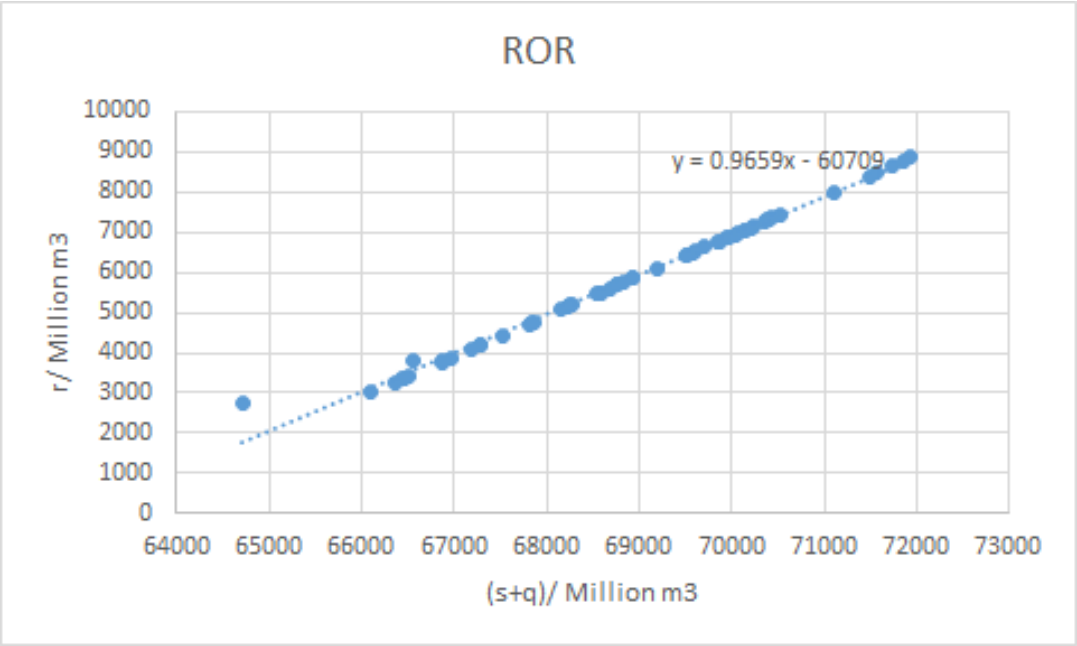
ROR
y = 0.9659x - 60709
r/ Million m3
(s+q)/ Million m3
10000
9000
8000
7000
6000
5000
4000
3000
2000
1000
0
64000
65000
66000
67000
68000
69000
70000
71000
72000
73000

Appendix D
Models

Statistical Models

Statistical models were applied in two ways in this study. First, models were used to produce one-month lead precipitation forecasts for each month of the rainy season. Next, another set of statistical models was developed to predict monthly streamflow as a function of monthly observed and forecasted precipitation. For both precipitation and streamflow models we applied a suite of parametric and non-parametric statistical models in order to determine the best modeling approach for the available data. Specifically, we applied a variable selected Generalized Linear Models (GLM), General Additive Models (GAM), Artificial Neural Networks (ANN), Random Forest (RF), and Bayesian Additive Regression Trees (BART). Each is described below.

Stepwise GLM

GLM is a linear statistical model that determines the response variable via OLS ordinary least squares, and utilizes a basic link function that describes the relationship between the predictors and response variables. Equation D.1 displays the structure of the GLM. The model used in this study uses a Gaussian distribution as the assumed link function.

$$Y = \beta_N X_N + \varepsilon \quad \text{(D.1)}$$

For prediction made using a Gaussian distribution the response used is centered around a mean of zero, thus the anomaly—a deviation from the long term mean—is the response variable. A separate GLM was derived for each of the four months in order to capture changing contributions of predictor variables over the course of the season. The Akaike information criteria (AIC) is used to maximize predictive accuracy by ensuring an

optimal relationship between model complexity and goodness of fit, thereby minimizing bias and variance in the models. Multicollinearity of predictors was addressed using a variance inflation factor (VIF) criterion in which all retained predictors were required to have VIF < 5.

The variables selected by the step method in the GLM function in R (representative of the AIC method) reveals the variables used in the analysis.

GAMs

GAMs, like GLMs, are linear likelihood-based regression model. GAMs, however feature a non parametric smoothing function that allows the model to capture and fit non linear trends in the predictor data. This study uses a cubic regression spline as the smoothing function. A link function is used to identify the relationship between response variable and the smoothed function of the predictors.

ANN

In addition to the linear and non linear parametric models, Artificial Neural Networks (ANN) are used in our analysis as a non-parametric machine learning alternative. ANNs consist of a network of nodes and links that utilize a non parametric approach to connect predictors to the response. ANNs have three basic types of layers. Predictor data is relayed from an input layer to a response in an output layer via a hidden layer. Data is weighted and fed forward from the input layer to the hidden layer where a function is determined and corrected via cross validated tuning and bias application. The hidden layer functions are then used to determine the response variable.

Tree-based data mining techniques

Other non-parametric approaches used are tree-based data mining techniques. Trees have the capacity to capture fit non-linear relationships between predictors and the response. Two examples of complex tree based methods are Random Forests (RF) and Bayesian Additive Regression Trees (BART). RF utilizes multiple decision trees to make predictions. A bootstrapped sample of the data is used to grow the trees, with an out-of-bag sample used to estimate accuracy of prediction. Random forest predictions are made by allocating a vote to each tree (classification) or averaging across all trees (regression). BART models also aggregate over multiple trees. In addition to summing over multiple trees, BART also regularizes the prior parameter of the model. BART implements a prior over tree space and calculates a posterior using a Bayesian backfitting Markov Chain Monte Carlo (MCMC) algorithm (Chipman, 2010) in order to make a prediction.

Precipitation Data

The statistical prediction of precipitation in the Blue Nile headwaters depends on the selection of data. Past analyses in Ethiopia have highlighted the large scale drivers that affect rainfall variability in the highlands and in the source regions of the Blue Nile (Gisselle et al 2004, Korecha and Barnston 2007, Diro et al. 2011, Berhane et al. 2014). Based on these previous studies, we selected a set of climate indices, sea surface temperature patterns and pressure indicators as predictors for the statistical models. These include:

1. El-Nino Southern Oscillation (ENSO) Nino 3.4, defined as the SST between 5S and 5N and from 120-170W, calculated using NOAA's OICCTV2 Optimal Interpolation Sea Surface Temperature Version 2.

2. The Southern Oscillation Index (SOI), a standardized mean monthly SLP between Tahiti and Darwin.
3. The Multivariate ENSO Index (MEI) the combined normalized first principle component (PC) of surface temperature, SST, SLP, winds and total cloudiness over the tropical pacific.
4. Pacific Decadal Oscillation (PDO) index, the leading PC of monthly SST anomalies in the northwest and eastern equatorial Pacific.
5. North Atlantic Oscillation (NAO) index,
6. Bombay Monthly SLP: is the SLP anomaly located on 19^0N and 72.8^0E
7. Arabian Penninsula SLP: 15^0-28^0N and 40^0-57^0E
8. St. Helena SLP: 20^0-27^0S and 10^0-25^0W
9. Indian Ocean SST: two areas were used as predictors, a) 10^0S-10^0N and 50^0-70^0E and (Ind1) b) 10^0S-0^0 and 90^0-110^0E (Ind2), (Gisselle et al 2004).

Indices (predictors 1-5) were obtained through the KNMI Climate Explorer (https://climexp.knmi.nl/). SLP was extracted from the National Centers for Environmental and Predictions- National Center for Atmospheric Research (NCEP-NCAR) Reanalysis 1 data obtained from the National Oceanic and Atmospheric Administration (Kalnay et al. 1996). Observed SST anomalies were extracted from the Kaplan Extended SST version 2 dataset, which is produced at 5 x 5 degree resolution (Reynolds et al. 1994, Parker et al. 1994, Kaplan et al. 1998). These data were obtained from the NOAA/OAR/ESRL PSD, Boulder Colorado USA (http://www.esri.noaa.gov/psd/).

Precipitation data used in this study was derived from the Climate Hazards Group (CHG)

and Florida State University's CenTrends monthly precipitation dataset. The dataset was developed using a large set of archived station data interpolated to produce a high resolution century long (1900-2015) time record of gridded East African precipitation. Statistical analyses were performed in R open source software package version 3.1.2. All data was standardized over the period of analysis 1950-2009.

Hydrology Data

Data for the construction of the hydrology model required precipitation data (see Precipitation data section for sources), and air temperature drawn from the Climate Research Unit (CRU) CRU TS3.21 dataset, developed at University of East Anglia. In Addition Flow data was derived from Global Runoff Data Center (GRDC) GRDC Station no. 16663800, which includes gauged discharge data from 1912-1982. Statistical analyses were performed in R open source software package version 3.1.2. All data was standardized over the period of analysis 1950-2009.

Model Evaluation

The statistical models are evaluated and compared for predictive accuracy by using three different metrics, the Pearson correlation coefficient (corr; larger is better), the Mean Absolute Error (MAE, smaller is better) and the Mean Squared Error (MSE, smaller is better). The Pearson correlation measures the direction of the linear relationship between the predicted values and the observed values, while the MAE and the MSE are direct measures of error. The MSE is used because of the metric's sensitivity to larger errors and outliers, while the MAE is the cumulative measure of the calculated error. A k-fold Random Holdout Cross Validation (RHCV) was performed in order to assess the model prediction. A k-fold RHCV randomly disaggregates the data, fits and trains the model to

one portion of the data set, and makes a prediction on the remaining portion. This process is repeated a specified number of times.

The RHCV-based error metrics for each model are then compared in order to test for significant differences between models and between each model and a null forecast that always predicts the long-term mean. Significance was assessed at the 95% confidence level, using a Bonferroni correction for multiple hypothesis testing.

Methods

Precipitation Models

Predictions of precipitation were made with predictors at 1-month lead time for each of the predicted four months of the June-July-August-September (JJAS) Kiremt rainy season. Predictor variables were selected from Atlantic, Indian, and Pacific Ocean SST and SLP patterns (see data section for description of the climate variables used). All predictors and the response variable were standardized. Two different analysis were conducted from the k-fold RHCV: (a) error comparison across all models for all holdouts and (b) ensemble prediction using the best performing model.

The k-fold RHCV required 60 years of data, from 1950-2009. The model was run 300 times, leaving out 10 years of data as validation for each run. The remaining 50 years of data was used to train the model. The results of the 300 iterations of 10 years of precipitation prediction were compiled and compared across all models, including a null model. 300 values of MAE and MSE of each model were averaged (Table 1) and a Bonferroni corrected t-test was administered to test statistical significance.

The k-fold RHCV was also used to determine the range of model errors for each of the years from 1982-2009. All predictions made for a particular year during the 300

iterations, and a distribution of errors for each year is attained. Figure 1 shows the quartile of predictions for each of the years from 1982-2009.

Hydrology Models

The hydrological models in this dissertation are statistical models that mimic the hydrological processes that convert precipitation into streamflow upstream of the Ethiopia/Sudan border. In order for the models to remain simple, the Blue Nile watershed is assessed as a whole and it is assumed that the basin characteristics that affect the hydrological processes -soil type, land cover, human consumption of water- remain relatively unchanged for the duration of the analysis. The general structure of the models (equation D.2) relates the standardized values of streamflow to current and previous standardized precipitation and temperature values (Shortridge at al 2015).

$$Q_t = (P_{t-2}, P_{t-1}, P_t, T_{t-2}, T_{t-1}, T_t) + \varepsilon \quad \text{(D.2)}$$

A k-fold RHCV process was used to determine the models with the best predictive capacity. Observed data of precipitation and flows spans 1965-2009, but with a gap for the period 1997-2001. This 38-year data record was fitted 300 times with 10 years randomly held out. The MAE, MSE and correlations of the 300 10 year predictions was compared and assessed for statistical significance.

Selection of the best performing model was used to determine the forecasted ensemble stream flows. Forecasted flows were derived through a leave-one-out (LOO) process where a chosen model was trained on the 37-year record and used to predict the remaining year. For this, the ensemble forecasted precipitation was input in order to calculate the forecasted flows. Therefore, P_{t-2}, P_{t-1}, and T_{t-2}, T_{t-1} are observed values, while

P_t is the forecasted precipitation at 1-month lag derived from the statistical models. T_t used in the LOO analysis is the climatological mean. This was repeated 38 times to determine the ensemble 1-month lag forecasted flows for the Blue Nile region.

Precipitation Forecast Model Results

Precipitation Stepwise GLM Variable selection

Variable selection of the precipitation stepwise GLM model is presented in Table 1 below. These variables were selected for each model as predictors for the 1-month precipitation forecast using the AIC selection.

Month	**Variables**
June	Ind 2, SOI, Nino3.4
July	Ind 1, PDO
August	St. Helena, Ind 1
September	Bombay, MEI, PDO, Atlantic

Table D.1: The variables used for Precipitation prediction by the GLM method using AIC selection method.

Holdout Analysis and Precipitation Model Selection

The performance of each model in the k-fold RHCV analysis is presented in table 2. Bold values highlight the model with the best performance. Results show the variable selected GLM consistently outperforms the other models with lower MSE and MAE values, as well as higher correlations. Table 2 shows the performance metrics averaged for all 300 iterations. The superior performance of the variable selected GLM is evident in all months for all metrics except for July, when RF is the best performing model according to the MAE metric. This single exception notwithstanding, the consistency with which the GLM outperforms other models at a statistically significant level indicates that the

model is able to capture relationships between precipitation and the selected climate indicators more reliably than the other tested modeling techniques.

MSE	**GLM**	**GAM**	**RF**	**ANN**	**BART**	**Mean**
June	**0.89**	0.97	1.09	1.03	1.07	1.04
July	**0.86**	1.05	0.89	0.99	0.93	1.01
August	**0.83**	0.86	1.00	1.01	0.99	1.04
September	**0.56**	0.58	0.64	0.92	0.66	1.03
MAE	**GLM**	**GAM**	**RF**	**ANN**	**BART**	**Mean**
June	**0.75**	0.79	0.85	0.83	0.84	0.83
July	0.78	0.82	**0.74**	0.77	0.76	0.77
August	**0.73**	0.73	0.79	0.79	0.79	0.81
September	**0.60**	0.62	0.67	0.78	0.68	0.81
Corr	**GLM**	**GAM**	**RF**	**ANN**	**BART**	
June	**0.40**	0.32	0.08	0.18	0.09	
July	**0.37**	0.28	0.29	0.30	0.27	
August	**0.46**	0.43	0.26	0.38	0.26	
September	**0.67**	0.66	0.60	0.60	0.60	

Table D.2: The average correlation (corr) and Mean Square Error (MSE) for the standardized precipitation predictions for all models. Best performing models are highlighted in bold text.

The predictors retained in the stepwise GLM differ from month to month over the JJAS period (Table D.3). Most notably, the ENSO influence is present throughout the season, but the power of ENSO predictors is much larger in late season (especially September) than in early season. Indian Ocean predictors, meanwhile contribute more to predictive skill early in the season. Overall, model performance is stronger later in the season (Table D.2), which is consistent with previous studies that have shown stronger teleconnections for Blue Nile precipitation towards the end of the rainy season (Berhane et al., 2014).

	June			
	Estimate	**Std. Error**	**t-value**	**Pval**
(Intercept)	0.00	0.12	0.03	0.98
Indian2	-0.32	0.16	-1.94	0.06
SOI	-0.47	0.18	-2.58	0.01
Nino34	-0.45	0.29	-1.52	0.13

	July			
	Estimate	**Std. Error**	**t-value**	**Pval**
(Intercept)	0.03	0.12	0.27	0.79
Indian1	-0.54	0.14	-3.93	0.00
PDO	0.23	0.11	2.15	0.04
	August			
	Estimate	**Std. Error**	**t-value**	**Pval**
(Intercept)	0.00	0.11	0.00	1.00
StHelena	-0.21	0.12	-1.71	0.09
Indian1	-0.38	0.12	-3.17	0.00
	September			
	Estimate	**Std. Error**	**t-value**	**Pval**
(Intercept)	0.14	0.10	1.37	0.18
Bombay	0.25	0.10	2.63	0.01
MEI	-0.84	0.13	-6.56	0.00
PDO	0.23	0.11	2.08	0.04
Atlantic	0.14	0.10	1.45	0.15

Table D.3: Stepwise GLM statistics showing model structure and influence of selected variables

Ensemble Precipitation Forecast

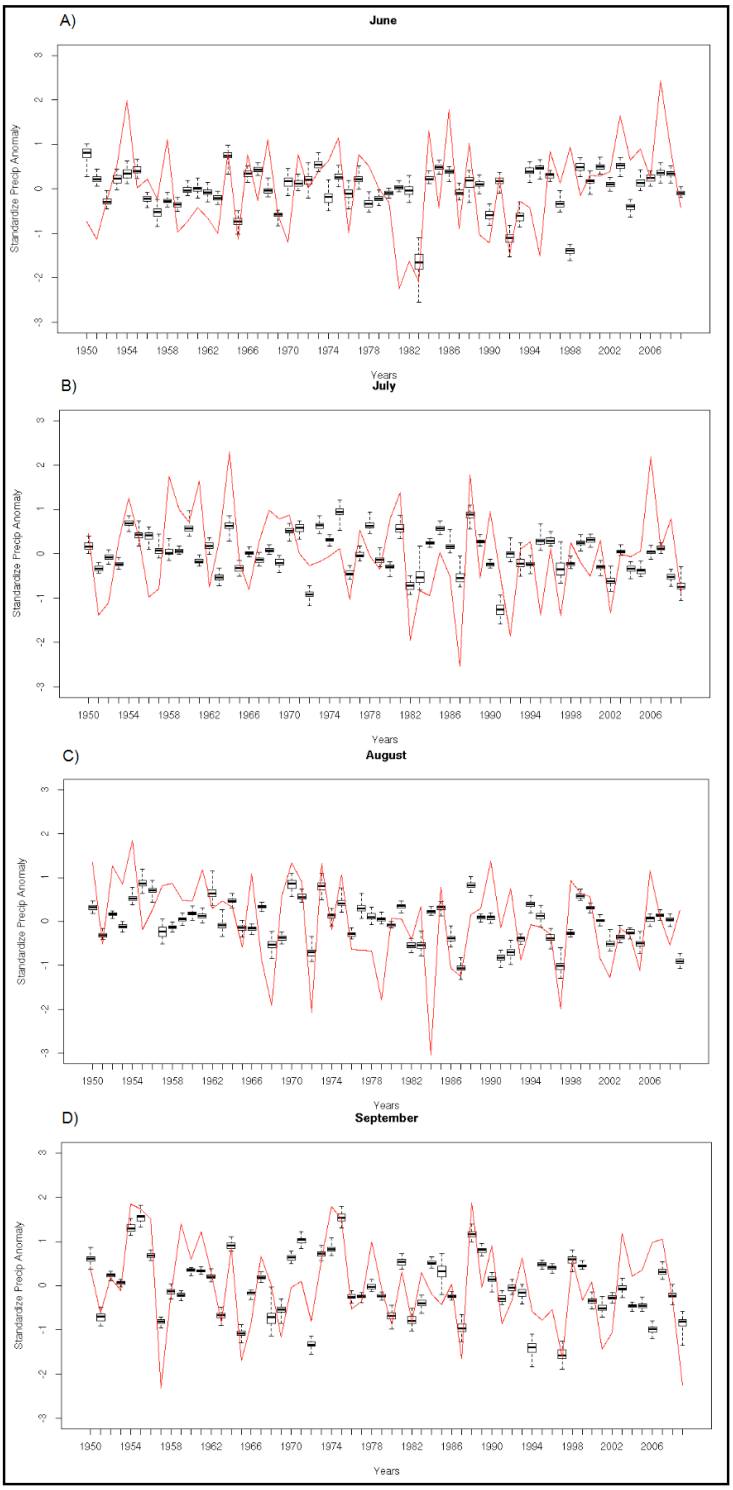

Figure D.1: A time series of precipitation JJAS standardized precipitation anomaly forecasts at 1-month lead for the Blue Nile region from 1982-2010. The predicted range of forecasted precipitation for each of the JJAS months is displayed in Figure 1. The

minimum, 25%, median, 75% and maximum values for GLM predictions are displayed on the box plots with the red line representing observed precipitation.

Hydrology Forecast Model Results

Hydrology Stepwise GLM Variable selection

Variable selection of the hydrology stepwise GLM model is presented in Table D.4 below. These variables were selected for each model using the AIC selection.

Month	**Variables**
June	Pjn,Pap,Pma,Tjn
July	Pjl,Pma,Tjl,Tma,Tjn
August	Pau,Pjn,Pjl,Tjn,Tjl
September	Psep,Pau,Pma,Tau

Table D.4: The variables used for hydrology GLM model using AIC selection method.

Holdout Analysis and Hydrology Model Selection

A second k-fold RHCV analysis was conducted to compare the same suite of statistical models in order to assess their ability to predict flow as a function of precipitation and temperature. Comparisons between the five statistical models and the null (mean model) are performed in terms average correlation, MAE and MSE of the standardized flows for all 300 holdouts run for each model during each month of the rainy season (Table D.5). GLM consistently and significantly produces the lowest MAE and MSE compared to all other.

MSE	GLM	GAM	RF	ANN	BART	Mean
June	**0.42**	0.47	0.73	0.69	0.62	0.98
July	**0.36**	0.44	0.52	0.70	0.49	1.05
Aug	**0.45**	0.57	0.60	0.77	0.52	1.01
Sep	**0.49**	0.58	0.62	0.85	0.57	1.04
MAE	**GLM**	**GAM**	**RF**	**ANN**	**BART**	**Mean**
June	**0.49**	0.50	0.60	0.66	0.56	0.71
July	**0.45**	0.49	0.55	0.69	0.53	0.83
Aug	**0.52**	0.59	0.62	0.72	0.57	0.69
Sep	**0.54**	0.60	0.62	0.75	0.60	0.80
Corr	**GLM**	**GAM**	**RF**	**ANN**	**BART**	
June	**0.72**	0.69	0.53	0.64	0.62	
July	**0.82**	0.79	0.78	0.75	0.77	
Aug	**0.74**	0.67	0.67	0.63	0.72	
Sep	**0.74**	0.68	0.67	0.53	0.71	

Table D.5: The average correlation (corr) and Mean Square Error (MSE) for the standardized flow predictions for all models. Best performing models are highlighted in bold text.

The structure of the hydrology stepwise GLM is presented in Table D.6.

June				
	Estimate	**Std. Error**	**t-value**	**Pval**
(Intercept)	0.00	0.09	0.00	1.00
Tjn	0.40	0.10	3.84	0.00
Pap	0.40	0.09	4.33	0.00
Pma	0.60	0.10	6.20	0.00
Pjn	0.64	0.10	6.42	0.00
July				
	Estimate	**Std. Error**	**t-value**	**Pval**
(Intercept)	0.00	0.09	0.00	1.00
Tma	0.09	0.20	0.46	0.65
Tjn	0.21	0.15	1.43	0.16
Tjl	0.02	0.15	0.17	0.87
Pma	0.29	0.15	2.01	0.05
Pjn	0.64	0.11	5.90	0.00
Pjl	0.46	0.10	4.55	0.00
August				
	Estimate	**Std. Error**	**t-value**	**Pval**
(Intercept)	0.00	0.10	0.00	1.00
Tjn	0.08	0.15	0.51	0.61
Tjl	-0.05	0.14	-0.36	0.72
Pjn	0.15	0.12	1.26	0.22
Pjl	0.51	0.12	4.34	0.00
Pau	0.45	0.11	3.92	0.00
September				
	Estimate	**Std. Error**	**t-value**	**Pval**
(Intercept)	0.00	0.11	0.00	1.00
Tau	-0.10	0.11	-0.88	0.38
Pau	0.41	0.11	3.63	0.00
Psep	0.51	0.11	4.59	0.00
Pma	0.15	0.11	1.35	0.19

Table D.6: Hydrology stepwise GLM statistics showing model structure and influence of selected variables

Flow forecasts

Predicted precipitation from the GLM forecast model (Figure D.1) for each JJAS month from 1982-2009 at 1-month lead time was input to the GLM hydrology model for each JJAS month to produce flow predictions (Figure D.2).

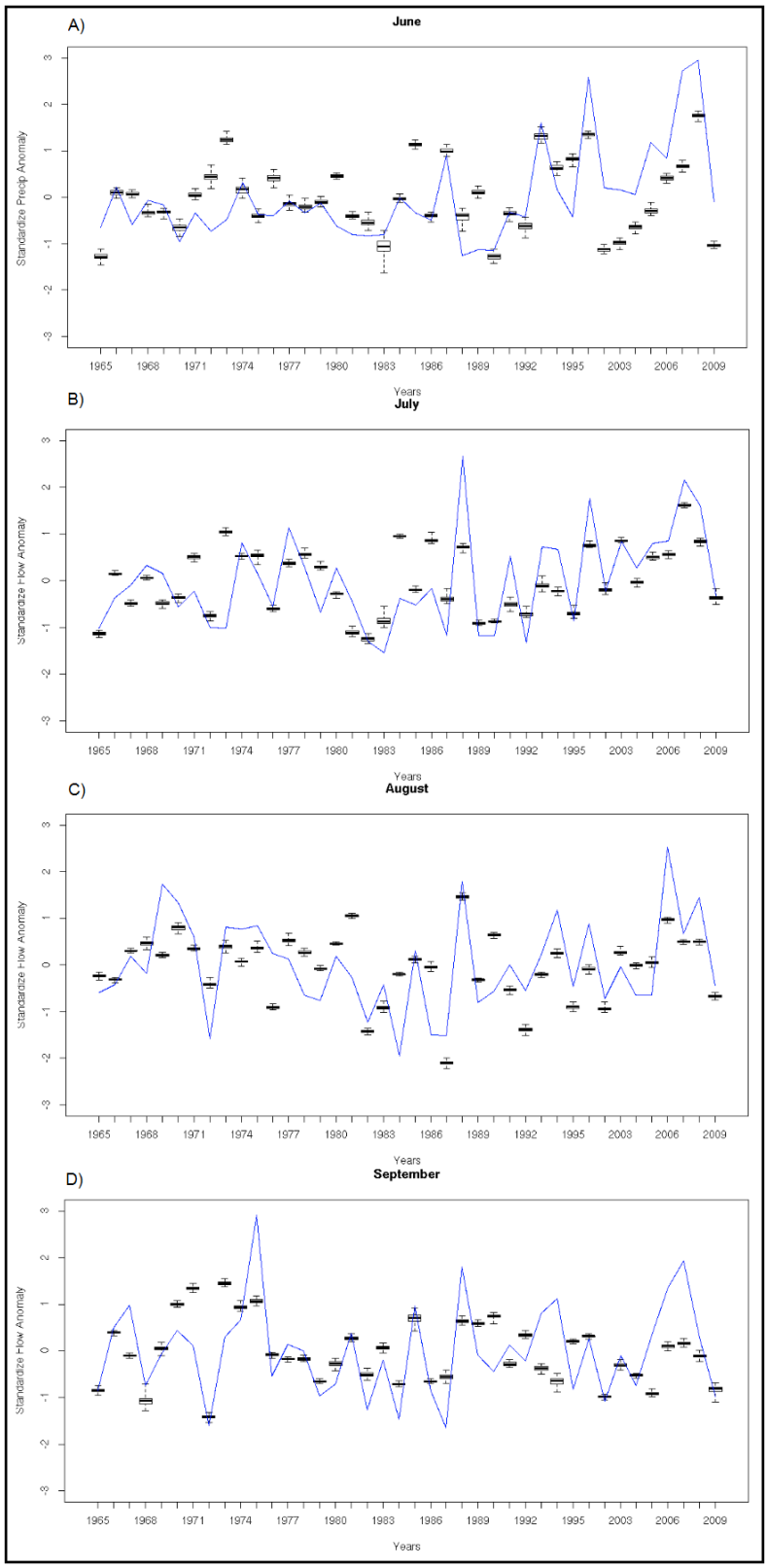

Figure D.2: Ensemble flow forecasts generated using GLM precipitation predictions at 1-month lead time. The minimum, 25%, median, 75% and maximum values for predictions are displayed on the box plots. The blue line is observed monthly flow.

Curriculum Vitae

Education

JOHNS HOPKINS UNIVERSITY Baltimore, MD 2016
PhD Candidate, Earth and Planetary Sciences

JOHNS HOPKINS UNIVERSITY Baltimore, MD 2013
MA, Masters of Arts, Earth and Planetary Sciences

TEXAS A&M UNIVERSITY College Station, TX 2007
MEng. Masters of Engineering-Civil Engineering

THE COLLEGE OF WOOSTER Wooster, OH 2005
Bachelor of Arts-Physics
Minor-Political Science

Journals

Satti, S., Zaitchik, B., & Siddiqui, S. (2015). The question of Sudan: a hydro-economic optimization model for the Sudanese Blue Nile. *Hydrology and Earth System Sciences*, *19*(5), 2275-2293.

Satti, S., Zaitchik, S., Badr, H., Tadesse, T. Understanding and enhancing dynamical seasonal forecast prediction through objective regionalizing. *In preparation (expected submission to Journal of Applied Hydrometeorology and Climatology in May 2016).*

Satti, S., Zaitchik, B., Regonda, S., Value versus Accuracy: application of a seasonal forecast to a hydro-economic optimization model for the Sudanese Blue Nile. *In preparation (expected submission to Journal of Hydrology: Regional Studies in June 2016).*

Satti, S., Zaitchik, B., Block P., Peters-Lidard, C. Value versus Accuracy: application of a seasonal forecast to a hydro-economic optimization model for the Sudanese Blue Nile. *In preparation (expected submission to Water Resources Research in June 2016).*

Presentations

Satti S, B Zaitchik and S Siddiqui S., Badr, H., Shukla, S., Peters-Lidard, C., (2016) Value versus Accuracy: application of a seasonal forecast to a hydro-economic optimization model for the Sudanese Blue Nile. (Poster). National Council for Science and the Environment. Meeting. January 19-21. Washington DC.

Satti S, B Zaitchik and S Siddiqui (2013) Determining the effect of climate change and development of water resources management in the Sudan. American Geophysical Union Fall Meeting. (Poster). December 9-13. San Francisco, CA.

Relevant Work Experience

Johns Hopkins University Baltimore, MD 2012 - Present
Research Assistant

Johns Hopkins University Baltimore, MD 2013 - 2014
Environment, Energy, Sustainability and Health Institute Fellow

- Research: The future of water, food and energy in Sudan

Johns Hopkins University Baltimore, MD 2013 & 2016
Teaching Assistant
- Climate Change: Science and Policy

Water Research Institute Accra, Ghana April 2010 – March 2011
Researcher
- Performed climactic and hydrologic modeling for the Pru Basin and the Ankobrah Basin of the Western region of Ghana

Dodson & Associates Inc. Houston, TX January 2008 – December 2009
Civil Engineer/Hydrologist
- Conducted water resources analysis by modeling existing and proposed channels and modifications
- Designed and analyzed existing storm water collection systems
- Developed drainage design reports, and conducted analysis, comparisons and design recommendations

Dannenbaum Engineering Houston, TX May 2007-August 2007
Engineering Intern, Hydrology Department
- Worked with hydrology department on projects involving Geographic Information Systems, as well as hydrology and hydraulics

Engineering Computer Skills and Software

R Statistical Tool
MATLAB
General Algebraic Modeling System
HEC-RAS: open channel hydraulic modeling
HEC-HMS: hydrologic modeling
WinStorm: hydrologic modeling for sewer systems
GIS: interface that incorporates maps and modeling
EPANet: hydraulic systems for water supply
XPSWMM: unsteady modeling for storm water with 2 dimensional capabilities
SWMM5: hydraulic modeling for storm watering
HEC-1: hydrology modeling
HEC-2: hydraulic modeling
SWAT: Soil and Water Assessment Tool.
ERDAS Imaging

Languages and Certifications

English, Arabic, French
Texas EIT Certification No. 41664

Honors and Associations

Texas Floodplain Managers Association
Member
Engineers Without Borders
Member
Wilson Compton Sr. Scholarship
2002-2005
Mabel Gillespie Scholarship
2002-2005
J&M Johnston Scholarship
2002-2005

Women's Board Academic Scholarship
2005
Joyce and Don Dunlap Scholarship
2007
Senior Independent Study Thesis
Honors

Project Experience

Sam Houston Tollway East Drainage Design

- Served as project engineer for the drainage analysis and design recommendations for drainage system along the Sam Houston Tollway.
- Performed a hydrologic and one-dimensional unsteady hydraulic analysis of the existing drainage system.
- Developed a report outlining the proposed mitigation and the impact analysis on the existing site.

Fort Bend County Drainage Design Criteria Manual

- Served as project engineer in the development of the hydrologic and hydraulic design manual for Fort Bend County.
- Duties included reviewing criteria manuals for surrounding counties, researching potential alternative solutions, analyzing requests and comments from Fort Bend County.

City of Portland Drainage Design Analysis

- Served as project engineer in the development of a regional two-dimensional unsteady model of a project area within the city of Portland.
- Duties included recognizing areas of flooding, recommending improvement scenarios, and developing a report detailing improvements and impacts analysis.

Buffalo Bend Wetlands Design

- Served as project engineer in the development of a hydrologic and hydraulic design of functioning wetlands.
- Findings from this project were submitted, and presented at the October 2009 Texas ASCE meeting.